Role of endocytic trafficking during Dpp gradient formation

DISSERTATION

zur Erlangung des akademischen Grades

Doctor rerum naturalium

(Dr. rer. nat.)

vorgelegt

der Fakultät Mathematik und Naturwissenschaften

der Technischen Universität Dresden

von

Dipl.-Biochem. Periklis Pantazis

geboren am 09.10.1975 in Hannover

Gutachter: Dr. Marcos González-Gaitán

Prof. Dr. Bernard Hoflack

Prof. Dr. Christian Klämbt

Eingereicht am: 01.11.2004

Tag der Verteidigung: 14.01.2005

"Των γραμμάτων οι μεν ρίζες πικραί εισί,
αλλά οι καρποί γλυκείς."

ΑΡΙΣΤΟΤΕΛΗΣ

Acknowledgement

During the past 3,5 years in the International Max Planck Research School at the Max Planck Institute of Molecular Cell Biology and Genetics in Dresden, many people provided help, support and friendship for which I am very grateful.

First of all, I would like to thank Dr. Marcos González-Gaitán for his continuous support during the period of my PhD. He has been a stimulating discussion partner offering countless advices and critically reviewing my work.

I wish to thank the members of my thesis advisory committee (TAC), Prof. Dr. Bernard Hoflack and Prof. Dr. Marino Zerial, for their feedback and scientific advices.

I want to thank Prof. Dr. Bernard Hoflack and Prof. Dr. Christian Klämbt for accepting to review my thesis.

The members of my lab provided an inspiring environment during my work. I am grateful to Anna, Antje, Naomi, Anja, Tanja, Olivier, Maximilian, Christian, Eugeni, Franck and - in particular - to Dana and Veronica!

Prof. Dr. Frank Jülicher, Dr. Karsten Kruse, and Tobias Bollenbach at the Max Planck Institute for the Physics of Complex Systems… thanks a lot for an excellent cooperation. There is so much more to gain when you are privileged to analyze the same issue from a different perspective.
Tobias, you have been a strong support during my work. Danke Dir!

For listening, numerous help and advice I am thankful to Giovanna, Eric, and Thorsten. I also thank the Photolab-team for printing… and talking. Kosta and Christine, it was fun to have some “Greeks” around!

My parents…: Μαμά και μπαμπά, ευχαριστώ για όλλα!

My brother Christos, my sister Athina and my brother-in-law Kosta for listening and talking… about so much more things but science!

Θείο Φώτη for innumerable discussions on the phone… ευχαριστώ για όλλες τις συμβουλές σου!

A special thank goes to my relatives in Greece… Αθηνά, Ρίτσα και Σπύρο.
It is always a great pleasure to see you again!

Helga and Adolf… Danke für die erholsamen Aufenthalte in Hannover!

All the friends who accompanied and supported my way!

Finally, I am particularly indebted to the most prominent person in my life … Nadine μου … her presence is the most invaluable treasure I can imagine.
Με πολλή αγάπη, ο Λάκης σου!

Summary

Morphogens are secreted signalling molecules that are expressed in restricted groups of cells within the developing tissue. From there, they are secreted and travel throughout the target field and form concentration gradients. These concentration profiles endow receiving cells with positional information. A number of experiments in *Drosophila* demonstrated that the morphogen Decapentaplegic (Dpp) forms activity gradients by inducing the expression of several target genes above distinct concentration thresholds at different distances from the source. This way, Dpp contributes to developmental fates in the target field such as the *Drosophila* wing disc.

Although the tissue distribution as well as the actual shape and size of the Dpp morphogen concentration gradient has been visualized, the cell biological mechanisms through which the morphogen forms and maintains a gradient are still a subject of debate. Two hypotheses as to the dominant mechanism of movement have been proposed that can account for Dpp spreading throughout the *Drosophila* wing imaginal target tissue: extracellular diffusion and planar transcytosis, i. e. endocytosis and resecretion of the ligand that is thereby transported through the cells.

Here, I present data indicating that implications of a theoretical analysis of Dpp spreading, where Dpp transport through the target tissue is solely based on extracellular diffusion taking into account receptor binding and subsequent internalization, are inconsistent with experimental results. By performing Fluorescence Recovery After Photobleaching (FRAP) experiments, I demonstrate a key role of Dynamin-mediated endocytosis for Dpp gradient formation. In addition, I show that most of GFP-Dpp traffics through endocytic compartments at the receiving epithelial cells, probably recycled through apical recycling endosomes (ARE). Finally, a Dpp recycling assay based on subcellular photouncage of ligand is presented to address specifically the Dpp recycling event at the receiving cells.

Table of contents

ACKNOWLEDGEMENT I

SUMMARY III

TABLE OF CONTENTS IV

1 INTRODUCTION 1

1.1 Positional information and pattern formation by morphogens 1

1.2 Morphogens in *Drosophila* wing development 3

1.3 Dpp signalling in *Drosophila* 7

1.4 Regulating Dpp signalling in *Drosophila* wing development 9

1.5 Dpp: a long-range morphogen in *Drosophila* wing development 12

1.6 Visualizing Dpp during *Drosophila* wing development 13

1.7 Mechanisms for morphogen gradient formation in the *Drosophila* wing 15

1.7.1 Morphogen gradient formation by extracellular diffusion 16

1.7.2 Morphogen gradient formation by active transport through the tissue 17

1.8 Mathematical models and Dpp gradient formation by restricted diffusion 22

1.9 The DBT and the DBTS model of Dpp gradient formation 24

1.10 Aim of the thesis 32

2 MATERIALS AND METHODS 33

2.1 Buffers and Solutions 33

2.2 Used equipment 38

2.3 Fly pushing 38

2.3.1 Maintenance of flies 38

2.3.2 Mutant strains 39
2.3.3 Transgenic strains 39
2.3.4 GAL4-mediated ectopic gene expression 40
2.3.5 Mosaic analysis 41
2.3.6 Blockage of Endocytosis at Receiving Cells 42
2.3.7 PAGFP-Dpp rescue 43

2.4 Cell biology 43
2.4.1 S2 cell maintenance 43
2.4.2 S2 cell transfection 43

2.5 Biochemistry 44
2.5.1 Preparation of cell extracts from *Drosophila* third instar larvae 44
2.5.2 Determining protein concentration by the Bradford dye-binding method 44
2.5.3 SDS-PAGE (SDS-Polyacrylamide gel electrophoresis) 45
2.5.4 Coomassie-Brilliant-Blue colouring of proteins 46
2.5.5 Western Blot 46
2.5.6 Immunodetection of a Western Blot 47

2.6 Histology and Imaging 48
2.6.1 Antibodies 48
2.6.2 Immunostaining 49
2.6.3 Dextran uptake 50
2.6.4 Cryosectioning 51
2.6.5 Preparing samples for *in vivo* imaging 51
2.6.6 Fluoresence Recovery After Photobleaching (FRAP) 51
2.6.7 Photoactivation 53

2.7 Molecular Biology 54
2.7.1 Polymerase chain reaction (PCR) 54
2.7.2 Gel-Electrophoresis of DNA 55
2.7.3 TOPO® cloning and transformation of chemical competent cells 55
2.7.4 Transformation 56
2.7.5 Subcloning into the pUAST/Caspertubulin vector 56
2.7.6 Preparing DNA for injection 57

3 RESULTS 58

3.1 Testing experimentally the DBTS model of Dpp gradient formation 58
3.1.1 Establishing antibodies and staining procedures detecting levels of total and cell surface receptor Tkv and extracellular Dpp 58
3.1.2 The DBTS model is inconsistent with the observed receptor concentrations in *shi* ^{ts1} clones 62
3.1.3 The DBTS model is inconsistent with the observed receptor concentrations in the “shibire rescue assay” 64

3.1.4 The DBTS model is inconsistent with observed extracellular ligand concentrations in the “shibire rescue assay” 67

3.2 Testing experimentally the role of Dynamin-mediated endocytosis in Dpp gradient formation - Determining the effective diffusion coefficient of GFP-Dpp 69

3.3 Characterizing Dpp trafficking along the endocytic pathway 78
3.3.1 Establishing antibodies to detect Rab proteins 78
3.3.2 Establishing an in vivo internalization assay 83
3.3.3 GFP-Dpp is localized in endosomal structures at the receiving cells 85

3.4 Establishing a Dpp recycling assay 87
3.4.1 Generating a photoactivatable GFP-Dpp (PAGFP-Dpp) fusion 88
3.4.2 Photoactivating PAGFP and PAGFP-Dpp in S2 cells 89
3.4.3 Visualizing PAGFP and PAGFP-Dpp in wing imaginal discs 90
3.4.4 A functional PAGFP-Dpp fusion 92
3.4.5 Dynamics of photoactivated PAGFP-Dpp 93
3.4.6 Subcellular photoactivation of PAGFP with a confocal laser-scanning miscroscope (C-LSM) 96
3.4.7 Subcellular photoactivation of PAGFP with a two-photon laser-scanning microspcope (2P-LSM) 97
3.4.8 Photoactivation of PAGFP-Dpp with a two-photon laser-scanning microscope (2P-LSM) 99

4 DISCUSSION 101

4.1 Why the DBTS model fails to explain Dpp propagation 102

4.2 Dynamin-dependent Dpp transport 103

4.3 Addressing the role of Dynamin-mediated endocytosis for Dpp movement: using FRAP as a tool 106

4.4 Dpp movement along the endocytic pathway 108

4.5 A Dpp recycling assay 109

5 REFERENCES 111

APPENDIX 127

Abbreviations 127

Movie description 129

Publications during PhD **131**

Statement / Versicherung **132**

1 Introduction

1.1 Positional information and pattern formation by morphogens

Our hands have five different fingers which are arranged in a particular order. This may seem quite trivial but the achievement of this arrangement during embryogenesis is an intriguing question in developmental biology. How do equivalent cells know where they are located within a tissue so that they form in a reliable manner the appropriate structure for their position?

At the onset of development, all cells are equipotent. During embryogenesis, they diversify as they proliferate to build up the final shape. To differentiate properly, it has been suggested that morphogens, secreted signalling molecules, tell cells about their positional information, i. e. their specific position within the tissue in a developing system. Once knowing their respective positional information, they contribute to the final spatial pattern in the entire organism (Wolpert, 1969). A morphogen is a “form-generating” molecule that is involved in the differentiation of cells by providing positional information encoded by its final concentration pattern within the developing tissue (Turing, 1952). The hypothesis of positional information (Wolpert, 1969) proposes that a morphogen is produced and secreted from a local group of cells and spreads through the target field to make a concentration gradient. This gradient endows the cells with their respective positional information. The information about the distance of the receiving cells from the morphogen-producing cells is encoded by the pattern of morphogen concentration. Above different threshold concentrations a distinct set of target genes is activated.

Secreted signalling molecules should fulfil three criteria to function as a morphogen:

I) To be distributed in a concentration gradient emanating from a restricted spatial source,

II) to act directly and at long distance to regulate expression of target genes, and

III) to specify distinct spatial domains of gene expression above different thresholds of concentration (Fig.1).

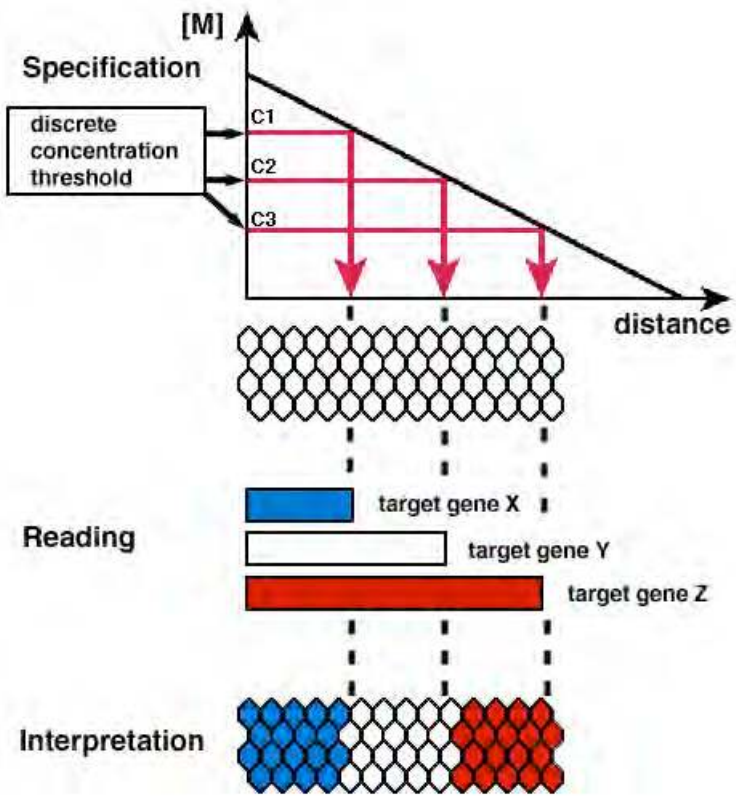

Fig. 1: Positional information by morphogen gradients
A morphogen (M) is released (left) into a field of undifferentiated cells to form a concentration gradient. Cells read the gradient by expressing different target genes above discrete concentration thresholds (target gene X above high concentration c1, target gene Y above medium concentration c2 and target gene Z above low concentration c3). The positional information is further processed to acquire fates that allow them to become blue, white and red.

Studies in *Drosophila* and vertebrates have identified members of the Hedgehog (Hh), Wingless (Wg), and TGF-β families of signalling molecules as morphogens. However, Wg seems not to be a classical morphogen, since the gradient does not activate directly different genes above different concentration thresholds, but rather maintains distinct gene expressions in a concentration-dependent manner (Martinez Arias, 2003).

Morphogens in the TGF-β family comprise Activin, bone morphogenetic protein 4 (BMP4), and Squint, which pattern the *Xenopus* and zebrafish dorsal/ventral (D/V) axis and regulate embryonic development (Chen and Shier, 2001; Dosch et al., 1997; Gurdon et al., 1994). Another example is Sonic Hedgehog (Shh) – a vertebrate member of the Hh family – that has been shown to function as a morphogen during the development of the chicken neural tube. It emanates from the notochord generating a ventral-dorsal activity gradient along the axis of the neural tube to promote directly the specification of interneurons and motor neurons (Briscoe et al., 2001; Ericson et al., 1997). Shh is also expressed in the posterior part of the developing vertebrate limb bud, from which it spreads to specify anterior/posterior (A/P) patterning of the limb bud (Riddle et al., 1993; Yang et al., 1997). It remains to be shown whether Shh can act directly at long distance.

In *Drosophila* development, one TGF-β molecule acting as a morphogen is the Decapentaplegic (Dpp) ligand, which contributes to the pattern of the dorsal ectoderm in the early embryo (Ferguson and Anderson, 1992a, 1992b; Ray et al., 2001; Wharton et al., 1993). Together with the morphogens Hh and Wg, Dpp also dictates the cell fate of the entire developing *Drosophila* wing (Basler and Struhl, 1994; Ingham and Fietz, 1995; Lecuit et al., 1996; Nellen et al., 1996; Neumann and Cohen, 1996; Zecca et al., 1995; Zecca et al., 1996).

1.2 Morphogens in *Drosophila* wing development

The *Drosophila* adult epidermis develops from distinct sets of epidermal cells, known as imaginal discs (Held, 2002). During embryogenesis, they are set aside from the larval epidermis and arise as pockets in the embryonic ectoderm. In the larva they grow fast until the pupal stage during which they evaginate to form the body wall and the appendages. In *Drosophila* larvae 19 larval imaginal discs can be distinguished by characteristic shape, size and pattern: 9 pairs for the head and the thorax, and a medial one for the genitalia. Besides them, the abdominal

epidermis of the adult fly derives from primordial cells called histoblast nests (Fig. 2). Unlike discs, they do not grow during larval stage and are integrated in the differentiated abdominal epidermis of the larva.

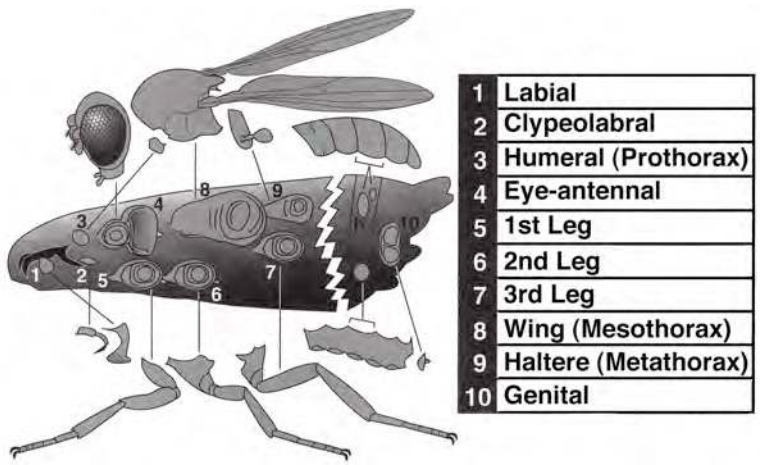

Fig. 2: Imaginal discs and their cuticular derivatives (modified from Held, 2002) Approximate placement of the discs (1-10) and their products in the adult fly. h (histoblast nests)

An extensively studied model system for identifying and analyzing morphogens and their function during development has been the wing imaginal disc. Like the other discs, it is a flattened, two-sided sac comprising a columnar cell epithelium and an overlying squamous cell layer, the peripodial epithelium (Held, 2002) (see also Fig. 7C, page 14). The characteristic distribution of the wing imaginal disc cuticular derivatives allows drawing a fate map of the wing disc: the wing pouch gives rise to the final wing blade, which is surrounded by a region which makes the hinge and pleura of the adult body and separates the wing from the most proximal region, the notum (Bryant, 1975). Topologically, the wing imaginal disc can be subdivided into anterior (A) and posterior (P) compartments along the anterior/posterior (A/P) axis, which do not mix with each other. In addition, the wing imaginal disc can be divided into dorsal (D) and ventral (V) compartments along the dorso/ventral (D/V) axis (Fig. 3).

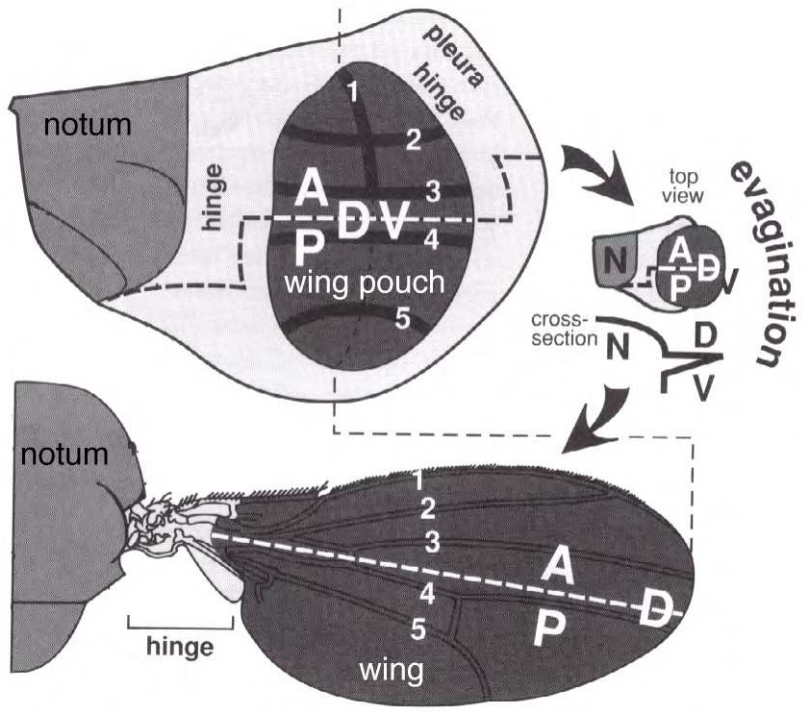

Fig. 3: Fate map of the wing imaginal disc (modified from Held, 2002)
The wing pouch as well as the adult wing is darkly shaded, the Notum (N) is medium shaded and the hinge with the pleura is lightly shaded. The thick dashed line marks the anterior/posterior (A/P) compartment boundary. During evagination the wing pouch expands and folds along the dorso/ventral (D/V) line. The thick black lines in the wing pouch are prevein zones (1-5).

The identity of the cells located in the P compartment is imprinted by the selector gene *engrailed* (*en*) (Simmonds et al., 1995; Tabata et al., 1995). Under the control of Engrailed, Hh is expressed in cells of the P compartment (Tabata and Kornberg, 1994) and upregulates or activates several target genes in nearby cells over a range of 10 cells into the A compartment, including *patched* (*ptc*), and the morphogen *dpp* (Maschat et al., 1998; Strigini and Cohen, 1997; Vervoort et al., 1999; Wang and Holmgren, 1999). In addition, Hh activates *engrailed* (*en*) at the late 3rd larvae instar only (Blair, 1992; Tabata and Kornberg, 1994; Guillén et al., 1995; Sanicola et al., 1995).

Dpp, which is expressed in an anterior cell stripe adjacent to the A/P compartment boundary, functions in turn as a morphogen that controls the fate beyond the central part. It is secreted from the central domain and induces in both compartments several target genes including *spalt (sal)*, *optomotor-blind*

(*omb*) and *vestigial* (*vg*) (Kim et al., 1995; Kim et al., 1996; Lecuit et al., 1996; Nellen et al., 1996).

In an analogous way to Engrailed, the protein Apterous imprints the cells in the dorsal compartment (Diaz-Benjumea and Cohen, 1993), inducing expression of the gene *fringe* (Irvine and Wieschaus, 1994). The latter activates the Notch receptor pathway at the D/V border (Kim et al., 1995), which results there in the induction of Wg (Doherty et al., 1996; Neumann and Cohen, 1996). Wg presumably maintains the differential expression of target genes (Martinez Arias, 2003), including *achaete* (*ac*), *Distalless* (*Dll*) and *vg* (Cubas et al., 1991; Diaz-Benjumea and Cohen, 1995; Kim et al., 1995; Neumann and Cohen, 1997; Skeath and Carroll, 1992; Zecca et al., 1996) (Fig. 4).

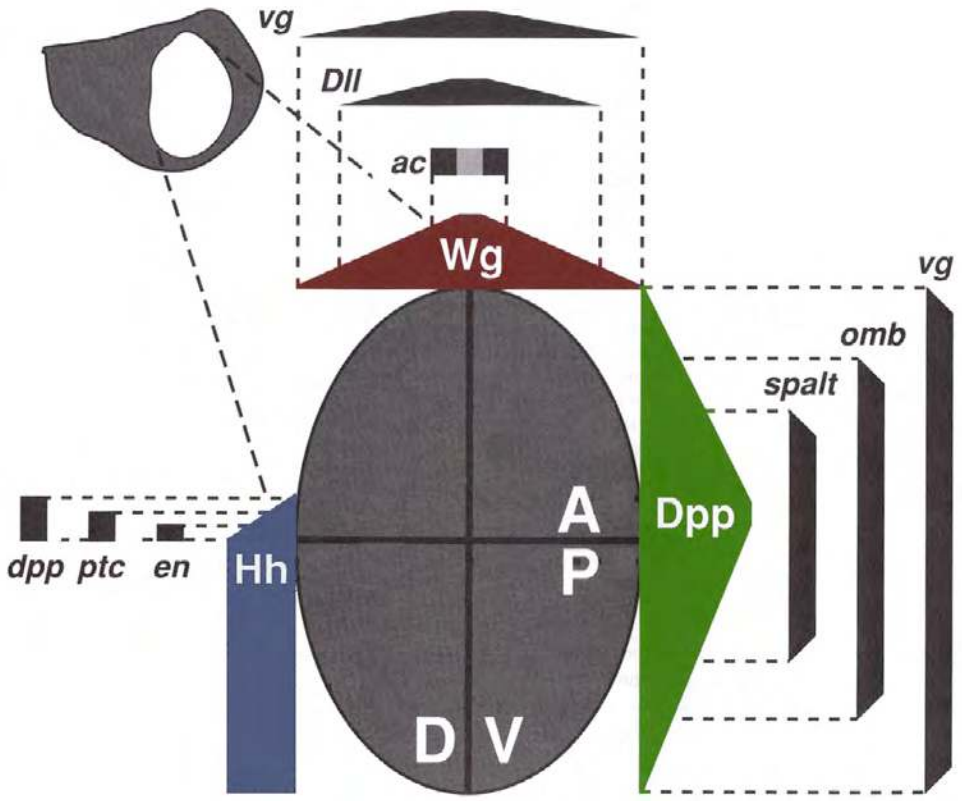

Fig. 4: Morphogen activity gradients in the wing imaginal disc (modified from Held, 2002) The wing pouch is enlarged from the wing imaginal disc as an oval. The solid lines indicate the anterior/posterior (A/P) and the dorso/ventral (D/V) compartment boundaries. The blue, green and brown areas show the activity gradient extents of the morphogens Hedgehog (Hh), Decapentaplegic (Dpp) and Wingless (Wg). Outer bars mark the expression domains of the target genes.

1.3 Dpp signalling in *Drosophila*

Based on the analysis of phenotypes of several alleles of the *dpp* gene (Spencer et al., 1982), Decapentaplegic has been shown to be involved in the development of at least 15 (Greek: decapente-) of the 19 imaginal discs. By Northern and cDNA analysis of the *dpp* locus, five differently spliced dpp transcripts were found (St Johnston et al., 1990), which encode a single open reading frame (ORF) (Newfeld et al., 1997). Dpp belongs to the TGF-β superfamily (reviewed in Massagué, 1998) and is closely related to the BMP2/4 subfamily (75 % amino acid sequence identity) (Sampath et al., 1993). Like other members of this family, Dpp is translated as a precursor and is cleaved into a C-terminal part which signals intercellularly, and a N-terminal part that is released and dimerizes (Gelbart, 1989; Panganiban et al., 1990). The proteolytic cleavage occurs at two sites, and is mediated by the metaloprotease furin (Cui et al., 1998; Cui et al., 2001). Apart from Dpp, at least six other TGF-β secreted ligand members have been identified in *Drosophila*:

- dActivin (Kutty et al., 1998),
- dActivin2 or ALP23B (Activin like protein at 23B) (Faucheux et al., 2001),
- Glass bottom boat 60A (Gbb 60A) (Doctor et al., 1992; Wharton et al., 1991),
- Maverick (Nguyen et al., 2000),
- Myoglianin (Lo and Frasch, 1999), and
- Screw (Arora et al., 1994).

Among them, Screw and Gbb 60A have been shown to modulate Dpp activity in the embryo and imaginal discs, respectively (Arora et al., 1994; Haerry et al., 1998; Khalsa et al., 1998).

Dpp, like the other members of this family, signals through a conserved mechanism of related serine/threonine receptor kinases. On the basis of their structural and functional properties they are divided into two families: type I and type II TGF-β receptors (reviewed in Raftery and Sutherland, 1999). Both receptor types are glycoproteins with a single membrane-spanning domain. In

Drosophila, three type I (Thick veins (Tkv), Saxophone (Sax), and Baboon (Babo)) (Brummel et al., 1994; Nellen et al., 1994; Penton et al., 1994; Xie et al., 1994), and two type II receptors (Punt (Put) and Wishful thinking (Wit)) have been identified (Letsou et al., 1995; Ruberte et al., 1995; Aberle et al., 2002; Marques et al., 2002). Among them, Tkv, Sax (Brummel at al., 1994)) and Put appear to serve primarily as type I and type II receptors for Dpp.

Upon binding of the dimerized Dpp ligand, Put, Tkv and Sax form a heterotetrameric receptor complex (Yamashita et al., 1994). Put then activates Tkv and Sax by multiply phosphorylating the GS (Glycine-Serine-rich) region, a highly conserved regulatory sequence next to the kinase domain on the cytoplasmic part of the type I receptor (Wrana et al., 1994). Activated Tkv and Sax phosphorylate in turn members of the receptor-regulated Smad (R-Smad) family of transcription factors at the C-terminus. SARA (Smad Anchor for Receptor Activation), an adaptor protein, is thought to recruit R-Smads to the activated receptor (Tsukazaki et al., 1998; Bennett and Alphey, 2002).

Phosphorylation of R-Smad triggers oligomerization with a “common-mediator” Smad (co-Smad), an obligate partner in the transcriptional complex. Upon complex formation, the Smads move to the nucleus where they regulate gene expression to elicit a diverse range of biological responses. In *Drosophila*, the genes *mothers against dpp* (*mad*) and *medea*, encoding a R-Smad and a co-Smad component required for Dpp signalling, were identified in genetic screens for enhancers of partial loss of function *dpp* mutant phenotypes (Raftery et al., 1995; Sekelsky et al., 1995). In addition, the DNA-binding transcription factors Schnurri (Shn) and the coactivator *Drosophila* CREB-binding protein (dCBP) have been identified as nuclear proteins that modulate their transcriptional activity (Arora et al., 1995; Waltzer and Bienz, 1999). Upon pathway activation a Smad/Shn complex represses Brinker (Brk) transcription, a default Dpp target genes repressor, to finally enable expression of Dpp target genes (Pyrowolakis et al., 2004) (Fig. 5).

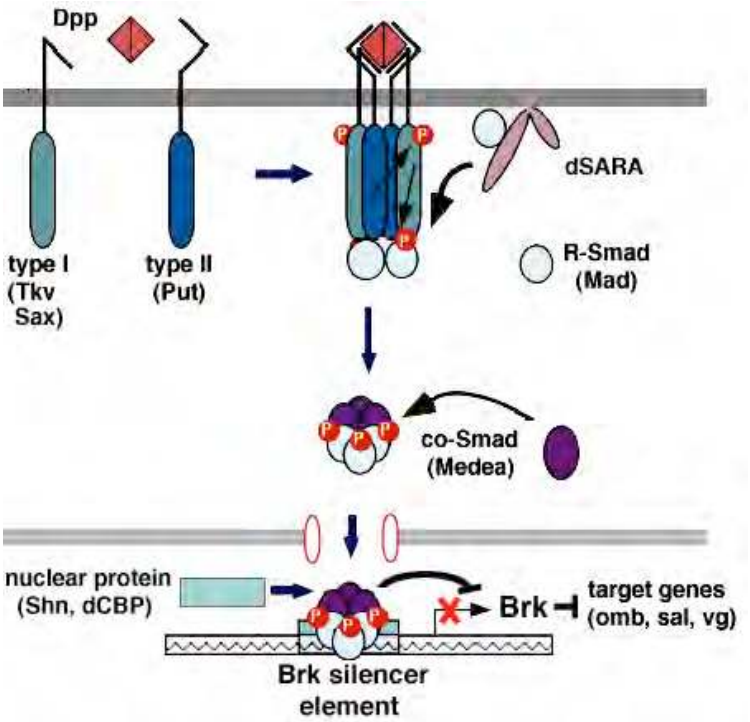

Fig. 5: Dpp signalling pathway (modified from Raftery and Sutherland, 1999)
Cooperative binding of dimerized Dpp to its type II receptor Punt (Put) and type I receptors Tkv and Sax leads to a ligand-receptor complex and subsequent phosphorylation of the type I receptors. Activated Tkv and Sax in turn phosphorylate the receptor-regulated Smad (R-Smad) Mothers against Dpp (Mad) which has been recruited by dSARA (Bennett and Alphey, 2002). Phosporylated Mad forms a transcriptional complex with the "common-mediator" Smad (co-Smad) Medea and moves into the nucleus. There, the complex in concert with DNA-binding partners, e. g. Shn and dCBP, binds to Brk silencer elements (Pyrowolakis et al., 2004), releasing default target gene repression by Brk. Finally, transcription of the target genes *spalt (sal)*, *optomotor-blind* (*omb*) and *vestigial* (*vg*) is enabled.

1.4 Regulating Dpp signalling in *Drosophila* wing development

A spatial and temporal regulation of transcription of Dpp signalling components has been shown to be important to ensure precise control of ligand action (reviewed in Parker et al., 2004). The signalling output can be modified at each step in the Dpp pathway: extracellular, intracellular and nuclear.

Glypicans, that comprise a family of heparin sulphate proteoglycans (HSPGs) tethered to the cell membrane by a glycosylphosphatidylinositol (GPI) anchor (reviewed in Filmus and Selleck, 2001), have been found to modulate Dpp signalling (Jackson et al., 1997). In *Drosophila*, two glypican homologues were

identified: Division abnormally delayed (Dally) and Dally-like (dly). *Dally* mutants were identified due to their effects on cell division in the *Drosophila* eye imaginal disc (Nakato et al., 1995). The precise action of Dally on Dpp signalling is still unclear (Jackson et al., 1997), yet it is assumed that it acts by altering either the local distribution of the ligand or its interaction with the receptor Tkv and Put. It is also possible that the distribution and activity of the ligand are modulated by the Dpp receptor Tkv itself. Dpp negatively regulates *tkv* expression (Lecuit and Cohen, 1998). Subsequently, the level of *tkv* expression is higher at the periphery of the wing disc, where Dpp signalling is low, and lower in the central region, where Dpp signalling is high (Lecuit and Cohen, 1998). Increasing Tkv level might shape the Dpp gradient itself by sequestering and internalizing local Dpp. In addition, the distribution of Tkv may sensitize cells at the periphery of the wing imaginal discs to lower levels of Dpp (Lecuit and Cohen, 1998).

At the cellular level, cytoplasmic proteins can compete with receptor-regulated R-Smad for the binding to the receptor active site. Several studies have characterized a third Smad subfamily that inhibits the signalling function of the other two Smads (Fig. 5). In *Drosophila*, Daughters again dpp (Dad) has been shown to function as a member of the inhibitor Smad (i-Smad) subgroup (Tsuneizumi et al., 1997). It represses Dpp activity by competing with Mad for binding to Tkv (Inoue et al., 1998), and coincident overexpression of Dad rescues overgrowth to wild-type caused by excess of Mad (Tsuneizumi et al., 1997). In addition, Dpp signalling is modulated by Smad ubiquitin regulatory factors (Smurfs), E3-ubiquitin ligases that selectively target the receptors and Smad proteins for degradation (Zhu et al., 1999). In *Drosophila*, loss of *dSmurf* leads to an increase in Dpp signalling (Podos et al., 2001).

A critical step in Dpp signalling is the nuclear translocation of the R-Smad/co-Smad complex to activate distinct target genes. In the context of nuclear Smad activity in *Drosophila*, the transcriptional release of repression has been analyzed. Dpp signalling target genes are repressed in the absence of ligand by the repressor Brinker (Brk) (Jazwinska et al., 1999a). Brk functions as a default active repressor of Dpp responsive target genes (Kirkpatrick et al., 2001). Thus,

brk mutant somatic clones express Dpp target genes in a cell-autonomous manner, indicating that Brk functions to keep these genes silent (Jazwinska et al., 1999a; Minami et al., 1999). Furthermore, mutants of *brk* turn on target genes in the absence of Dpp signalling (*mad* or *tkv* mutant), suggesting that Dpp inhibits *brk* transcription directly to overcome Brk repression on target genes (Campbell and Tomlinson, 1999; Jazwinska et al., 1999a; Jazwinska et al., 1999b). Consistent with this, the *brk* transcription level forms a gradient that overlaps and opposes Dpp activity levels (Campbell and Tomlinson, 1999; Jazwinska et al., 1999a) (Fig. 6).

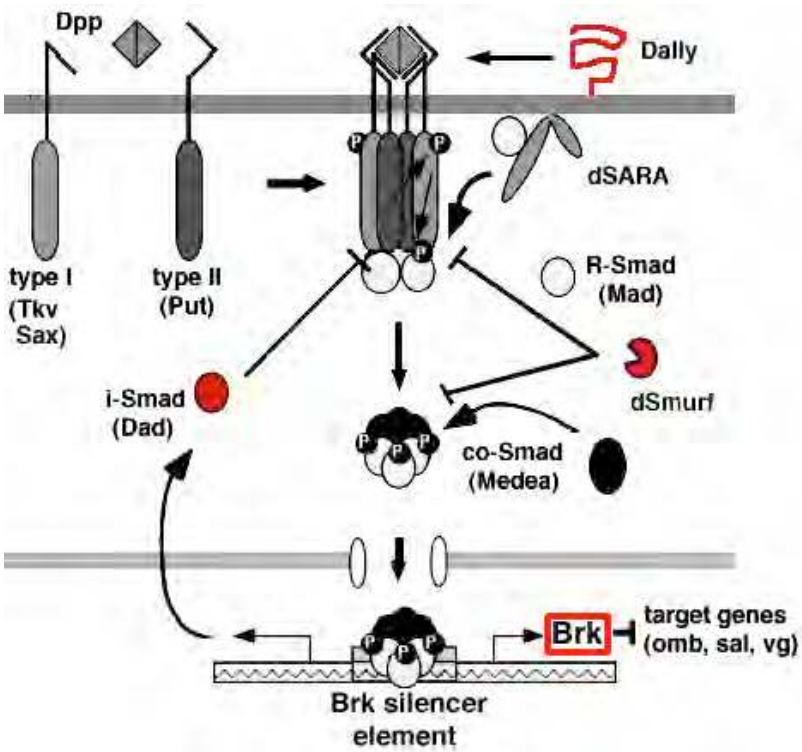

Fig. 6: Regulating Dpp signalling (modified from Raftery and Sutherland, 1999)
The glypican Dally is thought to alter either the local distribution of Dpp or its interaction with the receptor Tkv and Put, thereby enhancing Dpp signalling. In a negative feedback loop, Dpp signalling activates the transcription of the inhibitory Smad (i-Smad) Daughters against dpp (Dad), which represses Dpp signalling. *dSmurf* negatively regulates the cellular response to Dpp signalling by selectively targeting the receptors and Smad proteins for degradation. Brk functions as a default active repressor, resulting in the suppression of Dpp target genes expression.

1.5 Dpp: a long-range morphogen in *Drosophila* wing development

Evidence showing that Dpp acts as a morphogen in the wing imaginal disc came from experiments demonstrating that it acts directly on target cells in a concentration-dependent manner (Lecuit et al., 1996; Nellen et al., 1996). Dpp is expressed in a stripe of anterior cells along the border between the A and P compartments (Basler and Struhl, 1994), and was thought to be secreted into either direction within the wing pouch's entire A/P axis (Fig. 4). Two genes, *omb* and *sal*, were identified as targets of Dpp in the wing imaginal disc, showing expression domains centred in the A/P compartment boundary. Consistently, *omb* and *sal* expression domains disappear in *dpp* loss of function wing discs (Posakony et al., 1990; Spencer et al., 1982). Dpp induction of *omb* and *sal* was shown to be direct, since the same result was obtained with *tkv* and *mad* loss of function clones (Lecuit et al., 1996; Nellen et al., 1996). In addition, the *omb* and *sal* expression domains expanded when *dpp* or a constitutively active Tkv receptor, tkv^{Q253D}, were expressed ubiquitously or outside their normal domain. However, only the *dpp* clone induced target gene expression into the surrounding wild-type tissue. The cell-autonomous effect of ectopically expressed tkv^{Q253D} in inducing the target genes indicates that Dpp does not trigger a signalling relay mechanism. Rather, it functions directly on target cells. In addition, Dpp upregulates *omb* and *sal* expression at different concentration thresholds, since concentric circles of target gene expression induced by ectopic expression of *dpp* revealed that *omb* was expressed in a wider domain than *sal* (Nellen et al., 1996). This result was consistent with the expression domains of *omb* and *sal* centred in the A/P compartment boundary. These findings indicate that Dpp functions as a morphogen in *Drosophila* wing development.

1.6 Visualizing Dpp during *Drosophila* wing development

According to the model of positional information, a morphogen is expressed in a restricted group of cells within the developing tissue. From there, it is secreted and travels throughout the target field and forms a concentration gradient (Wolpert, 1969). A number of experiments in *Drosophila* demonstrated that Dpp, Hh and Wg form activity gradients by inducing the expression of several target genes at distinct distances from their source. This way, the morphogens specify developmental fates in the target field such as the *Drosophila* wing disc.

In order to determine the tissue distribution as well as the actual shape and size of the morphogen concentration gradient, several attempts were undertaken to visualize morphogen gradients. As for Hh and Wg, antibody staining as well as morphogen-GFP (green fluorescent protein) fusion proteins without affecting their signalling activity have been employed (Tabata and Kornberg, 1994; Pfeiffer et al., 2002; Strigini and Cohen, 2000; Torroja et al., 2004). In the case of Dpp, the lack of sensitive antibodies has prevented detection of endogenous Dpp morphogen outside the producing cells. To investigate the Dpp morphogen gradient, a functional GFP-tagged Dpp fusion was generated (Entchev et al., 2000; Teleman and Cohen, 2000).

As expected from a morphogen, GFP-Dpp fluorescence is also present beyond the Dpp expressing cells with the intensity decreasing and detectable up to 40 cell diameters away from the source. In addition, GFP-Dpp appears at the receiving cells primarily in intracellular punctuate structures confined to the apical part of the columnar wing imaginal disc epithelium. More basolateral, GFP-Dpp can also be found in a diffuse extracellular staining reflecting cell profiles (Entchev et al., 2000). Furthermore, GFP-Dpp moves in all directions and hence is detectable symmetrically around expressing GFP-Dpp clones (Entchev et al., 2000), confirming previous results that cells ectopically expressing Dpp activate downstream targets in all directions (Lecuit et al., 1996; Nellen et al., 1996). In a set of experiments it was also shown that morphogen gradients form rapidly. The temperature-sensitivity of the GAL4 system was exploited to turn on production

of GFP-Dpp. To do so, the tissue was shifted at a defined time from 16 °C (at which GAL4 is less efficient) to 25 °C (at which GAL4 is completely active) and the formation of the gradient was monitored after different time points (Entchev et al., 2000). It was demonstrated that Dpp moves at a rate of around five cell diameters per hour until a steady-state situation was reached at about 6 - 8 hours after onset of GFP-Dpp expression. Similar results were found using a temperature-sensitive allele of *hh* to control the timing of Dpp production (Teleman and Cohen, 2000). Hh signalling induces Dpp transcription (Basler and Struhl, 1994) and at the restrictive temperature, the Dpp gradient disappeared due to absence of expression. A rapid reformation of the gradient was monitored when shifting to the permissive temperature. Furthermore, a degradation assay revealed that GFP-Dpp is rapidly degraded and is no longer detectable after three hours chase period (Teleman and Cohen, 2000).

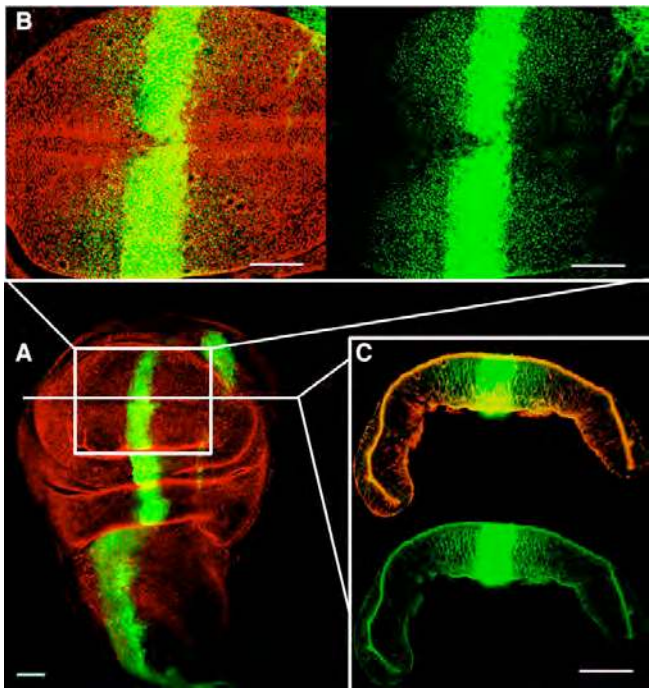

Fig. 7: Visualizing Dpp in the developing wing disc (modified from Kruse at al., 2004)
A) Double staining of a developing wing disc showing the Dpp source marked by GFP (green) and cell profiles labelled with phalloidin (red). B) GFP-Dpp localization in the wing pouch corresponding to the white box in A. Phalloidin staining (red) labels cell profiles in the left panel. C) Cryostat z-section of a GFP-Dpp expressing wing disc corresponding to the white line in A. Phalloidin staining (red) labels cell profiles in the upper panel. Scale bars: 50 µm.

1.7 Mechanisms for morphogen gradient formation in the *Drosophila* wing

Although the tissue distribution as well as the actual shape and size of the morphogen concentration gradients have been visualized, the cell biological mechanisms through which each particular morphogen group forms and maintains a gradient are still a subject of debate (reviewed in González-Gaitán, 2003; Vincent and Dubois, 2002). Several hypotheses as to the dominant mechanism of movement have been proposed that can account for morphogen spreading throughout the target tissue (reviewed in González-Gaitán, 2003; Vincent and Dubois, 2002).

It has been suggested that gradient formation might be explained by simple diffusion of the morphogen through the extracellular space (McDowell and et al., 2001). During embryogenesis, cell proliferation and subsequent cell displacement has been proposed to contribute to the spreading of morphogens (Pfeiffer et al., 2000), but additional mechanisms must exist to transport them from cell to cell. One possibility is that morphogens are actively transported along cell extensions called “cytonemes” from receiving cells to the source (Ramirez-Weber and Kornberg, 1999). Alternatively, active vesicle-mediated movement of morphogens has been proposed that is supported by the presence of morphogens in intracellular punctuate structures at the receiving cells. In this context, transport of morphogen through the target tissue consisting of repeated rounds of endocytosis and resecretion has been suggested: a process called planar transcytosis (Entchev et al., 2000).

1.7.1 Morphogen gradient formation by extracellular diffusion

The simplest process by which a morphogen gradient could be formed is diffusion of the secreted ligand throughout the extracellular space of the target tissue. To prevent saturation of the system at the steady-state situation, removal of the morphogen and subsequent degradation is also required (Fig. 8). Implantations of Activin-coated beads in *Xenopus* seem to provide evidence that gradient formation indeed might occur due to extracellular diffusion (reviewed in Gurdon et al., 1998). Activin gradient formation occurs over a distance of 200 µm in approximately three hours. During gradient formation, internalization seems not to be essential for transport since Activin distribution is not affected in the absence of endocytosis at 4 °C (McDowell et al., 2001). This implies that Activin movement might occur by passive diffusion through the extracellular space. However, the shape of the gradient seems to be affected by the TGF-β receptor levels indicating that morphogen movement involves ligand/receptor interaction.
Proteoglycans can also affect morphogen gradient formation. They are thought to modulate morphogen signalling by concentrating the ligand on the cell surface and facilitating its interaction with the receptor (see chapter 1.4). Besides this, they could sequester morphogens and hinder their diffusion, or could protect them from degradation thereby facilitating their diffusion through the extracellular space (reviewed in Nybakken and Perrimon, 2002; Selleck, 2000). The movement of the morphogen depends also on its intrinsic biochemical properties. The morphogen Hh is subject to post-translational modifications by two covalently bound lipid moieties: cholesterol at the C-terminal domain and palmitoyl acid at the N-terminal domain of the mature Hh protein (Porter et al., 1996; Chamoun et al., 2001). Therefore, Hh is likely to be tethered to the plasma membrane. Perhaps as a consequence of this, the Hh gradient range is much shorter than the 40 cell diameters spanning Dpp gradient, extending only to four cells in the developing *Drosophila* wing. It is however still controversial whether cholesterol modification limits or expands the Hh gradient range. In mesenchymal cells of the mouse limb, cholesterol modification is essential for

long-range Hh movement (Lewis et al., 2001), whereas in epithelial cells of the *Drosophila* imaginal wing disc non-cholesterol modified Hh can spread further away from its source. In principle, these interactions could prevent passive diffusion of morphogens through the extracellular space. This possibility has led to the suggestion that morphogen transport could be mediated by mechanisms involving a system of vesicular transport.

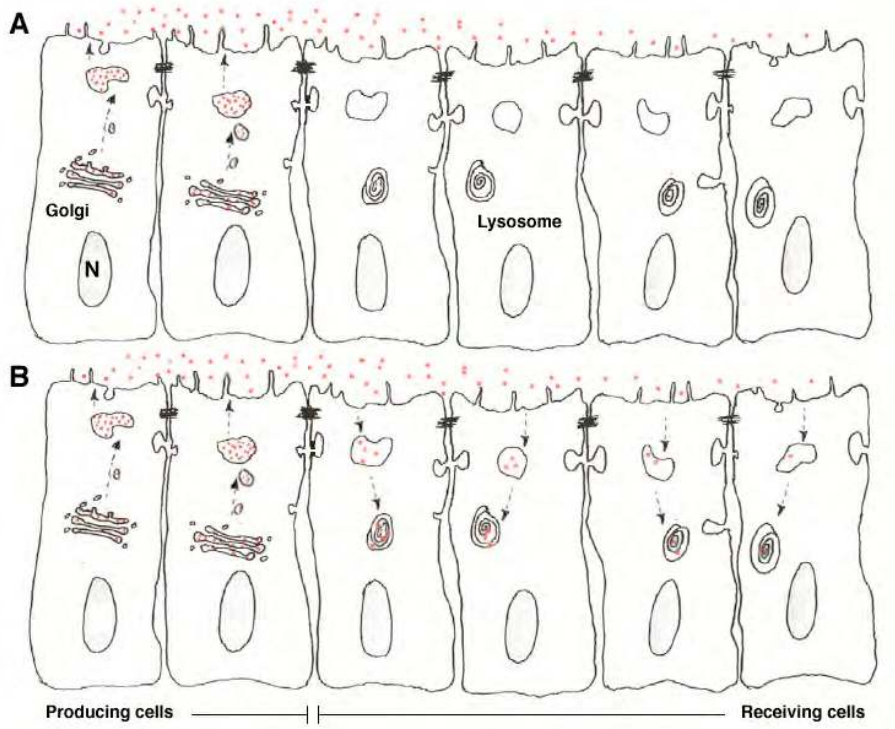

Fig. 8: Mechanisms for morphogen gradient formation (modified from Dudu at al., 2004) A) Gradient formation by simple diffusion of morphogens (red) through the extracellular space. B) Gradient formation by restricted diffusion of morphogens (red) by endocytosis and subsequent degradation. Note that extracellular diffusion can also occur along the basolateral side of the wing epithelium. N (nucleus).

1.7.2 Morphogen gradient formation by active transport through the tissue

Cytonemes

The discovery that cells at the periphery of wing imaginal discs extend actin-based long projections, called cytonemes, towards the A/P compartment boundary where Dpp is expressed, suggested that these processes might play a

role in morphogen transport (Ramirez-Weber and Kornberg, 1999). Their formation requires FGF and has been detected *in vivo* as well as in cell culture. In addition, they form rapidly (more than 15 µm per minute), and allow cells far away from the source to make direct contact with cells expressing morphogens. Although they still require functional analysis, cytonemes could transport morphogens from the source to the receiving cells (Fig. 9).

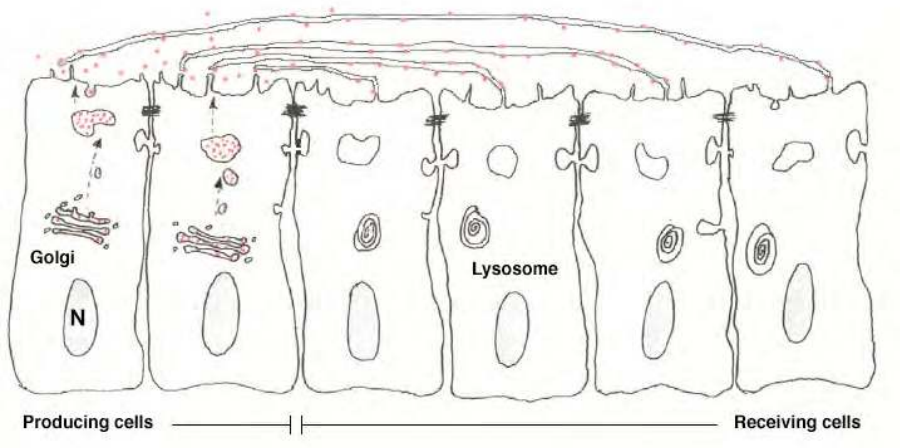

Fig. 9: Mechanism for morphogen gradient formation (modified from Dudu at al., 2004) Gradient formation by long cellular projections (cytonemes) that reach out toward the localized morphogen production source. N (nucleus).

Planar transcytosis

Another mechanism to explain morphogen transport throughout the target tissue is that the ligands spread by consecutive rounds of endocytosis and resecretion: a process called planar transcytosis (Entchev et al., 2000). The proposal that intracellular Dpp trafficking accounts for its long-range spreading emerged from experiments in which endocytosis was impaired in a distinct patch of cells: the „shibire rescue assay“ and the „shibire shadow assay“ (Entchev et al., 2000). In the “shibire rescue assay”, endocytosis was blocked in the target tissue by using a thermosensitive Dynamin mutation *shibire* (*shi* ^{ts1}) (Chen et al., 1991), whereas the source was rescued by expressing a Dynamin transgene. In this condition, Dpp is not internalized in the target cells and its range is restricted to the first 4 – 5 cell rows adjacent to the source. In the “shibire shadow assay”, a patch of shibire mutant cells, which cannot perform endocytosis, confronted long-range

Dpp spreading from the production source. In this situation, Dpp fails to move across the clone and forms a shadow of no or less Dpp distal to the clone. Since Dpp moves rapidly and in all directions, the shadow is transient and finally filled from the sides of the clone. These results suggested that internalization is required for Dpp propagation. In addition, the Dpp receptor is also necessary for Dpp internalization and long-range movement. A patch of cells mutant for *tkv* (*tkv*^{8}) did not internalize Dpp. As a consequence Dpp accumulated in the extracellular space around the mutant cells. However, accumulation of Dpp was restricted to the mutant cells facing the Dpp producing source. This indicates that Dpp is not able to move further into the patch of *tkv* mutant cells, implying a process where Dpp propagation throughout the target tissue requires Dynamin-dependent, receptor-mediated endocytosis (Fig. 10).

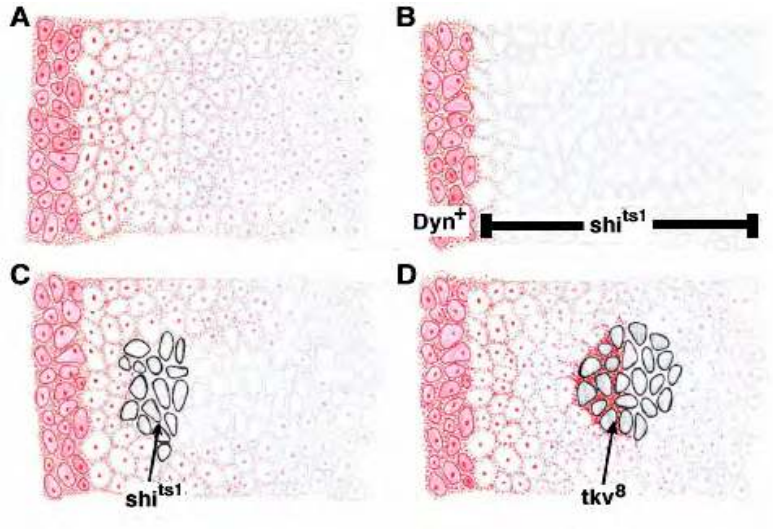

Fig. 10: Experiments addressing Dynamin-dependent, receptor-mediated endocytosis during Dpp propagation (modified from González-Gaitán, 2003)
A) Long-range Dpp gradient (red) that appears in the extracellular space as well as internalized in receiving cells. B) "Shibire rescue assay": endocytosis is blocked in the receiving tissue by using a thermosensitive Dynamin mutation *shibire* (*shi* ^{ts1}), whereas the source is rescued by expressing a Dynamin transgene (Dyn^{+}). Dpp is not internalized in the target cells and its range is restricted to cells adjacent to the source. C) "Shibire shadow assay": a patch of *shibire* mutant cells that cannot perform endocytosis confront long-range Dpp spreading from the production source. Dpp fails to move across the clone and forms a shadow distal to the clone. D) *Tkv* mutant cells: A patch of cells mutant for *tkv* do not internalize Dpp. Hence, the ligand accumulates in the extracellular space around the mutant cells facing the Dpp producing source.

Based on the proposed model, trafficking of Dpp at the receiving cells involves a number of intermediate compartments. Internalized ligands are targeted to the early endosome, where they are sorted either to degradation in the late endosome and lysosome, or recycled back to the plasma membrane through the recycling endosome. Each particular step is controlled by a small GTPase of the Rab (Ras related in the brain) family (reviewed in Zerial and McBride, 2001).

Rab proteins with their downstream effectors have been shown to coordinate the tethering/docking of vesicles to their target compartment, leading to membrane fusion. They are also involved in vesicle budding and in the interaction of vesicles with cytoskeletal elements. Like other GTPases, Rab proteins are regulated as molecular switches that shuttle between GTP- and GDP-bound conformations. The GTP-bound form is considered the “active” form. The conformation changes are restricted to the membrane compartments where they are localized. There, Rab proteins seem not to intermix on the plane of the membrane, but occupy rather restricted membrane domains (Sonnichsen et al., 2000; DeRenzis et al., 2002). Early endosomes appear mainly composed of Rab5 and Rab4 domains. Recycling endosomes are enriched in Rab11 and Rab4 domains (Sonnichsen et al., 2000). Late endosomes are specified by the presence of Rab7 (reviewed in Feng et al., 1995).

A series of experiments in mammalian cells have assigned the different Rab proteins to individual trafficking steps: Rab5 controls the step from the plasma membrane to the early endosome, Rab4/Rab11 regulates the recycling route from the early/recycling endosome to the plasma membrane, and Rab7 controls transport between early and late endosomes (reviewed in Novick and Zerial, 1997).

In *Drosophila*, these regulatory factors are highly conserved in amino acid sequence (above 75 % identity). Consistent with the role of planar transcytosis in Dpp gradient formation, their mutant phenotypes indicated an indispensable role of endosomal dynamics in the Dpp signalling range. In the “Rab mutant assay”, mutants of Rab5 or Rab7 were expressed in the receiving cells. When endocytosis was impaired by expressing dominant negative Rab5 or degradation

was enhanced by expressing dominant gain of function Rab7, the signalling range was reduced. Conversely, an enhanced endocytosis by overexpressing Rab5 led to an expansion of the signalling range (Entchev et al., 2000). This data supports the idea that Dpp dispersal is mediated by endocytosis and resecretion of the ligand in the receiving cells (Fig. 11). However, the Dpp re-secretion event itself has not yet been directly monitored.

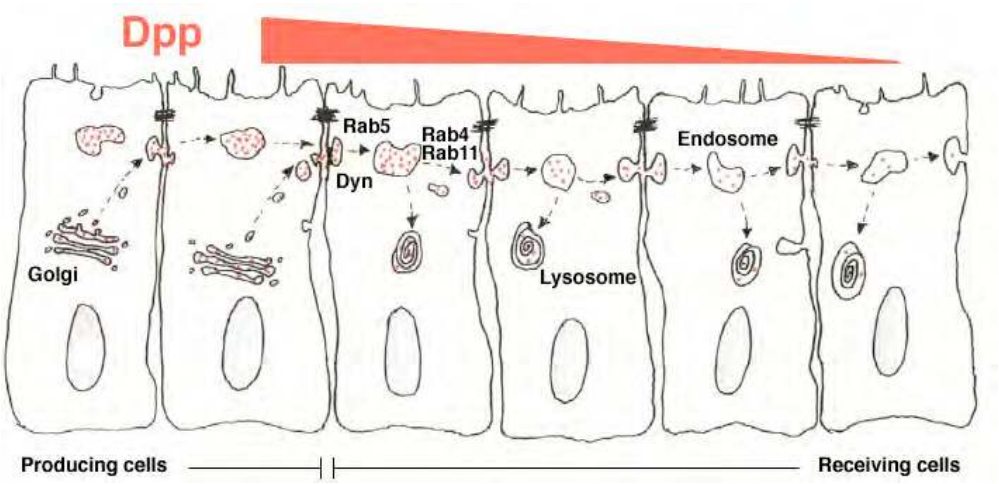

Fig. 11: Dpp spreading by planar transcytosis in the developing *Drosophila* wing (modified from Dudu et al., 2004)
Dpp (red) is expressed and released from in the producing cells into the extracellular space. It does not move far away by simple extracellular diffusion and is internalized in the receiving cells by receptor-mediated endocytosis involving Dynamin (Dyn). Here it accumulates in endosomes and is degraded or recycled back to the plasma membrane. The steps through the endocytic compartments are controlled by Rab proteins. In this way, Dpp spreads through the tissue forming a stable concentration gradient.

In contrast to the role of planar transcytosis in the Dpp gradient formation in the *Drosophila* wing disc, Wg gradient formation does not seem to require endocytic trafficking (Strigini and Cohen, 2000). Wg is present in endocytic compartments and in the extracellular space. It also moves rather rapidly (around 15 cells in 30 minutes) and in all directions. In contrast to Dpp in the “shibire shadow assay”, Wg is present in endosomal punctuate structures in wild type cells behind the *shi* ^{ts1} clone, indicating that Wg can move across the *shi* ^{ts1} mutant territory and is internalized by the adjacent wild type cells. Based on this result, it has been argued that planar transcytosis is not the mechanism of Wg trafficking in wing discs (Strigini and Cohen, 2000).

However, these experimental results were obtained in a steady-state situation. For those settings, no shadows with less or no Wg can be formed at the distal side of the *shi* ^{ts1} clone, since Wg molecules have already invaded this region from the sides substituting for previously present Wg. Taken together, to address appropriately the role of endocytosis during Wg spreading, a Wg propagation front should be facing a *shi* ^{ts1} clone as performed for Dpp in the “shibire shadow assay”.

Recently, it has been shown that, like Hh, Wg is palmitoylated (Willert et al., 2003), suggesting that it is tightly associated to the plasma membrane. Furthermore, Wg is present in the same endocytic compartments as “argosomes”, membrane exovesicles or lipid particles that can disperse over long distances in the wing epithelium (Greco et al., 2001). Based on these results, an alternative possibility has been suggested that such lipid carriers transport Wg through the receiving tissue. However, it needs to be addressed whether argosomes are trafficking by diffusion or planar transcytosis.

1.8 Mathematical models and Dpp gradient formation by restricted diffusion

Early quantitative studies based on mathematical models tried to distinguish which particular mechanism accounts for ligand dispersal (Crick, 1970). It has been argued that diffusion alone suffices for a morphogen to be propagated over several hundred micrometers during a period of several hours. The graded profile of the diffusible ligand would then provide receiving cells with their respective positional information. However, gradient formation must include binding of diffusing morphogen to its membrane receptors, which was not taken into account in early theoretical models (Crick, 1970). Consequently, ligand transport depends on complex non-linear kinetics, including kinetics of receptor binding/release and the kinetics of trafficking of ligands and receptors (Gierer, 1981; Gierer and Meinhardt, 1972; Koch and Meinhardt, 1994; Turing, 1952). Such theoretical models have argued that morphogen movement does not take

place by diffusion only (Kerszberg and Wolpert, 1998). Morphogens are instead transported by a mechanism in which receptor-bound ligand on one receiving cell is released to receptors of the neighbouring cells: a mechanism called “bucket brigade”. In addition, ligand trafficking in cells has been analyzed hypothetically and a possible role of transcytosis to enhance transport efficiency has been proposed (Chu et al., 1996; Lauffenburger and Linderman, 1993).

However, models of morphogen gradients must be designed with a high degree of reliability to ensure precise activation profiles. They should provide a reproducible distribution of morphogens in the case of e. g. changing production rates. Lately, a theoretical model discussing free diffusion has highlighted the importance of receptor-regulated degradation of free morphogen in establishing robustness and precision in Wg and Hh gradient formation (Eldar et al., 2003). It needs to be addressed whether planar transcytosis can also provide robustness in Dpp gradient formation (Bollenbach et al., submitted).

A recent mathematical analysis of Dpp spreading suggested though that diffusion alone suffices to form morphogen gradients (Lander et al., 2002). Morphogen transport was based on restricted extracellular diffusion using a model that takes into account free diffusion and receptor binding followed by endocytosis. This “diffusion, binding and trafficking” (DBT) model could generate ligand profiles that are consistent with observed gradients. Moreover, it has been argued that the model could generate results observed in the “shibire shadow assay” (Lander et al., 2002). To accomplish this, a block of endocytosis should induce a higher level of surface receptors and thereby should titrate out the pool of spreading free Dpp, hindering ligand transport (Fig. 12). Consistent with experimental results, this scenario generated a transient shadow. Results of these reaction diffusion equations in a one-dimensional geometry suggested that this description suffices to capture key features of this experiment.

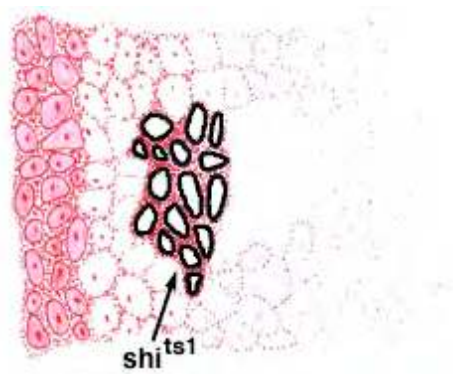

Fig. 12: The DBT model on Dpp movement in the "shibire shadow assay" (modified from González-Gaitán, 2003)
The DBT model assumes that endocytosis block would cause the accumulation of surface receptors (thick black line outlining cell profiles) at the shibire mutant cells thereby trapping Dpp (red) on its travel to form the gradient. As a consequence, the amount of extracellular Dpp at the clone would increase by a factor of 40, resulting in the formation of a shadow behind the mutant territory.

1.9 The DBT and the DBTS model of Dpp gradient formation

The DBT model assumes that transport is exclusively because of extracellular diffusion and takes into account binding to and release from the surface receptors. Neglecting the folding of the wing disc in the three-dimensional space, the transport of Dpp occurs essentially in two dimensions. Positions on this plane are specified by *x* and *y* coordinates. The transport of Dpp in the epithelium is characterized by the Dpp current $J=(J_x,J_y)$. This current is a vector with components J_x and J_y, quantifying the number of Dpp molecules that are transported per unit time across a line of unit length in *x* and *y* direction, respectively. If transport is exclusively because of diffusion, the current is generated by gradients (i. e. local differences) in ligand concentration. Formally, this can be written as:

$$\begin{pmatrix} J_x \\ J_y \end{pmatrix} = -D_o \begin{pmatrix} \frac{\partial A}{\partial x} \\ \frac{\partial A}{\partial y} \end{pmatrix}$$

where D_o is the diffusion constant characterizing diffusion in the extracellular space and *A* is the free extracellular ligand concentration.

The concentration of free ligands varies not only because of diffusion: ligands bind to and detach from cell surface receptors. In addition, receptors traffic through both the biosynthetic and endocytic pathways. They appear at the plasma membrane, are internalized into cells by endocytosis and are degraded in the lysosomes (Fig. 13).

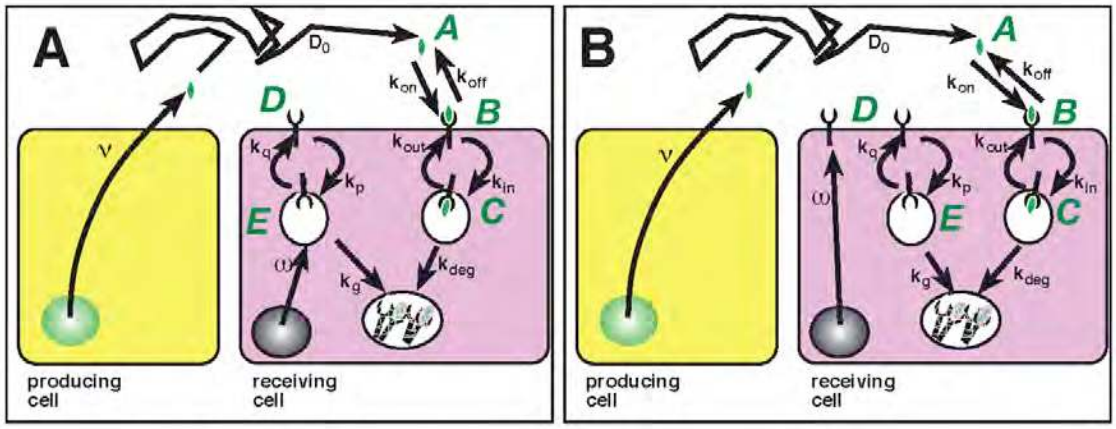

Fig. 13: Transport scheme in the DBT model on Dpp movement (from Kruse et al., 2004) A) Dpp ligand (green) is secreted with the rate ν into the extracellular space, where its transport is exclusively because of diffusion with the coefficient D_o (A). B is the concentration of ligand-bound receptors on cell surfaces, and *C* is the concentration of ligand-bound receptors inside cells. In addition, *D* and *E* are the concentrations of free receptors outside and inside cells. k_{on} and k_{off} rates define the binding and dissociation constants for the ligand-receptor binding. The rates of endocytosis and exocytosis of ligand-bound receptors are defined by k_{in} and k_{out} *rates*. The degradation rate of internalized ligands bound to receptors is denoted by k_{deg}. Receptors are produced with biosynthetic rate ω, internalized and recycled with rates k_p and k_q, and degraded with rate k_g. B) The same transport scheme is depicted with the biosynthetic route targeting the receptor directly to the plasma membrane (Alberts et al., 1994). Note that the parameter values used in the DBT model were measured for the EGF/EGF receptor system in B82 fibroblasts (Herbst et al., 1994; Lauffenburger and Linderman, 1993; Starbuck and Lauffenburger, 1992).

Since the DBT model considers the Dpp gradient formation in a particular area of interest (AOI), the boundary conditions have to be specified.

Along the boundary adjacent to the secreting cells at x=0 ('source boundary'; Fig. 14), cells expressing Dpp inject the morphogen into the AOI. A cell of width a (approximately 4 µm) secretes Dpp at a constant rate, measured in Moles/s (Fig. 13). A single cell contributes to a Dpp current into the AOI of magnitude $\nu/2a$ along the x-direction. Here, the factor 2 takes into account that Dpp leaves

the source in two directions (towards anterior and posterior) and only half of the secreted ligand reaches the posterior compartment. The total current entering the AOI is increased by a factor *d*/*a*, which is the number of contributing cells. Here, *d*≈20 mm denotes the width of the stripe of secreting cells (Fig. 14). Assuming that the Dpp source is homogeneous along the *y*-direction and that degradation of ligand in secreting cells is neglected, the source boundary condition at *x*=0 is thus given by:

$$J_x = \nu d / 2a^2 .$$

At $x=L_x$ - on the opposite side of the AOI with respect to the source ('distal boundary'; Fig. 14) - a current of ligand across this boundary is present which becomes small if the ligand concentration nearby is small. Choosing 200 µm for the width of L_x in the AOI, the current across the boundary sufficiently far from the source is small enough to be neglected and imposed to be zero.

At the remaining boundary lines $y=-L_y/2$ and $y=+L_y/2$ of the AOI ('side boundaries'; Fig. 14), also 'zero current' conditions across the boundary lines are imposed for L_x=200 µm. In the simplest situation, in which the whole system is homogeneous in the *y*-direction and for small *shi* ^{ts1} clones (up to 50 µm in both directions), this condition is satisfied.

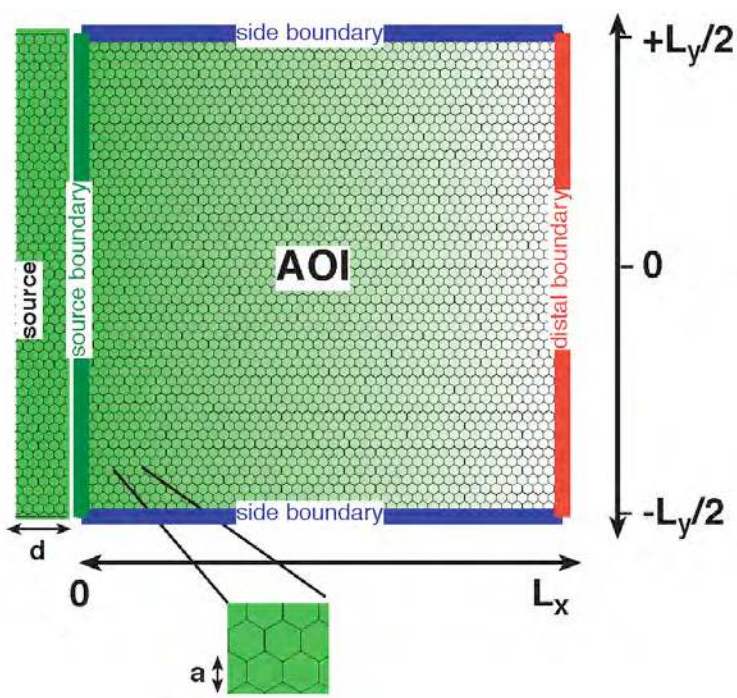

Fig. 14 (previous page): Area of interest (AOI) in the DBT model (from Kruse et al., 2004) Simplified geometry of the wing imaginal disc expressing GFP-Dpp used in the DBT model for the calculation of the boundary conditions. *Lx* and *Ly* correspond to 200 µm.

Interestingly, careful reanalysis of the DBT model used in Lander et al. (Lander et al., 2002) revealed that the DBT model cannot account for the observed transient shadows experimentally observed in the "shibire shadow assay" (Kruse et al., 2004). It rather generates permanent shadows behind the *shi* ^{ts1} clone, which are inconsistent with the experimental results (Entchev et al., 2000) (Fig. 15 and 16).

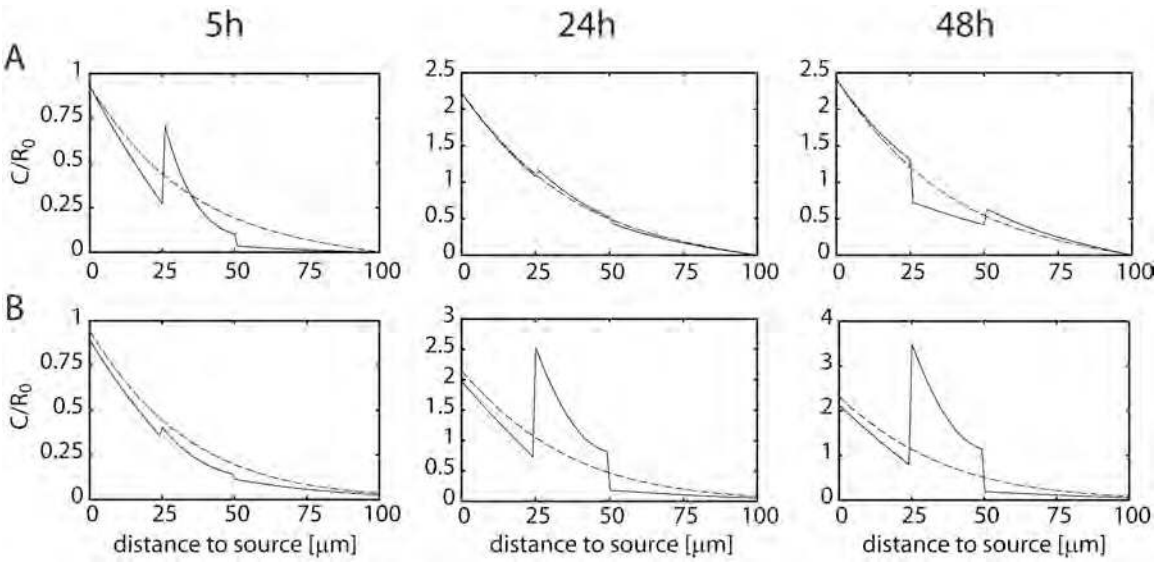

Fig. 15: Concentrations of internal-bound ligand (C) in the presence of a shibire clone calculated in the DBT from Lander et al. and the corrected DBT (modified from Kruse et al., 2004)

A) One-dimensional calculations of Lander et al. (Lander et al., 2002) for the DBT model. Profiles of internal-bound ligand after 5 hours, 24 hours, and 48 hours are shown. The endocytic block in the *shi* ^{ts1} clone is described by a tenfold reduction of receptor internalization rates (k_p, k_{in}). In addition, at time *t*=0, the surface receptor concentration is suddenly increased by a factor of 10 inside the clone as described in Lander et al. (Lander et al., 2002). Furthermore, the receptor production rate ω had also to be reduced by a factor of 10. After 5 hours the ligand concentration is reduced behind the clone as compared with the results of the same calculation in the absence of a clone (broken line). This corresponds to a shadow in the experiments. At 24 hours, the shadow is weak. This is not a steady state situation because after 48 hours, an accumulation of ligand behind the clone and depletion in the clone occur. B) Two-dimensional calculation of the DBT model, but with correct receptor production rate (not reduced by a factor of 10) and combined with a gradual increase of surface receptor concentration in the clone region. A shadow builds up which increases in time and persists. Note that the one-dimensional and two-dimensional calculations of the DBT model generate similar profiles. A,B) The clone extends from *x*=25 µm to *x*=50 µm, The broken line corresponds to a calculation without a clone, and the unbroken line to the calculation in the presence of a clone.

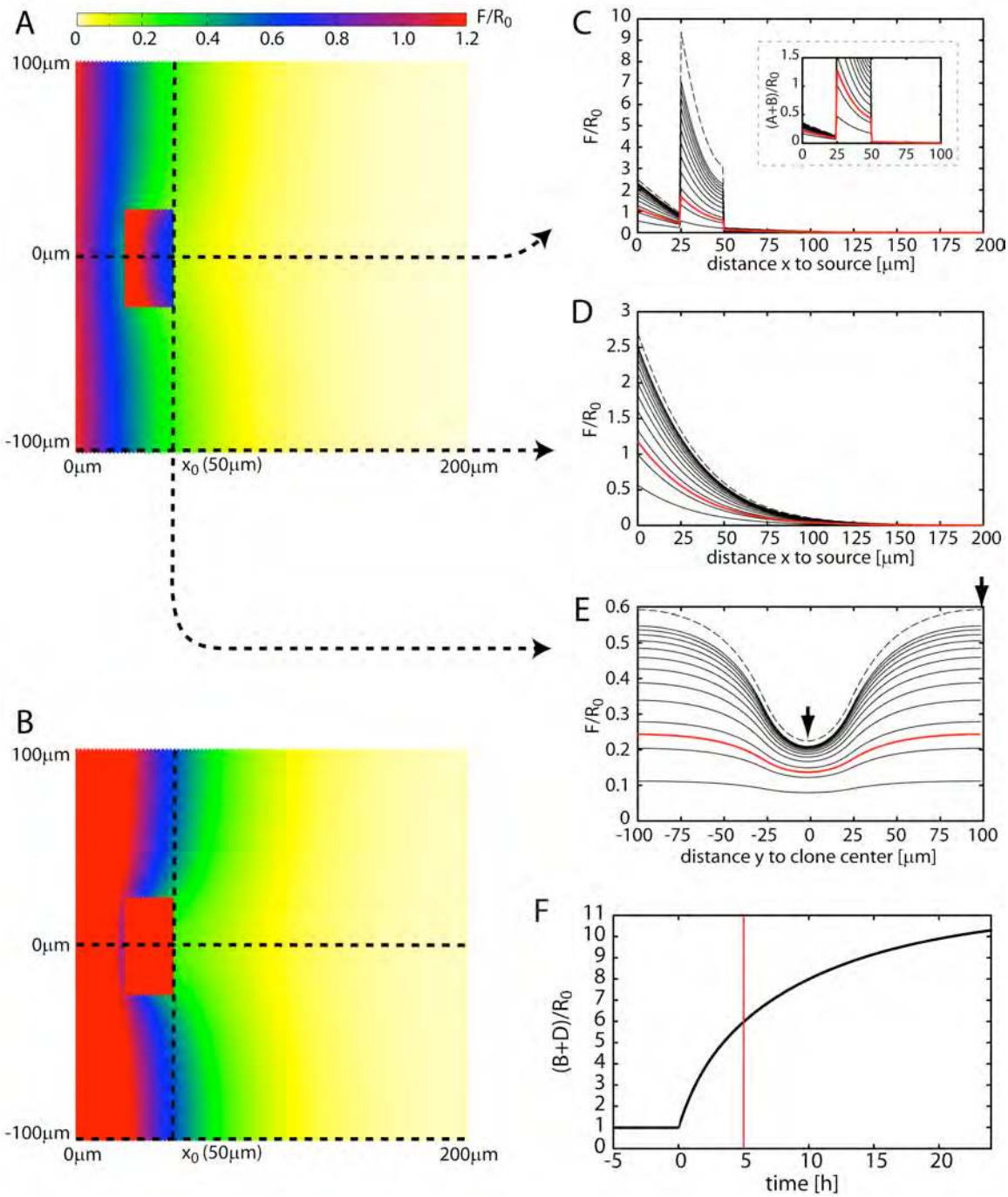

Fig. 16: Gradients in the DBT model describing a tissue with a *shi* ^{ts1} clone (modified from Kruse et al., 2004)

Dynamics of the total ligand distribution *F* in the DBT model in an area of interest (AOI) of size L_x=200 mm and L_y=200 mm. The AOI contains a rectangular region, inside which the internalization rates k_p and k_{in} are reduced by a factor of 10 after *t*=0. This region covers the intervals 25 µm<*x*<50 µm and -25 µm<*y*<25 µm and describes the effects of a temperature shift on a *shi* ^{ts1} clone. A) Colour-coded distribution of the total ligand concentration *F*=*A*+*B*+*C* at *t*=5 hours. B) Distribution of *F* after 48 hours, which is close to the steady state. C-E) Total ligand concentration *F* along the broken lines indicated in A,B. Unbroken black lines are separated by 2 hours. The red line represents the distributions

after 5 hours, the time when the observations were made in the experiments discussed in Entchev et al. (Entchev et al., 2000); the broken lines represent the steady state distributions. Note the accumulation of ligand in the clone by a factor of 10. Far away from the clone, the ligand distribution resembles the distribution in absence of a clone. The steady-state ligand concentration has a pronounced minimum behind the centre of the clone (E). The inset in C displays the profile of total extracellular ligand *A+B*. Note that the extracellular ligand accumulates in the clone by a factor of 10 after 5 hours of endocytic block and more than 40 times in the steady state. F) Total surface receptor concentration, B+D, in the centre of a *shi* ^{ts1} clone. Note the gradual increase of the surface-exposed receptor concentration by a factor of 10.

However, a modified version of this model, the DBT model with saturating cell surface receptor concentrations (DBTS), can generate transient shadows behind a *shi* ^{ts1} clone (Kruse et al., 2004) (Fig. 17). This model allows to describe the extreme case where the endocytic block is complete. Under this condition the DBT model becomes biologically meaningless, since the level of surface receptors tends to infinity. The DBTS defines a maximal receptor density on the cell surface R_{max}, at which the surface receptor levels saturate. This allows free variation of the internalization rates and even a set to zero. The DBTS model assumes that the rates of delivery to the plasma membrane of the free receptor k_q, and that of the bound receptor k_{out} are a function of the total surface receptor levels B and D as follows:

$$k_q = k_q^0\left(1 - \frac{B+D}{R_{\max}}\right)$$

$$k_{out} = k_{out}^0\left(1 - \frac{B+D}{R_{\max}}\right)$$

Here, the parameters k_q^0 and k_{out}^0 are equal to the originally introduced externalization rates. For small surface receptor concentrations (*B+D)*, the DBTS model corresponds to the original DBT model. As *B+D* approaches R_{max}, the externalization rates k_q and k_{out} tend to zero. This corresponds to a situation in which the externalization rates of the receptor depend on a limiting factor(s) that can thereby be saturated, such as the trafficking machinery, cargo receptors, etc. The profiles of total (Fig. 17B-F) and internal bound (Fig. 17A and inset in Fig. 17D) Dpp have been obtained by a calculation of the DBTS model in two dimensions and in the presence of a clone. Inside the clone, the internalization

rates k_p and k_{in} have been set to zero at t=0. The profile in the y-direction behind the clone displays a pronounced transient shadow similar to the experimental observation (Fig. 17B,D-F), followed by a weak persistent accumulation of ligand behind the clone ('anti-shadow') after long time periods (Fig. 17C-F).

In the DBTS model, the emergence of shadows in the "shibire shadow assay" is a consequence of a rapid 20 fold increase of surface receptor concentration inside the *shi* ^{ts1} clone (Fig. 17G). This leads then to the accumulation of extracellular Dpp at the clone by a factor of at least 20.

Fig. 17 (next page): Gradients in the DBTS model describing a tissue with a *shi* ^{ts1} clone (modified from Kruse et al., 2004)

A) Ligand distributions as described in Fig. 15, but obtained for the DBTS model for saturating surface receptors and zero internalization rates. A shadow is present at 5 hours and has disappeared at 24 hours. There is no internal-bound ligand inside the clone. The clone extends from *x*=25 µm to *x*=50 µm. The broken line corresponds to a calculation without a clone, and the unbroken line to the calculation in the presence of a clone. B,C) Colour-coded distribution like in Fig. 16 of the total ligand concentration *F=A+B+C* after 5 hours of endocytic block (B), and after 48 hours, corresponding to the steady state (C). D-F) Total ligand concentration *F* along the broken lines indicated in B,C. Unbroken black lines are separated by 2 hours. The broken lines represent the steady state distributions, the red line the distributions after 5 hours, the time when the observations were made in the experiments discussed in Entchev et al. (Entchev et al., 2000). The inset in D shows the concentration of internal-bound ligand, which vanishes inside the clone. The profile of the ligand concentration behind the clone is shown in F. At 5 hours, a clear shadow is present which vanishes and turns into a persistent anti-shadow. G) Total surface receptor concentration, *B+D,* in the center of the clone. Note the rapid increase of the surface-exposed receptor concentration by a factor of approximately 20 after 5 hours of endocytic block.

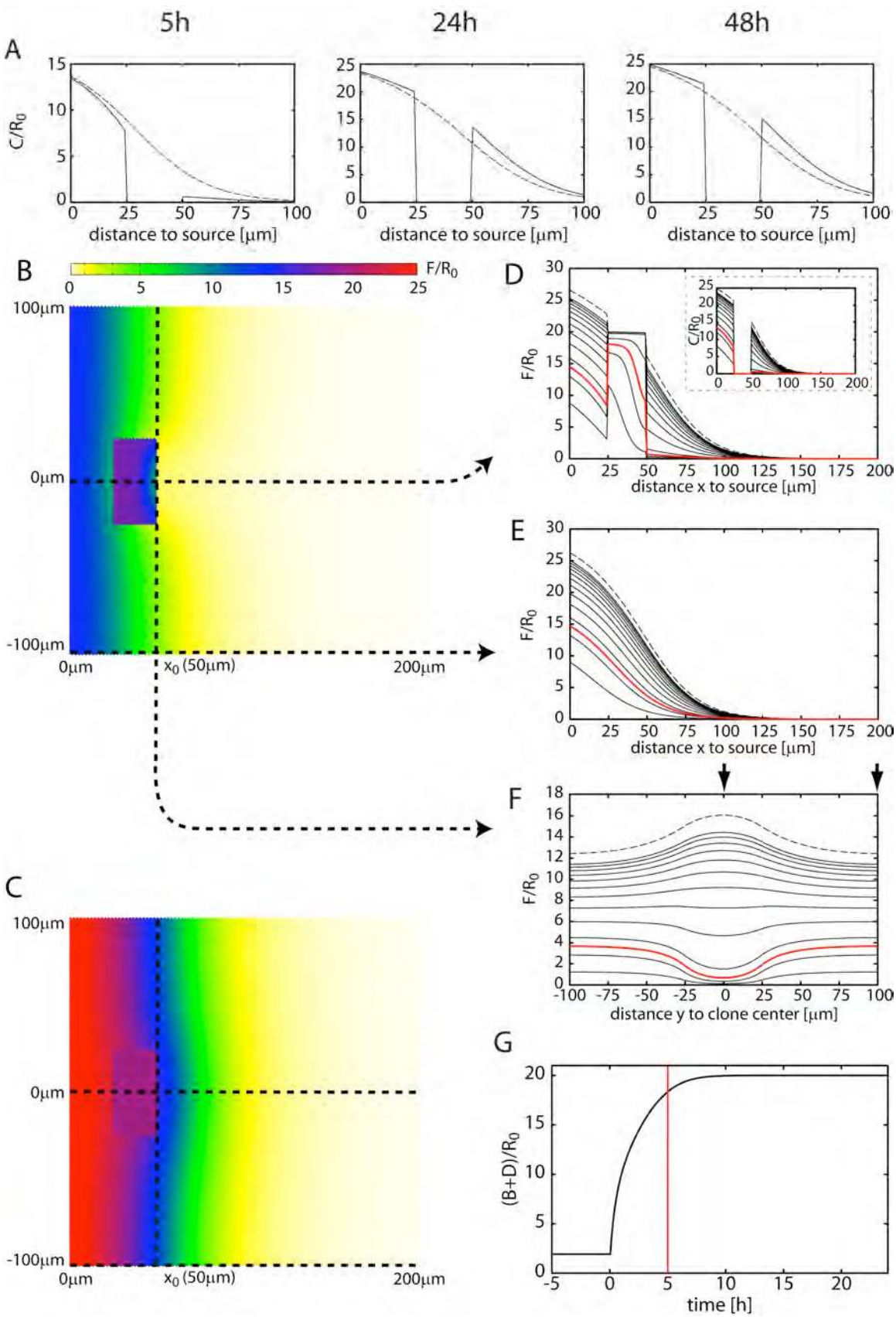
5h
24h
48h
A
C/R0
distance to source [µm]
B
F/R0
100µm
0µm
-100µm
0µm
x0 (50µm)
200µm
C
D
E
F
distance x to source [µm]
distance y to clone center [µm]
G
(B+D)/R0
time [h]

1.10 Aim of the thesis

During my thesis I seeked answers to four key questions:

I) Is the DBTS model sufficient to explain Dpp gradient formation?

- Does a block of endocytosis induce higher levels of surface receptors?
- Does a block of endocytosis sequester Dpp movement, while diffusing in the extracellular space?

II) What is the role of Dynamin-mediated endocytosis in Dpp gradient formation?

- Does block of endocytosis hinder Dpp movement *in vivo*?

III) Is Dpp trafficking along the endocytic pathway at the receiving cells?

- Is Dpp localized in early, late, and recycling endosomes marked by Rab proteins?

IV) Is Dpp recycled at the receiving cells?

2 Materials and Methods

2.1 Buffers and Solutions

1) *Drosophila* fly food:

150 g agar-agar
360 g yeast powder
200 g soy meal
440 g syrup
1.600 g malt

are dissolved in 16 l water and boiled. Then 30 g Nipagin in 100 ml EtOH together with 126 ml propionic acid added.

2) PBS:

137 mM NaCl
2,68 mM KCl
10,14 mM Na_2HPO_4
1,76 mM KH_2PO_4

3) S2 transfection mix:

3 µg DNA in 100 µl serum-free medium (Invitrogen) are combined with 18 µl Cellfectin (Invitrogen) in 100 µl serum-free medium and incubated for 20 minutes at room temperature.

4) Lysis Buffer:

50 mM Tris
150 mM NaCl
2 mM EDTA pH 7,4

to 50 ml one inhibitor-mix tablet (Roche) is added and solution is stored at 4 ºC

5) Sample buffer (5x):

0,35 ml 4 x stacking gel buffer[9)]

0,15 ml H_2O

0,16 g SDS

after incubation at 95 ºC to dissolve SDS

0,4 ml glycerol

0,1 ml mercaptoethanol

and a tiny bit of bromophenol blue are added.

Aliquots are stored at -20°C.

6) Electrode buffer:

25 mM Tris

192 mM glycine

0,1 % SDS, pH 8,4

7) Low Molecular Weight Calibration Kit for SDS Electrophoresis:

250 kDa (Myosin)

148 kDa (Phosphorylase β)

98 kDa (BSA)

64 kDa (Glutamic Dehydrogenase)

50 kDa (Alcohol Dehydrogenase)

36 kDa (Carbonic Anhydrase)

22 kDa (Myoglobin Red)

16 kDa (Lysozyme)

6 kDa (Aprotinin)

8) Running gel buffer (4x):

1,5 M Tris/HCl pH 8,8

stored up to three months at 4 ºC

9) Stacking gel buffer (4x):

0,5 M Tris/HCl pH 6,8

10) Coomassie-Brilliant-Blue solution:

0,85 g Coomassie Brilliant Blue G250 or

1 g Coomassie Brilliant Blue R (Roth GmbH)

450 ml CH_3OH

450 ml H_2O

100 ml CH_3COOH

detection limit: around 1 µg protein

11) Destaining solution:

200 ml CH_3OH

70 ml CH_3COOH

730 ml H_2O

12) Blotting buffer:

25 mM Tris

192 mM glycine

20 % CH_3OH

0,1 % SDS pH 8,1-8,5

13) Blocking solution:

5 g milk powder are added to 100 ml TBS buffer[14)]

14) TBS buffer:

154 mM NaCl

10 mM Tris pH 7,4

15) TBST buffer:

TBS buffer[14)] with 0,05 % Tween 20

16) BBS (10x):

100 mM Tris

550 mM NaCl

400 mM Kcl

70 mM $MgCl_2 \cdot 6H_2O$

50 mM $CaCl_2 \cdot 2H_2O$

200 mM glucose

500 mM sucrose

diluted in water to a final volume of 1 l pH 6,95

50 ml aliquotes stored at -20°C

17) BBT:

45 ml BBS (10x)[16)]

450 mg BSA

4,5 ml Tween 20 (10 %)

diluted in water to a final volume of 450 ml

aliquots stored at –20 ºC

18) PEM:

80 mM Na-Pipes

5 mM EGTA

1 mM $MgCl_2$ x 6 H_2O

pH adjusted to 7,4 with HCl

19) PEMT:

PEM[18)] and 0,05-0,2 % Triton X100

20) Blocking solution in PEMT:

PEMT[19)] and 0,5 % BSA

21) Staining solution in PEMT:

Blocking solution in PEMT[20)] and 1 % NGS

22) Mowiol:

60 g Mowiol 4-88 (Hoechst)

150 g Glycerol

150 ml H_2O

300 ml 0,2 M Tris pH 8,5

23) Dextran solution:

10 µl fluorescent Dextran 10.000 MW (Molecular Probes) (10 mg/ml)

490 µl Shields and Sang M3 insect medium (Sigma)

24) Loading buffer:

40 ml H_2O

6 g Ficoll

100 mg bromophenol blue

100 mg Xylene Cyanol FF

stored at room temperature

25) TAE (10x):

242,28 g Tris

57,1 ml glacial acetic acid

100 ml 0,5 M EDTA

diluted in water to a final volume of 1 l pH 8,0

26) TAE (1x):

100 ml TAE (10x)[25)] diluted with water to a final volume of 1 l stock solution

Not indicated chemicals were purchased from Fluka, Merck, Pharmacia, Promega, Riedel de Haën, Roth and Sigma.

2.2 Used equipment

- Waterbath: Julabo Labortechnik GmbH
- Icemachine: Ziegra
- Electrophorese chamber: Mighty Small SE 245 (BioRad)
- X-ray developing machine: Optimax (Protec)
- Heating block: Teche Dri-Block (Schütt Labortechnik)
- Table centrifuge: Biofuge fresco (Heraeus)
- Microscope: Stemi SV 11 (Zeiss)
- Schaker (37°C): ISF-1-W (Kühner)
- Thermomixer: Thermomixer compact/comfort (Eppendorf)
- UV-Transilluminator: Macro Vue UV20 (Hoefer)
- Western-Blot-apparatus: Trans-Blot SD (BioRad)
- Objective Heater System: Bioptechs
- PCR machine: GeneAmpPCR System 9700 (Perking Elmer)
- Gel documentation: GeneCAM Flexi (biostep)
- Vacuum centrifuge: Heto RC 10.22 Speedvac (Jouan)
- Fly incubator: Flyincubator I-36VL/D (Percinel Scientific)

2.3 Fly pushing

2.3.1 Maintenance of flies

Flies were kept in vials (~14 ml) containing *Drosophila* fly food[1)] at room temperature (25 ºC) except for the mutant strain *shi* ^{ts1} which was maintained at 18 ºC.

2.3.2 Mutant strains

shi ^{ts1}, *tkv*^{8}, *dpp*^{d8}, and *dpp*^{d12} are described in Flybase (http://flybase.bio.indiana.edu). *shi* ^{ts1} is a Dynamin thermo-sensitive mutation in the GTP binding domain (Chen et al., 1991) that rapidly blocks endocytosis when shifted at 34 ºC (but not at 32 ºC) in developing wing cells. *tkv*^{8} is a Thick veins receptor truncated at amino acid 144 before the transmembrane domain which presumably represents a null mutation of *tkv* (Nellen at al., 1994). *dpp*^{d8} and *dpp*^{d12} represent each breakpoint alleles of the *decapentaplegic* gene (St Johnston et al., 1990). The wing blade is almost entirely missing in *dpp*^{d8}/ *dpp*^{d12} animals, though some wing hinge structures are still present (Teleman and Cohen, 2000).

2.3.3 Transgenic strains

UAS-Dynamin^{+} flies carry a cDNA (GH23121 in the fly genome project) coding for the splicing variant DynaminΔ2S (Staples and Ramaswami, 1999). *UAS-Tkv* and *UAS-GFP-Dpp* were previously described in Nellen et al., 1996, and Entchev et al., 2000. Barry Dickson (Institute of Molecular Pathology, Vienna, Austria) provided the *UAS-GFP* flies. The *tub-DsRed* flies carry the construct inserted into a P element plasmid containing the promoter of the tubulinα1 gene and flanked at its 3' end by the 3' UTR of the tubulinα1 gene (Basler and Struhl, 1994). *UAS-GFP-DRab5* and *UAS-GFP-DRab7* were described in Entchev et al., 2000. For the generation of *UAS-GFP-DRab11*, the coding sequence (LD14551 in the fly genome project) was inserted C-terminal to EGFP and the fusion subcloned into the polylinker of the vector pUAST. *UAS-PAGFP* flies carry the coding sequence of PAGFP (Patterson and Lippincott-Schwartz, 2002) subcloned into the polylinker of the vector pUAST. The p*UAST-PAGFP-Dpp* vector was generated by cloning the coding sequence of PAGFP into the position of EGFP within the *pUAST-EGFP-Dpp* vector (Entchev et al., 2000).

2.3.4 GAL4-mediated ectopic gene expression

For the ectopic expression of various transgenic constructs in a wide variety of cell- and tissue-specific patterns of *Drosophila* we used the GAL4-mediated expression system (Brand and Perrimon, 1993). GAL4 is a transcription factor from yeast that can activate transcription in *Drosophila* (Fischer et al., 1988). To express GAL4, the *GAL4* gene is integrated in sites that are under the temporal and spatial control of various genomic enhancers. When a target gene of interest containing GAL4-binding sites (UAS or Upstream Activator Sequence) within its promoter is present in those cells where GAL4 is expressed, its transcription is initiated upon binding of GAL4 to the UAS (Fig. 18). The targeted ectopic gene expression is commonly present in the progeny of a genetic cross of a transgenic line expressing GAL4 and a line carrying the target gene of interest downstream from the UAS.

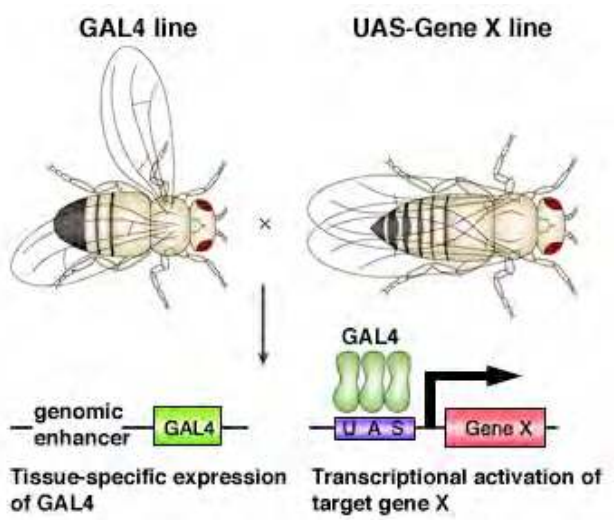

Fig. 18: Targeted expression using GAL4 (modified from St Johnston, 2002)

To drive expression of various transgenic constructs in the Dpp producing cells, *dpp-GAL4* was used. *Hedgehog-GAL4* (*hh-GAL4*) was employed when expression in the Dpp receiving cells of the posterior compartment was needed. For the analysis of anti-Rab antibodies, *vestigial-GAL4* (*vg-GAL4*) was used to drive the expression of the different GFP-Rab fusion proteins at the dorso/ventral

(D/V) boundary. For the analysis of Tkv antibodies, patched-*GAL4* (*ptc-GAL4*) was used to drive the expression of Tkv receptor anterior to the anterior/posterior (A/P) compartment boundary.

2.3.5 Mosaic analysis

FLP-FRT mitotic recombination

In the FLP-FRT mitotic recombination, homozygotic cells are generated in heterozygotic flies by inducing recombination between homologous chromosomes. Using the heat-shock-induced expression of FLPase leads to the recombination between FLPase recombination targets (FRTs) that have been inserted into the chromosome arm carrying the mutation to analyze. With the appropriate developmental time point and level of heat-shock, mitotic recombination produces a patch of cells or clone of genetically altered tissue (Fig. 19).

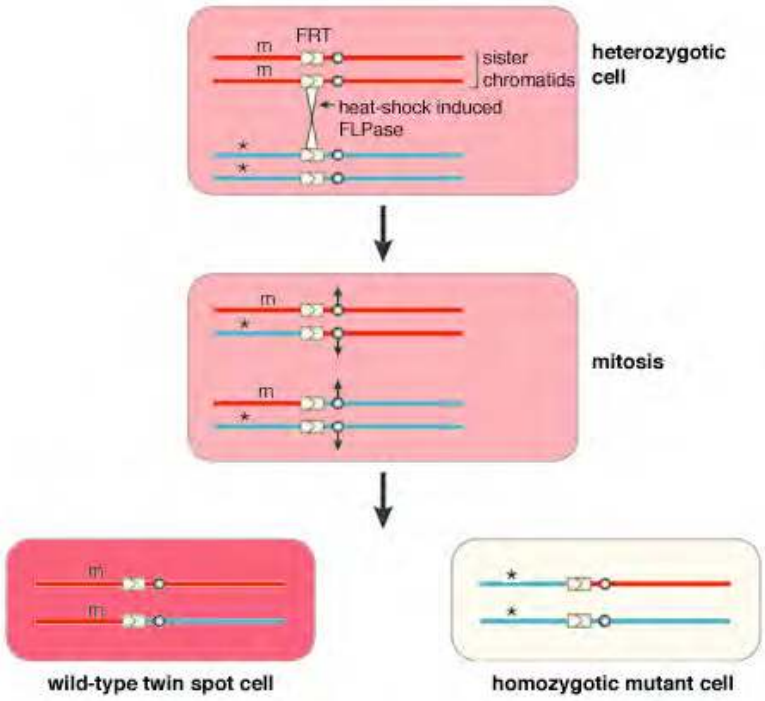

Fig. 19: FLP-FRT mitotic recombination (modified from St Johnston, 2002) (m: marker, ⋆: mutation)

The location of such a clone can be identified by the use of genetic (e. g. *tub-DsRed*) or histological markers (e. g. *ΠMyc* epitope marker construct followed using anti-Myc antibody). For the analysis of the Tkv antibody, *tkv*^{8} mutant Minute^{+}/FRT clones (Xu and Harrison, 1994) were generated by heat shock (30 minutes, 36 ºC) in three days old larvae (*HS-Flp/+; M(2)z ΠMyc FRT40A/tkv*^{8} *FRT40A*) and raised at 25 ºC to mid-third instar larvae. To induce ΠMyc transcription larvae were heat shocked at 38 ºC for one hour followed by at least one hour at 25 ºC to allow the translation of the *Π*Myc transcript prior to fixation. For the analysis of the cell surface Tkv receptor level in *shi* ^{ts1} FRT mutant clones, larvae of the genotype *shi* ^{ts1} *FRT18A/HS-NM8A FRT18A; HS-Flp/+* and *shi* ^{ts1} *FRT18A/tub-DsRed FRT18A; HS-Flp/+ were used.* Embryos were collected during one day at 18 ºC, larvae were raised for one day at 18 ºC and heat shocked (90 minutes, 38,3 ºC). Larvae were subsequently kept at 25 ºC until third instar larval stage. Afterwards, endocytosis was blocked either for three hours at 34 ºC followed by one hour at 38,3 ºC and one hour at 34 ºC to induce NMyc transcription and its translation or for five hours at 34 ºC in the case of larvae of the genotype *shi* ^{ts1} *FRT18A/tub-DsRed FRT18A; HS-Flp/+*. Dissection of wing discs was performed at 34 ºC.

2.3.6 Blockage of Endocytosis at Receiving Cells

shi ^{ts1}*; UAS-Dynamin*$^{+}$*/+; dpp-GAL4/UAS-GFP-Dpp* larvae were kept at the *shi* ^{ts1} permissive temperature (25 ºC or 18 ºC) to allow normal wing development until third instar larval stage. For the comparison of Tkv receptor levels in the endocytosis-defective receiving territory with that of the rescued secreting cells, endocytosis was blocked for 6 hours at 34 ºC and wing discs were dissected at 34 ºC and fixed. For the *in vivo* analysis of GFP-Dpp dynamics in the *shi* ^{ts1} mutant receiving tissue the dissected wing discs were kept at 34 ºC during the record of time-lapse movies.

2.3.7 PAGFP-Dpp rescue

For the demonstration of functionality of the generated transgenic constructs, the PAGFP-Dpp fusion was expressed in a *dpp* mutant background and tested for rescue. As for *PAGFP-Dpp, dpp^{d12}/CyO,Act-GFP; dpp-GAL4/TM6B* males were crossed to *UAS-PAGFP-Dpp/+; dpp^{d8}/CyO,Act-GFP females* and the rescued progeny of the genotype *UAS-PAGFP-Dpp; dpp^{d8}/dpp^{d12}; dpp-GAL4/+* were dissected and further analyzed.

2.4 Cell biology

2.4.1 S2 cell maintenance

The S2 cell line was derived from a primary culture of late stage (20-24 hours old) *Drosophila melanogaster* embryos (Schneider, 1972). This cell line was maintained at 25 ºC without CO_2 in both serum-containing and serum-free Schneider's medium (Invitrogen). Cells were passaged once per week.

2.4.2 S2 cell transfection

For the expression of cytosolic PAGFP and PAGFP-Dpp in *Drosophila* Schneider S2 cells, they were transiently transfected with 3 µg of DNA per well in 6-well plates using Cellfectin (Invitrogen). Prior to transfection cells were washed with PBS[2)] and put on wells with 800 µl serum-free medium and the transfection mix[3)]. After four hours of incubation, cells were washed with PBS[2)] and wells were filled with 2 ml serum-containing Schneider's medium each. 48 hours after transfection cells were submitted to further analysis.

2.5 Biochemistry

2.5.1 Preparation of cell extracts from Drosophila third instar larvae

For the analysis of the Tkv antibody, cell extracts from *Drosophila* third instar larvae were prepared for SDS-PAGE and subject to Western Blot analysis. All subsequent operations were performed at 4 ºC. 100 larvae were combined with 1 ml of Lysis buffer[4)] and disrupted with several passages though a 1 ml douncer (Wheaton). Once the embryos were homogenized, the homogenate was transferred to a tube and centrifuged for five minutes at 1.000 g in a Biofuge fresco centrifuge (Heraeus). The debris and the nuclei are then pelleted down. The supernatant, but not the white lipid coating from the walls of the tube, was transferred into a new tube and centrifuged for one hour at 100.000 g in a TLA55 rotor (Beckman). The pellet (p100) represents the membrane fraction and the supernatant (s100) the cytosolic fraction. Both fractions were solved in the same amount of Lysis buffer[4)] and the proteins precipitated (Wessel and Flügge, 1984). 0,1 ml of the respective fraction was merged to 0,4 ml of methanol, mixed and centrifuged in a Biofuge fresco centrifuge (Heraeus) at 9.000 g for 10 seconds. The step was repeated after adding 0,1 ml of chloroform. Finally 0,3 ml of water was mixed vigorously to the solution and centrifuged at 9.000 g for five minutes. The clear aqueous phase on top was removed carefully and 0,3 ml of methanol was added to the lower phase and interphase comprising the enriched proteins. Centrifuging for five minutes at 9.000 g subsequently pelleted them down. The supernatant was decanted, the protein pellet resuspended in Lysis buffer[4)] and ready for use or storage at -20 ºC.

2.5.2 Determining protein concentration by the Bradford dye-binding method

The protein concentration of the various *Drosophila* third instar larvae extracts (see section 2.5.1) were determined by the Bradford dye-binding method

(Bradford, 1976). The method is based on the binding of the dye *Coomassie-Brilliant-Blue G-250* to proteins in acid solution that results in a shift of the absorption maximum from 465 nm to 595 nm. 100 µl of the sample was diluted in PBS[2)] and combined with 100 µl of diluted dye solution (Roth GmbH) (1:2,5 in water). After five minutes of incubation at room temperature the absorption was measured at 595 nm and compared to a pure dye solution. The concentration of the sample was determined on the basis of a BSA (Bovine Serum Albumin)-calibration curve (c_{BSA}= 5–35 mg/ml in PBS[2)]).

2.5.3 SDS-PAGE (SDS-Polyacrylamide gel electrophoresis)

For the separation of purified proteins we used the SDS-PAGE (Laemmli, 1970). Sodium dodecyl sulphate (SDS) is an anionic detergent which denatures proteins by "wrapping around" the polypeptide backbone conferring a negative charge to the polypeptide in proportion to its length, i. e. equal charge or charge densities per unit length. In denaturing SDS-PAGE separations therefore, migration is determined not by intrinsic electrical charge of the polypeptide, but by molecular weight. A discontinuous system was employed that was composed of a resolving or separating (lower) gel and a stacking (upper) gel. The gels are cast with different porosities, pH and ionic strength to sharpen greatly the bands of the proteins to be separated. The gel was made of a 5 % stacking gel and usually a 12,5 % separating gel. Prior to loading on the SDS-PAGE gel, sample-buffer (5x)[5)] was added and the mixture was denaturated for five minutes at 95 ºC. The electrophoresis was performed at room temperature in electrode buffer[6)] at 70 mA for one hour. As molecular weight calibration 5 µl low molecular weight (LMW)-marker[7)] run parallel to the samples.
The gels were prepared as follows:

Components	Separating gel 12,5 % [µl]	Stacking gel 5 % [µl]
water	3.160	2.600
running gel buffer (4x)[8)]	1.875	
stacking gel buffer (4x)[9)]		880
Acrylamide solution (40 %)	2.345	500
10 % SDS	75	20
10 % APS	37,5	20
TEMED	7,5	10

Table 1: SDS-PAGE preparation

2.5.4 Coomassie-Brilliant-Blue colouring of proteins

Protein bands on SDS-PAGE gels were visualized by colouring them with Coomassie-Brilliant-Blue solution[10)]. After SDS-PAGE, the gels were submerged for 10 minutes in Coomassie-Brilliant-Blue solution[10)], then rinsed several times in destaining solution[11)] to remove excess dye that was not bound on proteins. After this procedure, proteins were visible as blue bands.

2.5.5 Western Blot

Western Blot is a method to transfer by electrophoresis proteins from a polyacrylamide matrix to a membrane. Antibodies combined with enhanced chemiluminescence enzyme substrates can then detect those immobilized proteins. As Western Blot system we used a semi-dry apparatus (BioRad). It consists of two flat electrode plates that enclose a Blot sandwich of several filter papers, the gel and a polyvinylidine difluoride (PVDF) membrane. Prior to blotting the hydrophobic PVDF membrane was activated with 100 % methanol for a few seconds followed by a wash in water. In parallel, the filter papers were soaked with blotting buffer[12)]. The wet filter papers, the gel and the activated membrane

were stacked up in a specific order facing the anode electrode plate (see Fig. 20).

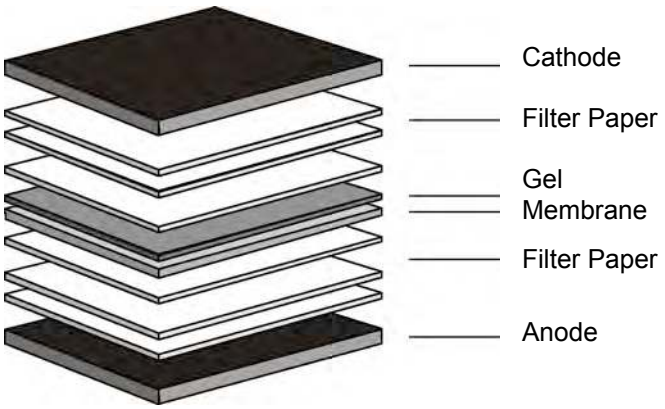

Fig. 20: Semi-Dry-Blott assembly

The transfer was performed at constant current of 1 mA/cm^2 for two hours. During electrophoresis, the negative charged proteins migrate towards the anode. After blotting, the membrane was dipped in Ponceau-S solution (Sigma) and washed once in water to verify the efficiency of transfer by detecting the red marked protein bands. In addition, the gel was stained with Coomassie-Brilliant-Blue solution[10)] to detect remaining proteins not transferred during this process. The PVDF membrane was then submerged with blocking solution[13)] overnight at 4 °C.

2.5.6 Immunodetection of a Western Blot

The detection of membrane-bound proteins was carried out with an enhanced-chemiluminescence (ECL) detection kit (Amersham Life Science) using Rabbit anti-Tkv (intracellular), 1:1.000; Rabbit anti-GST, 1:5.000. Membranes were incubated in Blocking solution[13)] overnight at 4 °C. Afterwards the membranes were incubated with the primary antibody in Blocking solution[13)] for one hour. Subsequent membrane washes with TBST buffer[15)] were followed by incubation with the horseradish peroxidase (HRP)-coupled secondary antibody in Blocking solution[13)] for one hour. After repeated washes with TBST buffer[15)], the detection took place with the ECL detection kit (Amersham Life Science). The technique is

designed around the peroxidase-coupled secondary antibody and the substrate luminol. In the presence of hydrogen peroxide, HRP catalyzes the oxidation of diacylhydrazides like luminol. An activated intermediate reaction product is formed, which decays to the ground state by emitting light. This emission was visualized by placing an X-ray film (Biomax ML, Kodak) onto the membrane. For repeated detections with different primary antibodies the membrane was submerged briefly in 100 % methanol, washed in TBST-buffer[15)] and blocked again with Blocking solution[13)].

2.6 Histology and Imaging

2.6.1 Antibodies

Rabbit anti-Tkv antibody was generated against two peptides corresponding to parts of the intracellular kinase domain (H_2N-SQQLDPKQFEEFKRAC-$CONH_2$ and H_2N- GFRPPIPSRWQEDDVC-$CONH_2$). Rabbit luminal anti–Tkv antibody was generated against two peptides corresponding to the luminal side of the Tkv peptide sequence outside the ligand binding cleft (H_2N-YEEERTYGCMPPEDNG-$CONH_2$ and H_2N-KEDFCNRDLYPTYTP-$CONH_2$). Rabbit anti–*Drosophila* Rab5/7/11 antibodies were generated against peptides corresponding to the C-terminal parts of the respective proteins (H_2N-TSIRPTGTETNRPTNN-$CONH_2$ for Rab5; H_2N-CKVDLDNRQVSTRRAQ-$CONH_2$ and H_2N-CTLGSQNNRPGNPDN-$CONH_2$ for Rab7; H_2N-CQKQIRDPPEGDVIRPS-$CONH_2$ for Rab11).
The immune sera were affinity chromatography purified using the corresponding peptides coupled to CNBr-activated Sepharose 4B (Amersham Biosciences). The specificity of the antibodies was tested by preincubating the purified antibody with 100 µg/ml of the respective peptide (or 500 µg/ml when performing the extracellular immunostaining protocol (see section 2.6.2)) for 30 minutes at room temperature and performing subsequently an antibody staining on Tkv overexpressing or Rab5/7/11GFP expressing discs. No fluorescent signal was

detected under these conditions, while preincubation with a control peptide did not affect the staining.

2.6.2 Immunostaining

Immunostainings were performed using Mouse anti-Myc (CalBiochem), 1:25 dilution; Rabbit anti-Tkv (intracellular and luminal), 1:1.250; Goat anti-GFP, 1:100; Rabbit anti-Rab5, 1:50; Rabbit anti-Rab7/11, 1:250; Mouse anti-Golgi, 1:100 (CalBiochem); Mouse anti-Fasciclin III (7G10, Hybridoma Bank), 1:1.000; Rabbit anti-pMad (Tanimoto et al., 2000), 1:2.000. Alexa 488-, Alexa 546-(Molecular Probes) and Cy5-(Dianova) coupled secondary antibodies were used at a dilution of 1:500. The anti-Tkv, the anti-Rab7/11 as well as the secondary antibodies were preadsorbed against fixed *Drosophila* embryos prior to immunostaining. Preadsorbtion was performed by incubating the antibody diluted 1:10 in BBT[17)] with 400 µl of fixed embryos overnight at 4 ºC.

Intracellular immunostaining

Drosophila third instar larvae were collected in glass dishes coated with Repel-Silane ES (Amersham Pharmacia Biotech) to avoid adhesion of the sample. Dissection of wing imaginal discs was performed in PEM[18)] by inverting the larvae cuticle with the attached imaginal discs being exposed to the solutions. They were subsequently fixed in 4 % paraformaldehyde (PFA) in PEM[18)] and permeabilized in 4 % PFA in PEMT[19)] for 40 minutes each. The dissected wing discs were washed twice with PEMT[19)] for 10 minutes, interrupted by a wash with 50 mM NH_4Cl in PEM[18)] for 10 minutes to remove as well as to quench free aldehydes. The tissue was then incubated in blocking solution in PEMT[20)] overnight at 4 ºC. After blocking, the samples were incubated with primary antibodies diluted in staining solution in PEMT[21)] for two hours at room temperature. Unbound primary antibody was removed by three washes with PEMT[19)]. Subsequent incubation with the appropriate secondary antibody diluted

in staining solution in PEMT[21)] for two hours was followed by washes with PEMT[19)] and PEM[18)], respectively. Finally, the wing imaginal discs were removed from the cuticle and mounted in Mowiol[22)].

Extracellular immunostaining

Extracellular GFP-Dpp and cell surface exposed Tkv were detected by incubating the dissected wing imaginal discs prior to fixation (Strigini and Cohen, 2000) with Goat anti-GFP antibody, 1:10 dilution, and Rabbit anti-Tkv (raised against the luminal domain of Tkv), 1:10 dilution, respectively. The *Drosophila* third instar larvae were dissected in insect medium M3 (Sigma) and incubated with the primary antibody diluted in Cl8 medium on ice for two hours. The samples were then washed three times with Cl8 medium to remove unbound antibody, fixed in 4 % PFA in PEM[18)] and permeabilized in 4 % PFA in PEMT[19)] for 40 minutes each. Subsequent procedure was according to the intracellular immunostaining (without blocking and primary antibody incubation). Fewer GFP-Dpp signal was found upon extracellular immunostaining due to the different staining procedure. In both immunostaining procedures fluorescent phalloidin (Molecular Probes) counterstaining was sometimes performed after the secondary antibody step to monitor cell profiles.

2.6.3 Dextran uptake

Fluid phase endocytosis assays with fluorescent Dextran 10.000 MW (Molecular Probes) were performed to distinguish early as well as late endocytic compartments in wing imaginal discs. Dissection of wing discs was performed less than five minutes in Cl8 medium. The samples were then transferred to a glass dish with 100 µl Dextran solution[23)] and incubated for 10 minutes at room temperature (25 ºC) to mark early endocytic compartments. The Dextran pulse was then stopped with three washes of chilled Cl8 medium in the same dish on ice and concluded with fixation in 4 % PFA in PEM[18)]. In a pulse-chase assay, a

chase of 40 to 60 minutes in 100 µl Cl8 medium followed the medium washes to mark late endocytic compartments prior to fixation in 4 % PFA in PEM[18]. Finally, the wing imaginal discs were removed from the cuticle and mounted in Mowiol[22].

2.6.4 Cryosectioning

Cryostat z-sections at Cryo-Star HM 560 (Microm) were performed with PFA-fixed developing wing discs incubated in 30 % sucrose solution in PBS[2] after immunostaining (see section 2.6.2) for at least twelve hours at 4 ºC and mounted with Tissue-Tek (Sakura).

2.6.5 Preparing samples for *in vivo* imaging

Wing imaginal discs were dissected in Cl8 medium. Meanwhile a chamber was prepared by cutting out a frame from a double-side adhesive tape on a glass slide. The chamber was filled with Cl8 medium and the lypophilic dye FM 4-64 (Molecular Probes) at a dilution of 1:1.000 was added. Upon intercalation into the membranes the lypophilic emits a strong fluorescent signal above 560 nm when excited with 488 nm light, thereby marking cell boundaries *in vivo.* The isolated wing imaginal discs were then transferred into the chamber and pushed gentle on the glass slide to stay attached during movie record. Finally, a coverslip was put on the chamber and sealed with nail polish.

2.6.6 Fluoresence Recovery After Photobleaching (FRAP)

Fluorescence Recovery After Photobleaching (FRAP) experiments were performed on LSM510 laser scanning confocal microscope (Carl Zeiss, Jena, Germany) with a 40x/1.3 numerical aperture (NA) Plan-Apochromat oil objective. GFP was excited with the 488 nm line of Argon laser and GFP emission was

monitored between 505-530 nm. During record, the samples were maintained at 25 ºC or at 34 ºC with an Objective Heater System (Bioptechs). In the GFP-Dpp receiving tissue a stripe of ~10 µm in width was bleached for approximately 30 seconds using the 488 nm laser line at 100 % laser power. Discs were monitored with low levels of 488 nm light (~3 % laser power) to avoid bleaching of GFP signal. Time-lapses were composed of two minutes intervals for approximately one hour. Longer time frames were not possible due to tissue collapse. For quantitation, the average fluorescent intensity of a region of interest in the bleached area was monitored using Zeiss software. Background fluorescence was measured in a random field outside the GFP-Dpp receiving tissue. The background-substracted fluorescence intensity normalized to the pre-bleach value was calculated. For the recovery kinetics, a fitting curve was calculated using the nonlinear least-squares Marquardt-Levenberg algorithm as implemented in gnuplot 3.7 for each experimental FRAP curve of normalized fluorescence intensity over time in seconds (Axelrod et al., 1976). The one-dimensional diffusion equation was solved assuming a homogeneous initial distribution inside and outside of the bleached area with a step like transition at its boundary. The resulting fitting curve for the averaged fluorescence in the region of interest was as follows:

$$f(t) \propto 1 - \left[2\sqrt{\frac{Dt}{\pi\omega^2}} \left(e^{\frac{-\omega^2}{4Dt}} - 1 \right) + \mathrm{erf}\left(\frac{\omega}{2\sqrt{Dt}} \right) \right] + c \qquad k = 0$$

where erf denotes the error function, $\mathrm{erf}(x) = \frac{2}{\sqrt{\pi}} \int_0^x e^{-y^2} dy$, D is the diffusion coefficient, k is the degradation rate (which is set to zero), ω is the width of the photobleached stripe, and c is an additional fit parameter necessary to account for the fact that there is some remaining fluorescence after bleaching. The resulting values for D correspond to apparent or effective diffusion coefficients (D'), assuming that the FRAP recovery of GFP-Dpp is due to a “random walk” of the ligand. Note that the estimate is independent of the transport machinery

underlying the random walk. In other words, it does not distinguish between extracellular diffusion, intracellular movement, receptor binding, etc.

2.6.7 Photoactivation

Photoactivation of PAGFP-Dpp and cytosolic PAGFP expressed in *Drosophila* wing imaginal discs was performed either on a Zeiss LSM510 laser scanning confocal microscope (Carl Zeiss, Jena, Germany) or on a two-photon Radiance2100 MP laser scanning microscope system (Carl Zeiss CellScience Ltd., Jena, Germany). Photoactivation on the confocal microscope was performed with high levels (~0.6 mW) of 405 nm laser light through a 40x Plan Neofluar 1.3 NA objective. Photoactivation on the two-photon microscope was performed with a femtosecond pulsed 825 nm laser. In this case, a 60x Plan Apochromat 1.2 NA objective was used. For the recovery kinetics of PAGFP-Dpp in the not activated circled region, a fitting curve was calculated for the experimental curve of normalized fluorescence intensity over time in seconds. Since the shape of the region differs comparing to the FRAP experiments with GFP-Dpp (i. e. a stripe versus a circle, respectively), the one-dimensional diffusion equation was solved assuming Gaussian initial distribution in the not activated area. The fitting curve for averaged fluorescence in the region of interest was as follow:

$$f(t) \propto 1 - e^{-kt}\left(1 - e^{\frac{-R^2}{R^2+4Dt}}\right)_{k=0}$$

where D is the diffusion coefficient, k is the degradation rate (which is set to zero), and R is the radius of the not photoactivated region. The resulting values for D again correspond to apparent or effective diffusion coefficients (D').

2.7 Molecular Biology

2.7.1 Polymerase chain reaction (PCR)

The polymerase chain reaction (PCR) provided an effective method to amplify DNA sequences used for cloning the transgenic constructs used in this work. The PCR leads to an exponential amplification of DNA, since the newly synthesized strands are also used as templates. With the use of a thermostable DNA polymerase this chain reaction can be run off without break. The automatization of this procedure is realized in a thermocycler. The components included in each reaction were:

Components	Amount
10 x reaction buffer (Stratagene)	5,0 µl
dNTPs [10 mM]	2,0 µl
upper primer [20 µM]	5,0 µl
lower primer [20 µM]	5,0 µl
Water	22,5 µl
Taq DNA polymerase (Stratagene)	0,5 µl
Template DNA [1 ng/µl]	10,0 µl

Table 2: PCR reaction mix

The programme used for the PCR was following:

PCR programme	Stages	Duration and Temperature
Denaturation	Preheating	5 min at 94 ºC
Cycles of amplification	Denaturation Primer annealing Primer extension	1 min at 94 ºC 1 min at around 60 ºC 1 min/kb at 72 ºC
Terminal extension	Primer annealing	10 min at 72 ºC
Closing	Cool off	4 ºC

Table 3: PCR programme

After amplification, the DNA was examined by agarose gel electrophoresis.

2.7.2 Gel-Electrophoresis of DNA

The amplified cDNA was – diluted in loading buffer[24)] – separated by electrophoresis in 0,7 % (w/v) agarose gel (PeqGold) in TAE (1x)[26)] at a constant voltage of 100 V. The separated DNA bands were visualized by adding ethidium bromide (3.8-Diamino-5-ethyle-6-phenylphenanthridiumbromide) to the gel (final concentration of approximately 0,5 µg/ml). The dye intercalates into the stacked base pairs of DNA exhibiting fluorescence at 590 nm when excited with UV light.

2.7.3 TOPO® cloning and transformation of chemical competent cells

For cloning of various transgenic constructs we used the TOPO®cloning technology (Invitrogen) to insert PCR products into the pCR®II-TOPO®cloning vector. This vector includes various restriction sites flanking the PCR product insertion site for easy removal of insert, kanamycin and ampicillin resistance genes for selection in *E.coli*. The vector is provided linearized and covalently bound to topoisomerase I at the 3' phosphate at each end. The resulting topoisomerase I-activated vector readily accepts PCR products with compatible overhangs lacking 5' phosphates. To do so, topoisomerase I recognizes and covalently binds the 3' thymine on the pentameric sequence 5'-(C/T)CCTT-3' at the 3' phosphate. It cleaves one strand of the DNA, allowing the DNA to unwind. The enzyme then relegates the DNA ends and is released. 1 µl of PCR product and 3 µl water were combined with 1 µl TOPO®cloning vector. After five minutes, the mixture was placed on ice and prepared for transformation.

2.7.4 Transformation

For transformation, TOP10 One Shot™ chemically competent *E.coli* cells (Invitrogen) were used. 5 µl of the ligation was directly added to 50 µl of competent cells previously thawed and incubated for 30 minutes on ice. The vials were then incubated for 30 seconds in a 42 ºC temperated waterbath and again placed on ice. After two minutes 250 µl of warmed LB medium was added and the mixture incubated at 37 ºC for one hour. The transformed cells were subsequently plated on LB plates containing 50 µg/µl ampicillin and kanamycin, respectively. Transformation was tested by clone selection followed by plasmid isolation (Quiagen Plasmid Mini/Maxi Kit) and DNA sequencing.

2.7.5 Subcloning into the pUAST/Caspertubulin vector

Various inserts present in the TOPO®cloning vector were then subcloned into the pUAST (Phelps and Brand, 1998) and CaSpeR vector (Pirrotta, 1988), respectively. To cut out the sequence of interest and the final vector, usually 1 µg of DNA was mixed with the corresponding restriction endonucleases (approximately 5 units) combined with the appropriate buffers in 15 µl reaction mixtures. Restriction took place at 37 ºC for one hour. The excised insert and the cut final vector were then separated by gel electrophoresis (see Section 2.7.2) and the corresponding DNA bands were cut out and transferred to 0,5 ml tubes filled at the bottom with a few (autoclaved) aquarium filter fibers covering a small hole. The tubes were then placed in 1,5 ml tubes and the DNA eluted by centrifuging those double tubes in the Biofuge fresco centrifuge (Heraeus) at maximum speed for 2 minutes. The obtained insert and the appropriate cut pUAST or CaSpeR vector were directly ligated respecting the 3 fold molar excess of insert combined with the T4 DNA ligase and the buffer (NEB Quick Ligation Kit) in a 10 µl reaction mixture at room temperature for 5 minutes. For

transformation, TOP10 One Shot™ chemically competent *E.coli* cells were used (see section 2.7.4).

2.7.6 Preparing DNA for injection

For the injection of the various transgenic constructs into *Drosophila white* embryos, impurity-free DNA was mixed with a helper plasmid encoding for a transposase to allow genomic integration of DNA of interest. 20 µg cloned DNA was diluted in 300 µl water, combined with 300 µl rotiphenol (Roth GmbH), mixed and centrifuged in the Biofuge fresco centrifuge (Heraeus) at 10.000 rpm for 2 minutes. The resulting upper phase was mixed with 300 µl phenol-chlorophorm (Roth) and subject to the same centrifugation step. Purification was again performed with 300 µl chlorophorm (Roth) instead. The upper phase comprising the purified DNA was precipitated by adding 750 µl 100 % ethanol and 30 µl 3M sodium acetate and pelleted by centrifuging in the Biofuge fresco centrifuge (Heraeus) at maximum speed for 15 minutes. After decanting the supernatant, the pellet was washed in 500 µl 70 % ethanol to remove left salts and centrifuged at maximum speed for 15 minutes. The resulting pellet was dried in a vacuum centrifuge (Jouan) for 5 minutes and resuspended in 30 µl water. Finally 6 µg of purified construct and 2 µg of helper were combined in a volume filled with water up to 200 µl. DNA was again precipitated by adding 500 µl 100 % ethanol and 20 µl 3M sodium acetate and pelleted by centrifuging in the Biofuge fresco centrifuge (Heraeus) at maximum speed for 15 minutes. Subsequent washes with 300 µl 70 % ethanol followed drying in the vacuum centrifuge. Finally, the pellet was resuspended in 20 µl water, centrifuged briefly and used for injection.

3 Results

3.1 Testing experimentally the DBTS model of Dpp gradient formation

3.1.1 Establishing antibodies and staining procedures detecting levels of total and cell surface receptor Tkv and extracellular Dpp

The theoretical analysis of Kruse et al. (Kruse et al., 2004) suggested that diffusion suffices to explain Dpp spreading throughout the target tissue. In the DBTS model, the Dpp transport is based on extracellular diffusion taking into account receptor binding and subsequent internalization. It is suggested that this "diffusion, receptor binding and trafficking with surface receptor saturation" (DBTS) model can generate ligand profiles consistent with observed gradients. Moreover, the mathematical model results in transient shadows of no or less Dpp as observed experimentally in the "shibire shadow assay" (Kruse et al., 2004). To accomplish this, it was assumed that a block of endocytosis induces a higher level of surface receptors and thereby titrates out Dpp while diffusing in the extracellular space, hindering ligand transport (Lecuit and Cohen, 1998).

First the cell surface receptor concentration was considered. The crucial precondition for forming a shadow in the DBTS model is a rapid accumulation of surface receptors in the *shi* ^{ts1} clone by a factor of 20 (Kruse et al., 2004). In order to compare this with the actual surface receptor levels in the clone, an antibody that specifically recognizes the Dpp receptor, Tkv, was generated. Confirming previous results (Teleman and Cohen, 2000), the receptor accumulates predominantly at the cell surface, although some intracellular vesicular structures can also be observed (Fig. 21A). The level of the Tkv protein parallels the accumulation of the Tkv transcript, which is distributed in a graded fashion complementary to the Dpp gradient (Lecuit and Cohen, 1998) (Fig. 21A). We performed three assays to address the specificity of the Tkv antibody: (1) The antibody detects overexpression levels of Tkv (above 5 fold as monitored by

RT-PCR (not shown)), induced by the GAL4 system using a *ptc-GAL4* driver (Fig. 21B), (2) the antibody is titrated out by incubating with the peptide used to raise the antibody prior to immunostaining (Fig. 21C) (see Materials and Methods), and (3) does not stain cells lacking Tkv in mutant *tkv*^{8} mosaics (Fig. 21D).

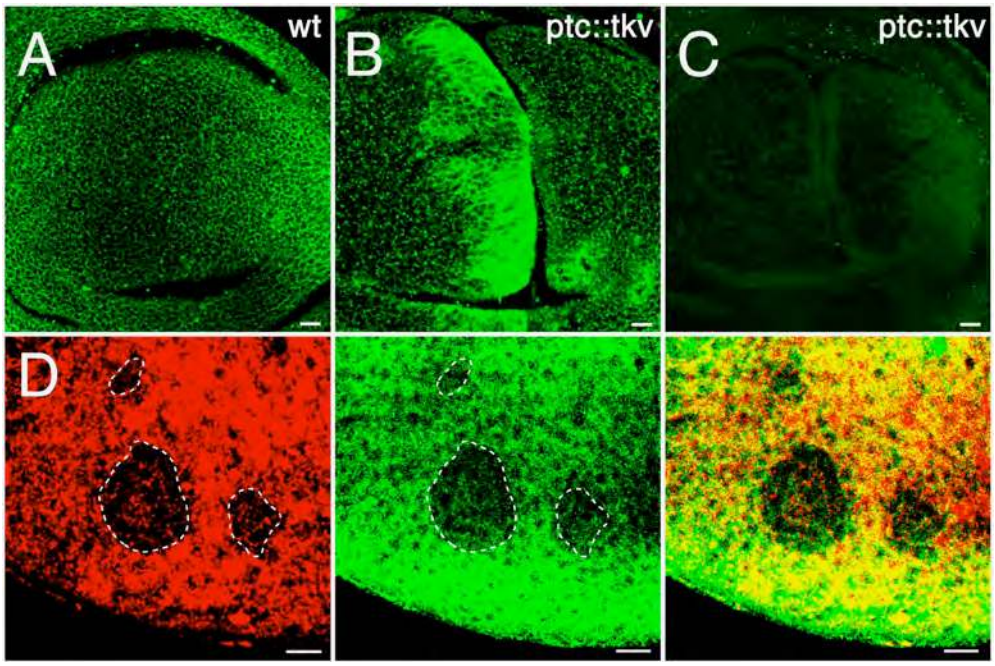

Fig. 21: Detecting total Thick veins in *Drosophila* wing disc
A) Wild-type third instar wing disc stained with anti-Tkv antibody. Thick veins predominantly outlines the cells and forms a gradient inversed with respect to the Dpp gradient. The Tkv counter-gradient has a shallow slope and might not be very apparent in some cases, depending on the imaging conditions. B,C) Tkv immunostainings of third instar wing discs expressing UAS-Tkv under the *ptc-GAL4* driver using anti-Tkv (B) or anti-Tkv blocked by its corresponding peptide antigen (C). Note that the anti-Tkv antibody detects overexpression levels of Tkv induced by the GAL4 system whereas it is abolished when performing a protocol where prior to immunostaining the antibody was incubated with its corresponding target polypeptide. Other polypeptides did not have any effect (see Materials and Methods). Fold in the wing pouch is caused by Tkv overexpression. D) Double labelling showing *tkv*^{8} clones marked by the absence of ΠMyc (red) and Tkv immunostaining (green). Genotype: *HS-Flp/+; M(2)z ΠMyc FRT40A/tkv*^{8} *FRT40A*. The anti-Tkv antibody does not stain cells lacking Tkv in mutant mosaics present in the notum of a third instar wing disc. Bars correspond to 10 µm.

In addition, it detects a corresponding band of 63 kDa in Western Blot experiments from developing larvae (Fig. 22). In agreement with the disc immunostaining, the band is nearly absent when performing a protocol where

prior to detection the antibody was incubated with its corresponding target polypeptide (Fig. 22).

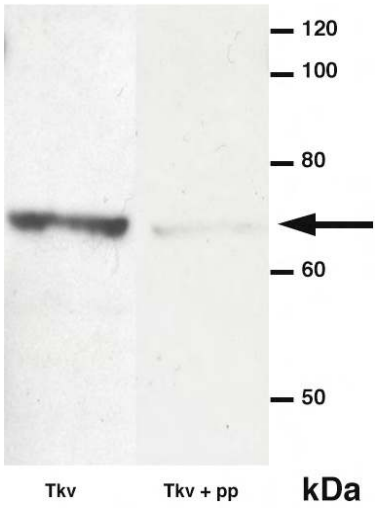

Fig. 22: Detecting total Thick veins in Western Blot
Western Blot of wild-type third instar larvae extract stained with anti-Tkv antibody. The antibody detects a band of approximately 63 kDa (left lane). The Thick veins corresponding band is nearly absent when the antibody was incubated with its target polypeptide prior to detection (right lane).

To visualize only the Tkv pool associated to the cell surface, an antibody directed against the luminal domain of Tkv (see Materials and Methods) was raised and the “extracellular immunostaining” protocol was performed on wing imaginal discs (Strigini and Cohen, 2000). During this staining procedure the tissue is incubated with the antibody at 4 °C prior to fixation. In the absence of endocytosis, the applied antibody has only access to the cell surface-exposed Tkv. In contrast to total Tkv, the level of the cell surface receptor is only decreased in a thin stripe of cells located anterior to the A/P boundary (Fig. 23A). As with the other Tkv antibody, the antibody staining in this condition can robustly detect overexpression of the receptor, induced by the GAL4 system using a *hh-GAL4* driver (Fig. 23B), and is titrated out by incubating it, prior to immunostaining, with the peptide used to raise the antibody (see Materials and Methods) (Fig. 23C).

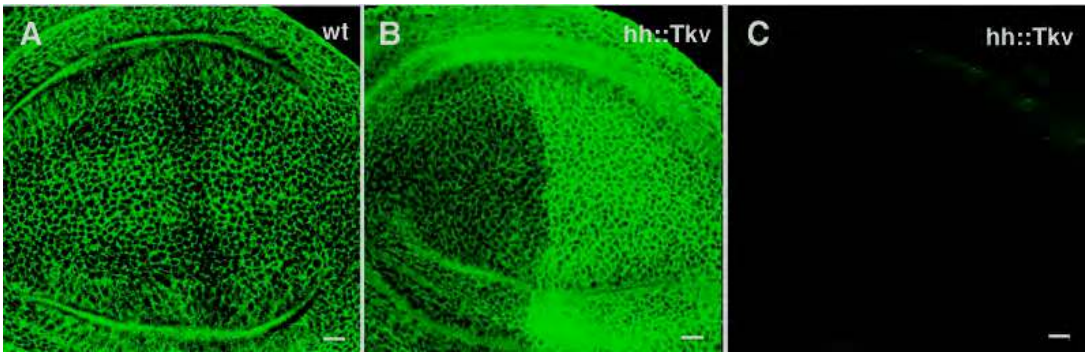

Fig. 23: Detecting cell surface Thick veins
A) Wild-type third instar wing disc showing immunostaining of cell surface exposed Tkv using the Tkv luminal antibody and the extracellular immunostaining protocol. The level of surface Thick veins is decreased within a narrow stripe of cells located anterior to the anterior-posterior compartment boundary. B,C) Immunostaining of cell surface exposed Tkv of third instar wing discs expressing UAS-Tkv under the *hh-GAL4* driver; using luminal anti-Tkv (B) or luminal anti-Tkv antibody blocked by its corresponding peptide antigen (C). Note that the luminal anti-Tkv antibody detects overexpression levels of cell surface exposed Tkv induced by the GAL4 system, whereas it is abolished when incubated with its corresponding target polypeptide. Bars correspond to 10 µm.

According to the DBTS model, the accumulation of surface receptors at the *shi* ^{ts1} clone sequesters free diffusing Dpp on its travel to form the gradient. As a consequence, the amount of extracellular Dpp at the clone would increase by a factor of approximately 20, resulting in the formation of a shadow behind the mutant territory (Kruse et al., 2004). Performing the extracellular immunostaining protocol with an antibody detecting GFP extracellular GFP-Dpp could be monitored (Fig. 24). Extracellular GFP-Dpp staining outlines the cell profiles and does not detect intracellular GFP-Dpp neither in the producing cells nor at the receiving tissue (Fig. 24B). Like total GFP-Dpp, steady-state extracellular GFP-Dpp is distributed in a long-range gradient at the target tissue. However, the fluorescence intensity profiles are less steep than total Dpp (Fig. 24C and 24D), indicating that intracellular Dpp accounts primarily for the visible GFP-Dpp gradient in the receiving territory.

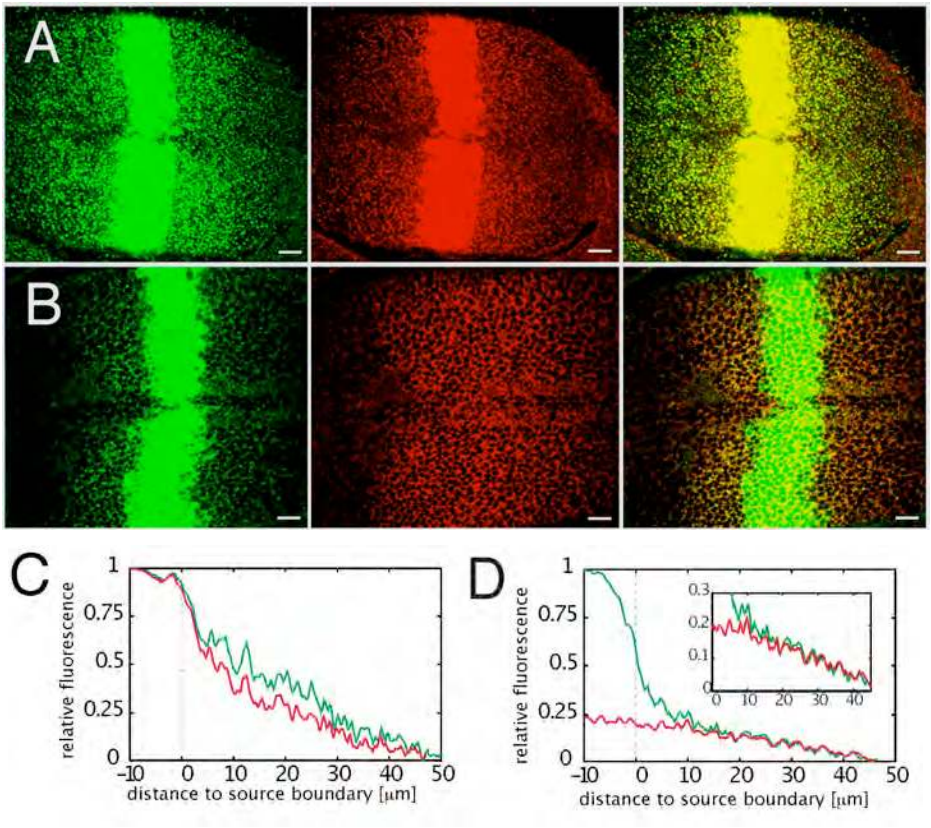

Fig. 24: Detecting extracellular GFP-Dpp
A,B) Double labelling showing GFP-Dpp distribution (green), total (A) or extracellular (C) GFP immunostaining (red) and overlays. C,D) Fluorescence intensity profiles of GFP-Dpp (green) and total (C) or extracellular (D) GFP immunostaining (red) in representative discs. Genotype in A-D: *dpp-GAL4/UAS-GFP-Dpp*. Bars in A and B correspond to 10 µm.

3.1.2 The DBTS model is inconsistent with the observed receptor concentrations in *shi* ^{ts1} clones

Capitalizing on the generated antibodies and staining conditions, the results of the DBTS model in the presence of a *shi* ^{ts1} clone were tested experimentally. First the levels of surface Tkv were analyzed in *shi* ^{ts1} mutant clones when endocytosis is blocked. Fig. 25 shows that in the *shi* ^{ts1} mutant cells after five hours at the restrictive temperature of 34 °C (the experimental conditions that generated the GFP-Dpp shadows in the “shibire shadow assay”), the levels of total Tkv are not significantly altered. In particular, receptors associated to the cell membranes are not changed. This result indicates that when endocytosis is

blocked during five hours, surface receptor levels do not change tenfold or more as predicted by the DBTS model (see Fig. 17G, page 31).

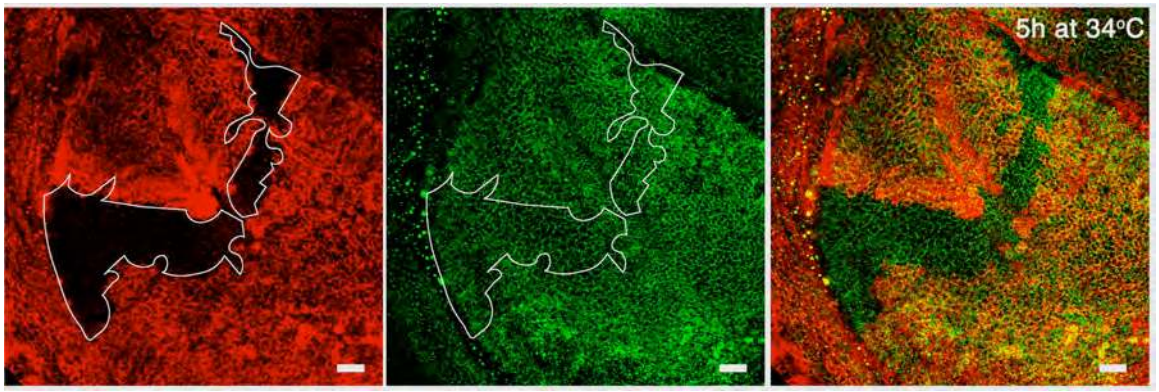

Fig. 25: Total Thick veins localization in *shi* ^{ts1} clones
Double labelling showing *shi* ^{ts1} clones after five hours at the restrictive temperature (see Materials and Methods) marked by the absence of Nmyc (red), and Tkv immunostaining (green). Genotype *shi* ^{ts1} *FRT18A/HS-NM8A FRT18A; HS-Flp/+*. Note that the levels of Tkv outlining the cells are not significantly changed within the mutant mosaics. White line outlines the mutant clone. Bars correspond to 10 µm.

To confirm that the Tkv pool associated to the cell profiles correspond to Tkv on the cell surface, the antibody directed against the luminal domain of Tkv (see Materials and Methods) was used with the extracellular immunostaining protocol (Strigini and Cohen, 2000). Fig. 26 shows that the levels of surface-exposed Tkv are not increased upon five hours of endocytic block in the *shi* ^{ts1} mutant clones.

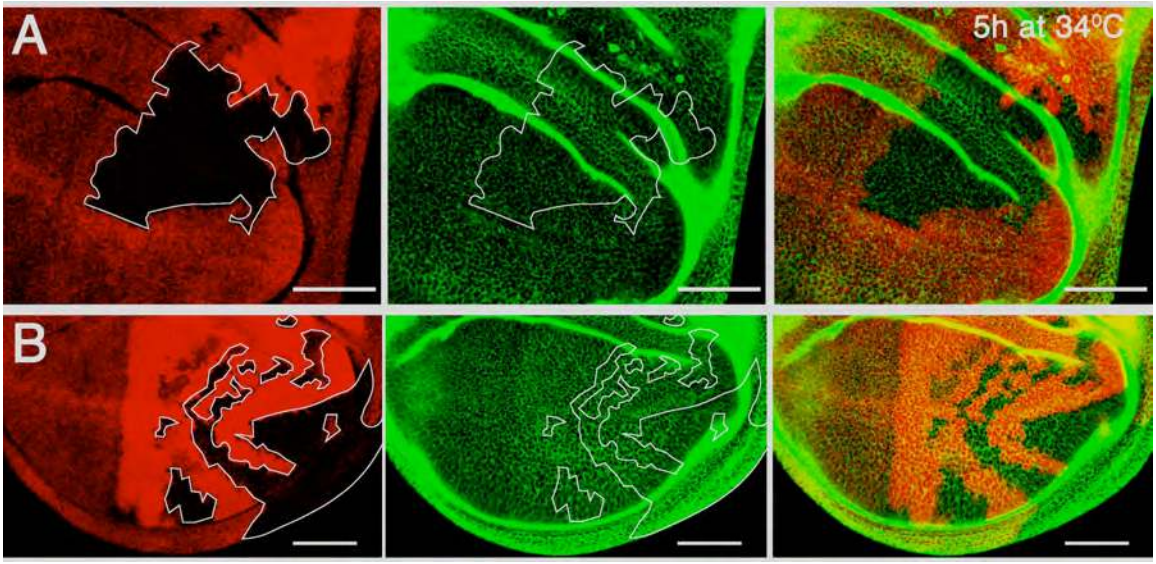

Fig. 26: Cell surface Thick veins levels in *shi* ^{ts1} clones
A,B) Double labelling showing *shi* ^{ts1} clones after five hours at the restrictive temperature marked by the absence of DsRed (red) and immunostaining of surface exposed Tkv using the Tkv luminal antibody and the extracellular immunostaining protocol (green; see Materials and Methods). Genotype: *shi* ^{ts1} *FRT18A/tub-DsRed FRT18A; HSFlp/+*. Note that the levels of surface exposed Tkv are not increased within the *shi* ^{ts1} mutant clones. White line outlines the mutant clone. Bars correspond to 50 µm.

Taken together, the observed shadow can therefore not result from a mechanism based on a high surface Tkv receptor concentration as proposed in the DBTS models (Kruse et al., 2004).

3.1.3 The DBTS model is inconsistent with the observed receptor concentrations in the “shibire rescue assay”

The “shibire rescue assay” permits to monitor how blocking endocytosis in the receiving cells influences the formation of the Dpp gradient on the levels of intracellular and extracellular ligand (Entchev et al., 2000). In this assay, the receiving cells cannot perform endocytosis at the restrictive temperature (34 °C) in a *shi* ^{ts1} mutant animal, whereas the secreting cells are rescued by expressing a *Dynamin*$^{+}$ transgene and can thus perform endocytosis normally (see Materials and Methods). At the permissive temperature (25 °C), a GFP-Dpp gradient is present in the target tissue. After a temperature shift to the restrictive

temperature, endocytosis is blocked at the receiving territory. Upon six hours of endocytic block, internalized GFP-Dpp has vanished and no gradient can be observed (Entchev et al., 2000).

To study whether block of endocytosis at the receiving tissue affects Tkv levels, the cell surface receptor levels were analyzed in the “shibire rescue assay” after endocytic block was performed. The corresponding heterozygous sibling larvae were taken as control. As for total Tkv, no significant increase in the total receptor levels could be uncovered neither between the shibire rescue disc and the control disc nor between the wild-type source and the receiving tissue (Fig. 27).

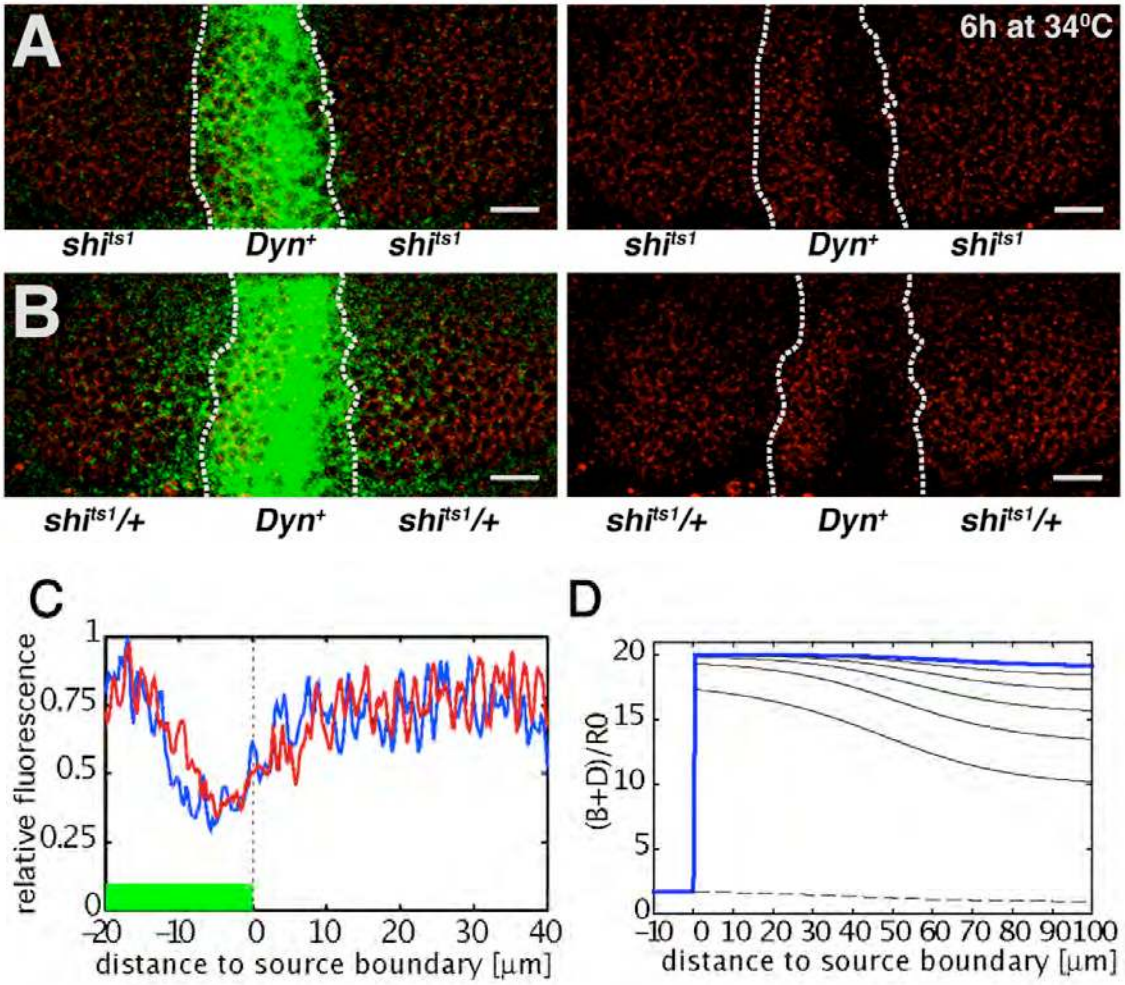

Fig. 27: Total Thick veins levels in the “shibire rescue assay”
A,B) Double labelling showing GFP-Dpp (green) and immunostaining of Tkv (red) from a *shi ^{ts1}; UAS-Dynamin^{+}/+; dpp-GAL4/UASGFP-Dpp* larva (A), or from a heterozygous *shi ^{ts1}/+* sibling (B) incubated at 34 °C for six hours. Note a downregulation of Tkv levels of unknown significance abutting the A/P boundary. C) Intensity profiles of Tkv

immunostaining in representative discs. Red trace, Tkv in a heterozygous *shi* ^{ts1}/+ sibling. Blue trace, Tkv in a hemizygous *shi* ^{ts1} sibling. D) Cell surface receptor distributions corresponding to the situation in the 'shibire rescue' experiment calculated in the DBTS model containing a region –10 µm<*x*<0 µm describing secreting cells. Total surface receptor concentration *B*+*D*. Broken lines indicate the concentrations at *t*=0 given by the steady-state value obtained for parameter values describing a wild-type tissue. The endocytosis block is modeled by setting the receptor internalization rates to zero for *x*>0 µm. The red lines show the concentration after six hours, the time at which the experimental observations are made. The calculations are performed in one dimension with an AOI of size *Lx*=200 µm. Note that in contrast to the DBTS model, Tkv levels at the cell surface do not change at the receiving tissue when endocytosis is abolished for six hours. However, the DBTS model does also not result in increased levels of total Tkv at the receiving territory (1,2 fold) corresponding to the situation in the 'shibire rescue' experiment. Broken lines in A and B delimit the *Dynamin*$^{+}$ rescued source. Bars correspond to 10 µm.

In addition, the levels of surface Tkv were not increased in the mutant cells as determined by extracellular immunostaining (Strigini and Cohen, 2000) using the antibody raised against the luminal domain of Tkv (Fig. 28).

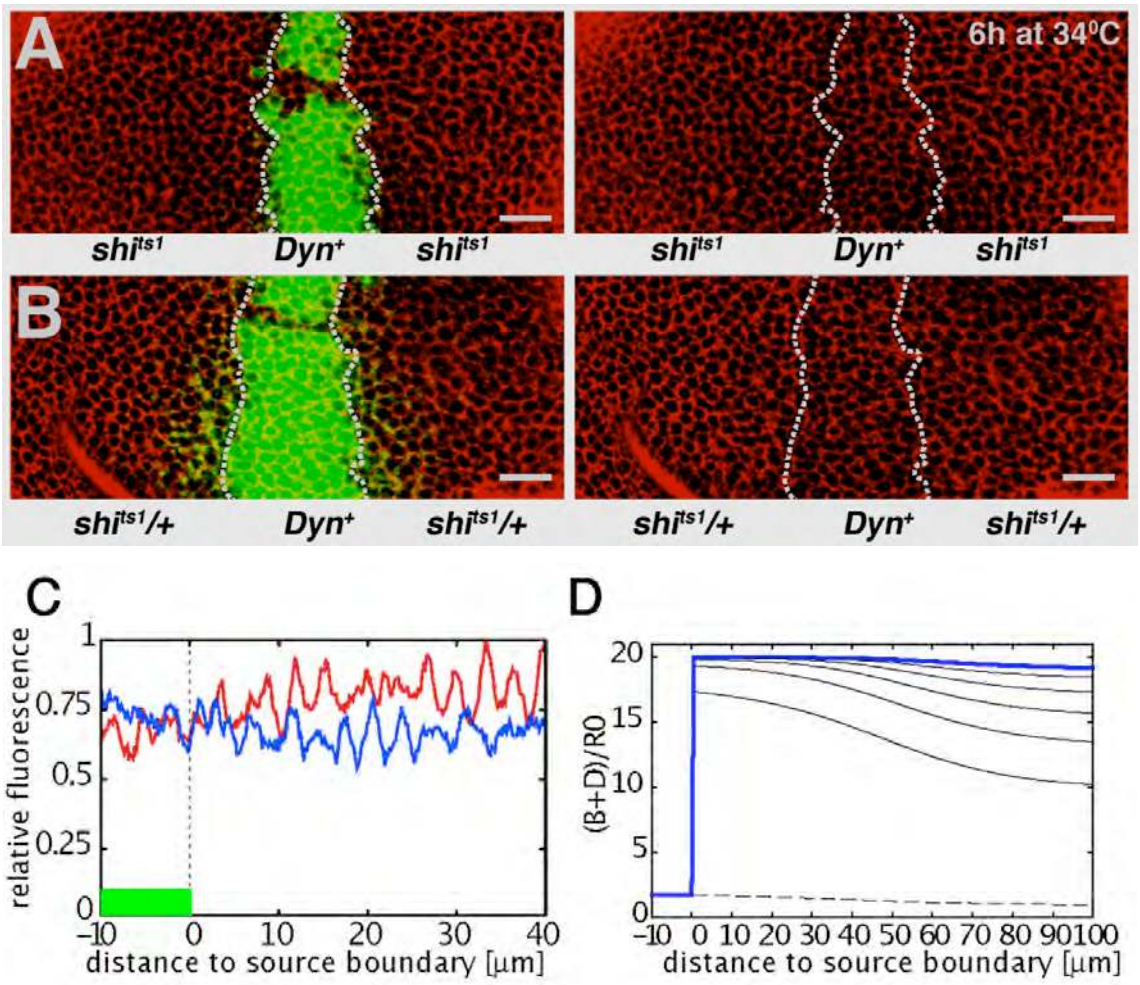

Fig. 28 (previous page): Cell surface Thick veins levels in the "shibire rescue assay"
A,B) Double labelling showing GFP-Dpp (green) and immunostaining of cell surface exposed Tkv using the Tkv luminal antibody and the extracellular immunostaining protocol (red) from a *shi ^{ts1}; UAS-Dynamin^{+}/+; dpp-GAL4/UAS-GFP-Dpp* larva (A), or from a heterozygous *shi ^{ts1}*/+ sibling (B) incubated at 34 °C for six hours. C) Intensity profiles of cell surface exposed Tkv immunostaining in representative discs. Red trace, Tkv in a heterozygous *shi ^{ts1}*/+ sibling. Blue trace, Tkv in a hemizygous *shi ^{ts1}*sibling. D) Cell surface receptor distributions corresponding to the situation in the 'shibire rescue' experiment calculated in the DBTS model containing a region –10 µm<*x*<0 µm describing secreting cells (see Fig. 27). Unlike the DBTS model, surface Tkv levels do not significantly change in the receiving tissue when endocytosis is abolished for six hours. Broken lines in A and B delimit the *Dynamin^{+}* rescued source. Bars correspond to 10 µm.

Comparing the obtained experimental data with the DBTS model leads therefore to the conclusion that high surface receptor levels cannot account for the shadows in the "shibire shadow assay".

3.1.4 The DBTS model is inconsistent with observed extracellular ligand concentrations in the "shibire rescue assay"

The extracellular GFP-Dpp levels were also investigated in the "shibire rescue assay". Here, the DBTS model generates a discontinuity of the levels of extracellular ligand by a factor of approximately 20 across the *shi^{ts1}* mutant boundary (Kruse et al., 2004) (Fig. 29D). To monitor the extracellular ligand levels, GFP immunostaining was performed in the "shibire rescue" disc after six hours at the restrictive temperature (34 °C). The corresponding heterozygous sibling larvae were again taken as control. In contrast to the model, amount of extracellular Dpp decreases at the receiving cells and the range of the extracellular gradient is reduced after six hours of block of endocytosis (Fig. 29). This indicates that a block of endocytosis does not lead to the sequestration of Dpp in the mutant territory.

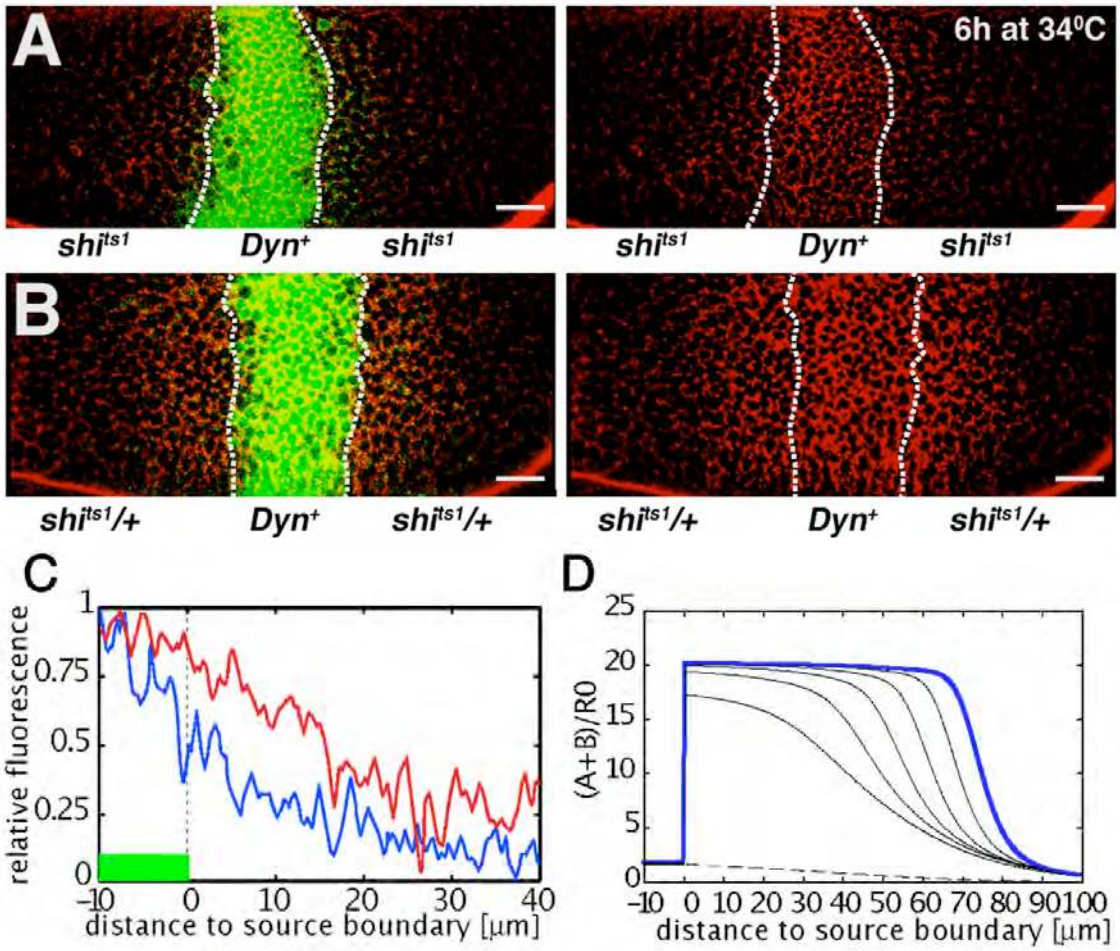

Fig. 29: Extracellular GFP-Dpp levels in the "shibire rescue assay"
A,B) Double labelling showing GFP-Dpp (green) and immunostaining of extracellular GFP-Dpp (red) from a *shi ^{ts1}; UAS-Dynamin^{+}/+; dpp-GAL4/UAS-GFP-Dpp* larva (A) or from a heterozygous *shi ^{ts1}/+* sibling (B) incubated at 34 °C for six hours. Note that the range of extracellular GFP-Dpp in the hemizygous wing disc is reduced after six hours of block at the restrictive temperature. (C) Intensity profiles of extracellular GFP immunostaining in representative discs. Red trace, GFP in a heterozygous sibling. Blue trace, GFP in a hemizygous sibling. Green box, secreting cells. D) Total extracellular ligand concentration *A+B*, corresponding to the situation in the 'shibire rescue' experiment calculated in the DBTS model containing a region –10 µm<*x*<0 µm describing secreting cells (see Fig. 25). Unlike the DBTS model, extracellular GFP-Dpp drops significantly in the receiving tissue when endocytosis is abolished. Broken lines in A and B delimit the *Dynamin^{+}* rescued source. Bars correspond to 10 µm.

Taken together, neither the surface receptor levels were elevated in conditions where endocytosis was abolished nor a massive accumulation of extracellular GFP-Dpp could be observed under this situation. The comparison of experimental data and theory therefore leads to the conclusion that high surface

receptor levels and massive accumulation of extracellular GFP-Dpp cannot be the reason for the shadows in the “shibire shadow assay”.

3.2 Testing experimentally the role of Dynamin-mediated endocytosis in Dpp gradient formation - Determining the effective diffusion coefficient of GFP-Dpp

To study directly the role of Dynamin-mediated endocytosis in Dpp gradient formation, the dynamics of GFP-Dpp movement in wing imaginal discs were analyzed *in vivo*. To do this, Fluorescence Recovery After Photobleaching (FRAP) experiments were performed (see Materials and Methods) (Axelrod et al., 1976; Koppel et al., 1976). The irreversible photobleaching of fluorescent molecules within a restricted region of a cell or tissue allows measuring two-dimensional lateral mobility of the molecule of interest (Lippincott-Schwartz et al., 2001; Reits et al., 2001). In particular, movement of GFP-Dpp was monitored in conditions where endocytosis at the receiving cells was either normal or blocked (“shibire rescue assay”). Third instar larval imaginal discs expressing GFP-Dpp at the domain of endogenous Dpp were used. Adjacent to the GFP-Dpp source, a narrow stripe of 10 µm (i. e. 3 - 4 receiving cells wide) was photobleached using a 488 nm laser. After photobleaching, the time course of the fluorescence recovery within this region was monitored by confocal time-lapse microscopy (see Materials and Methods as well as listed in the Appendix). The obtained FRAP recovery curves were quantitatively evaluated using a one-dimensional diffusion equation. The equation was solved assuming a homogeneous initial distribution inside and outside of the bleached area with a step like transition at its boundary. The resulting fitting curve for the averaged fluorescence in the region of interest was as follows:

$$f(t) \propto 1 - \left[2\sqrt{\frac{Dt}{\pi\omega^2}} \left(e^{\frac{-\omega^2}{4Dt}} - 1 \right) + \mathrm{erf}\left(\frac{\omega}{2\sqrt{Dt}} \right) \right] + c \qquad k = 0$$

where erf denotes the error function, $\mathrm{erf}(x) = \frac{2}{\sqrt{\pi}} \int_0^x e^{-y^2} dy$, D is the diffusion coefficient, k is the degradation rate, ω is the width of the photobleached stripe, and c is an additional fit parameter necessary to account for the fact that there is some remaining fluorescence after bleaching. The resulting apparent or effective diffusion coefficient (D') represents the driving force of the FRAP recovery of GFP-Dpp comprising free ligand diffusion as well as directed motion or binding events (Soumpasis, 1983).

First GFP-Dpp expressing wing imaginal discs at 25 °C were considered (Fig. 30). The region of interest next to the GFP-Dpp secreting cells was rapidly bleached using a high-intensity 488 nm laser pulse for approximately 30 seconds. Less than 20 % of the initial averaged fluorescence within the region remained after photobleaching. GFP-Dpp from the neighbouring areas moved subsequently into the bleached area. Recovered GFP-Dpp appears first as a diffuse fluorescent signal and later as bright fluorescent punctate structures. The kinetics of GFP-Dpp recovery correspond to a diffusion coefficient of D'= 0,0107 $\mu m^2/s$ ± 0,003 (n=4). The obtained value is approximately 1.000 fold lower than predicted for a molecule the size and shape of Dpp in solution (Groppe et al., 1998), probably reflecting Dpp binding to the receptor, transient interaction with the extracellular matrix, and cytoskeleton mediated movement.

Fig. 30 (next page): FRAP of GFP-Dpp at 25 °C
Third instar wing imaginal disc pouch projection (out of six individual sections) expressing GFP-Dpp (green) from a *dpp-GAL4/UAS-GFP-Dpp* larva. The GFP-Dpp gradient was imaged before (A), and 0 (B), 10 (C), 20 (D), 30 (E), 40 (F), and 50 min (G) after photobleaching of GFP-Dpp in a narrow stripe of 10 µm width. H) The recovery of the fluorescent signal was measured by confocal time-lapse microscopy and the fitting curves of the normalized fluorescence (n.f.) values over time in seconds (s) were plotted (see Materials and Methods). For quantitation of recovery kinetics, four independent FRAP time-lapse movies were analyzed. The resulting effective diffusion coefficient was D'= 0,0107 $\mu m^2/s$ ± 0,003 (n=4). Bars correspond to 10 µm.

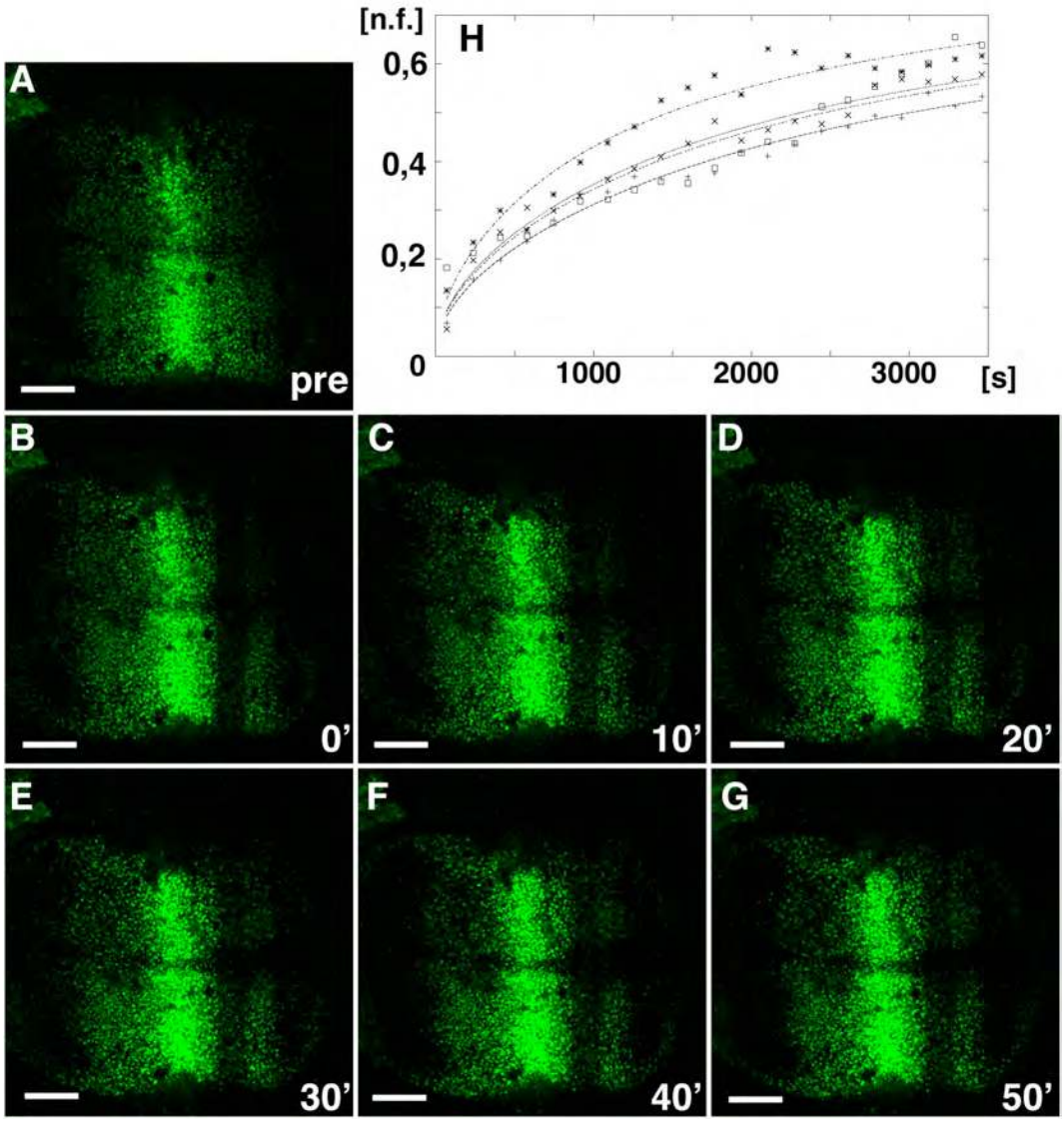

Next the recovery kinetics of a “shibire rescue” wing imaginal disc at the restrictive temperature (34 °C for at least 10 minutes before photobleaching) were determined (Fig. 31). Under this condition, the receiving cells cannot perform endocytosis in a *shi* ^{ts1} mutant animal, whereas the secreting cells are rescued by expressing a *Dynamin*$^{+}$ transgene and can thus perform endocytosis normally (see Materials and Methods).

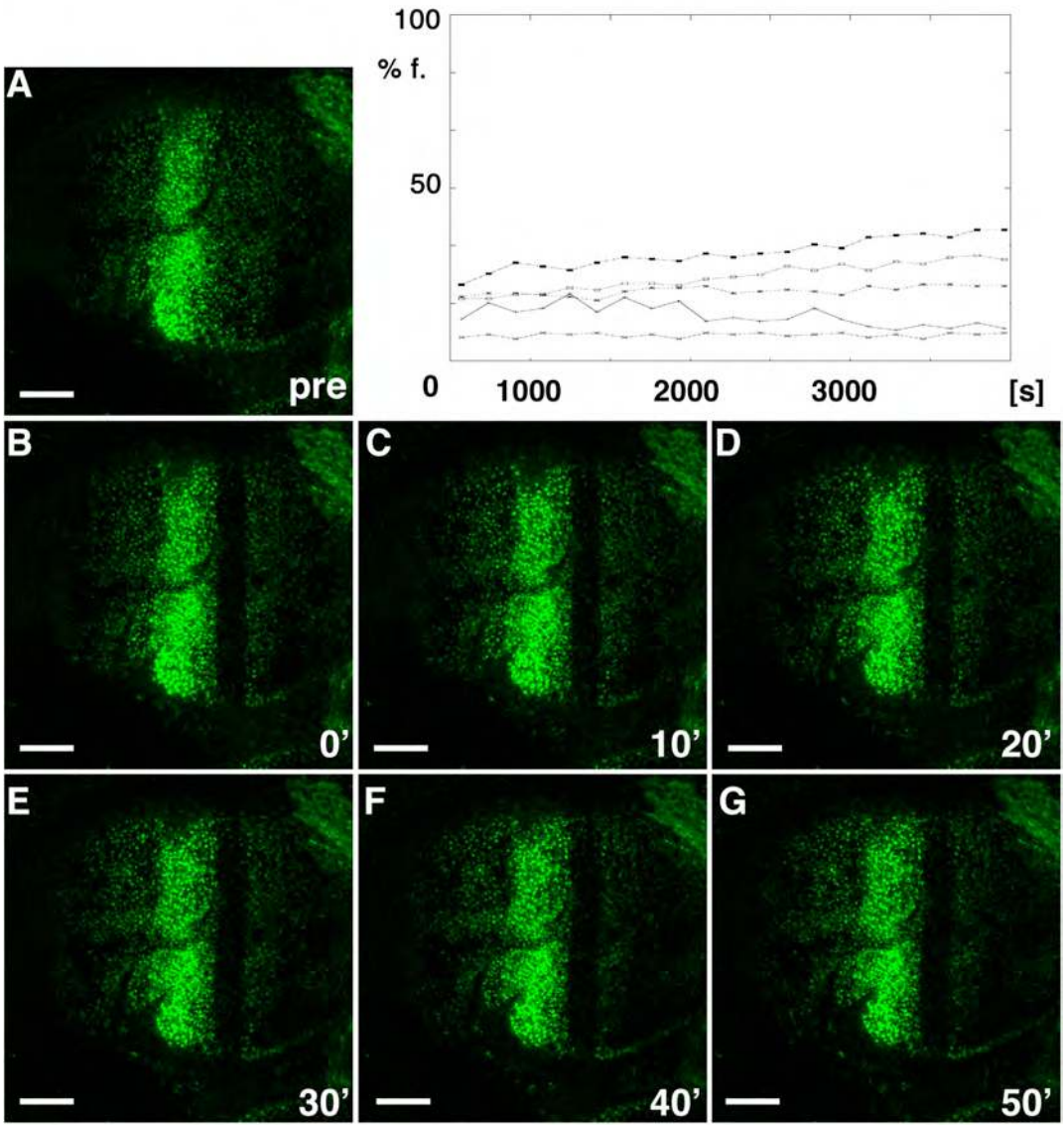

Fig. 31: FRAP of GFP-Dpp in a "shibire rescue" wing disc at 34 °C
Third instar wing imaginal disc pouch projection (out of six individual sections) expressing GFP-Dpp (green) from a *shi ^{ts1}; UAS-Dynamin^{+}/+; dpp-GAL4/UAS-GFP-Dpp* larva. The GFP-Dpp gradient was imaged before (A), and 0 (B), 10 (C), 20 (D), 30 (E), 40 (F), and 50 min (G) after photobleaching of GFP-Dpp in a narrow stripe of 10 µm width. H) The recovery of the fluorescent signal was measured by time-lapse microscopy and the curves of the normalized fluorescence in % to the pre-bleached fluorescence values were plotted over time in seconds (s) (see Materials and Methods). Five independent FRAP movies showed similar absence of recovery. Bars correspond to 10 µm.

After photobleaching, the time course of the fluorescence recovery within this region was monitored with low levels of 488 nm light and essentially no recovery could be observed when endocytosis was blocked in the bleached region (Fig. 31). The resulting FRAP curves revealed diffusion coefficients close to zero.

As controls, the recovery kinetics of GFP-Dpp at 34 °C as well as “shibire rescue” wing imaginal discs at the permissive temperature (25 °C) were determined (Fig. 32 and 33).

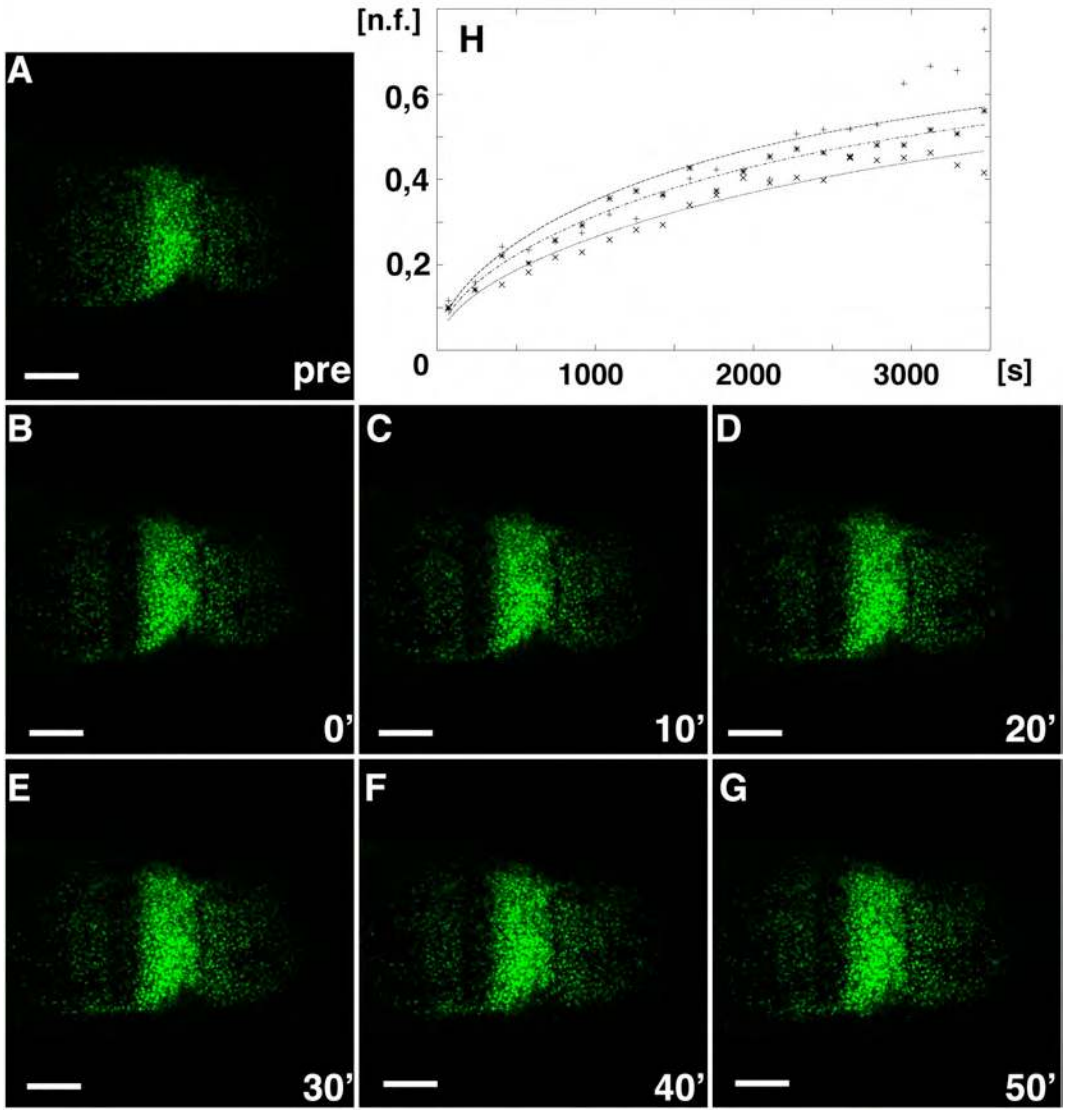

Fig. 32: FRAP of GFP-Dpp at 34 °C
Third instar wing imaginal disc pouch projection (out of six individual sections) expressing GFP-Dpp (green) from a *dpp-GAL4/UAS-GFP-Dpp* larva. The GFP-Dpp gradient was imaged before (A), and 0 (B), 10 (C), 20 (D), 30 (E), 40 (F), and 50 min (G) after photobleaching of GFP-Dpp in a narrow stripe of 10 µm width. H) The recovery of the fluorescent signal was measured by confocal time-lapse microscopy and the fitting curves of the normalized fluorescence (n.f.) values over time in seconds (s) were plotted (see Materials and Methods). For quantitation of recovery kinetics, three independent FRAP time-lapse movies were analyzed. The resulting effective diffusion coefficient was D’= 0,0078 µm^2/s ± 0,002 (n=3). Bars correspond to 10 µm.

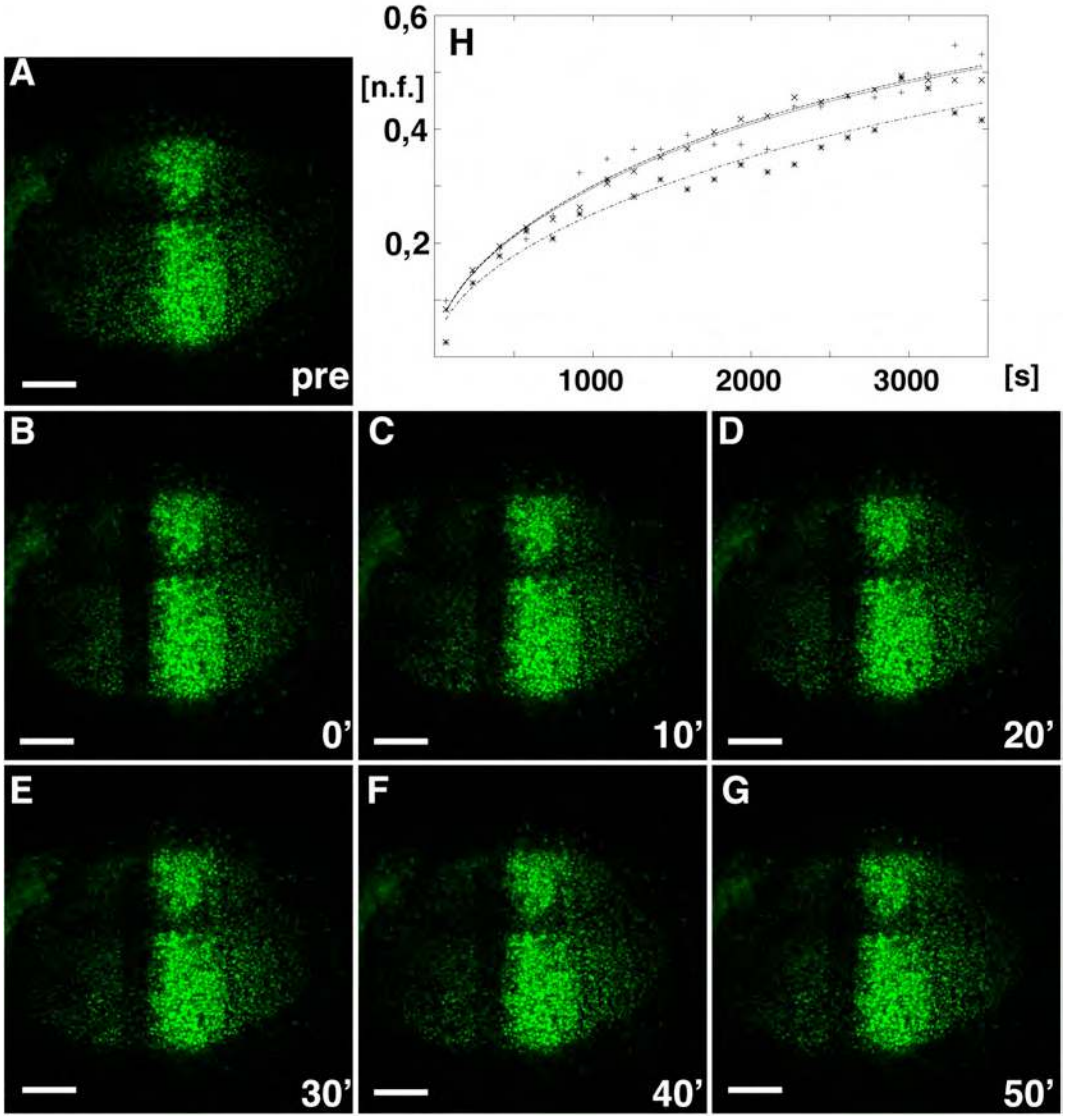

Fig. 33: FRAP of GFP-Dpp in a "shibire rescue" wing disc at 25 °C
Third instar wing imaginal disc pouch projection (out of six individual sections) expressing GFP-Dpp (green) from a *shi ^{ts1}; UAS-Dynamin^{+}/+; dpp-GAL4/UAS-GFP-Dpp* larva. The GFP-Dpp gradient was imaged before (A), and 0 (B), 10 (C), 20 (D), 30 (E), 40 (F), and 50 min (G) after photobleaching of GFP-Dpp in a narrow stripe of 10 µm width. H) For quantitation of recovery kinetics, three independent FRAP time-lapse movies were analyzed. The resulting effective diffusion coefficient was D'= 0,0063 µm^2/s ± 0,0014 (n=3). Bars correspond to 10 µm.

The recovery kinetics of GFP-Dpp at 34 °C are in the range of the GFP-Dpp ones at 25 °C (D'= 0,0078 µm^2/s ± 0,002 (n=3)), implying that under this experimental conditions ligand movement is still normal in wild-type receiving cells performing endocytosis. Furthermore, "shibire rescue" wing imaginal discs at the permissive temperature (25 °C) exhibit similar values for the effective diffusion coefficient

(D'= 0,0063 $\mu m^2/s$ ± 0,0014 (n=3)), indicating that the chosen experimental conditions are appropriate to study the dynamics of GFP-Dpp under conditions where endocytosis is abolished in the receiving territory. Interestingly, similar recovery kinetics were obtained when FRAP experiments were performed in "shibire rescue" wing imaginal discs at 32 °C (D'= 0,0061 $\mu m^2/s$ ± 0,004 (n=3)) (Fig. 34), indicating that endocytosis is not blocked at this temperature.

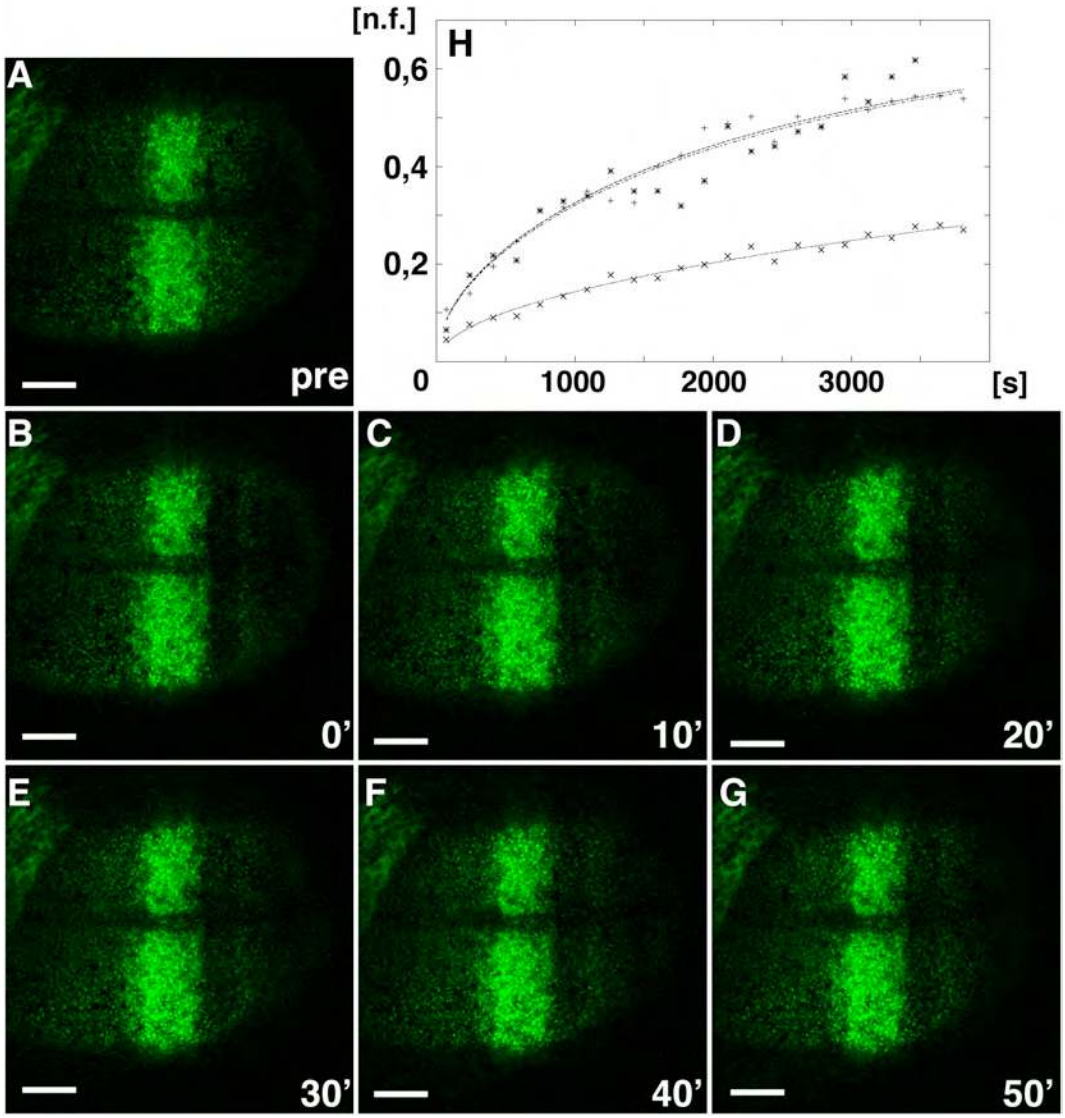

Fig. 34: FRAP of GFP-Dpp in a "shibire rescue" wing disc at 32 °C
Third instar wing imaginal disc pouch projection (out of six individual sections) expressing GFP-Dpp (green) from a *shi ^{ts1}; UAS-Dynamin^{+}/+; dpp-GAL4/UAS-GFP-Dpp* larva. The GFP-Dpp gradient was imaged before (A), and 0 (B), 10 (C), 20 (D), 30 (E), 40 (F),

and 50 min (G) after photobleaching of GFP-Dpp in a narrow stripe of 10 µm width. H) For quantitation of recovery kinetics, three independent FRAP time-lapse movies were analyzed. The resulting effective diffusion coefficient was D'= 0,0061 $\mu m^2/s$ ± 0,004 (n=3). Bars correspond to 10 µm.

Finally, a temperature-shift experiment was performed, where "shibire rescue" wing imaginal discs were imaged at 34 °C before and immediately after photobleaching. Following the dynamics of GFP-Dpp for approximately 10 minutes at the restrictive temperature, the wing imaginal disc was then cooled down gradually to 25 °C. These experimental conditions would allow monitoring fluorescence recovery of the bleached area after release of the temperature based endocytosis block at the receiving tissue. Indeed, after cooling down the tissue, slow recovery of GFP signal was recorded in the bleached area (Fig. 34). After approximately 10 minutes of gradual temperature decrease unbleached GFP-Dpp ligands from the neighbouring areas moved into the bleached area first as diffuse fluorescent signal and later as bright fluorescent punctate structures (Fig. 35). However, two additional experiments resulted in variable recovery kinetics. This is probably caused by the fact that the temperature control during the downshift was not reliable. Further work at the technical level will be necessary to validate the obtained result.

Fig. 35 (next page): FRAP of GFP-Dpp in a "shibire rescue" wing disc at 34 °C followed by a gradual decrease to 25 °C

Third instar wing imaginal disc pouch projection out of six individual sections expressing GFP-Dpp (green) from a *shi ^{ts1}; UAS-Dynamin^{+}/+; dpp-GAL4/UAS-GFP-Dpp* larva. The GFP-Dpp gradient was imaged before (upper panel), immediately, 10 min, 20 min, 30 min, 40 min, and 50 min after photobleaching of GFP-Dpp in a narrow stripe of 10 µm width. Release of temperature block occurred after 10 min of photobleaching. Note that a gradual increase of normalized fluorescence (n.f.) over time in seconds (s) can be observed after approximately 10 min of gradual temperature drop. Bars correspond to 10 µm.

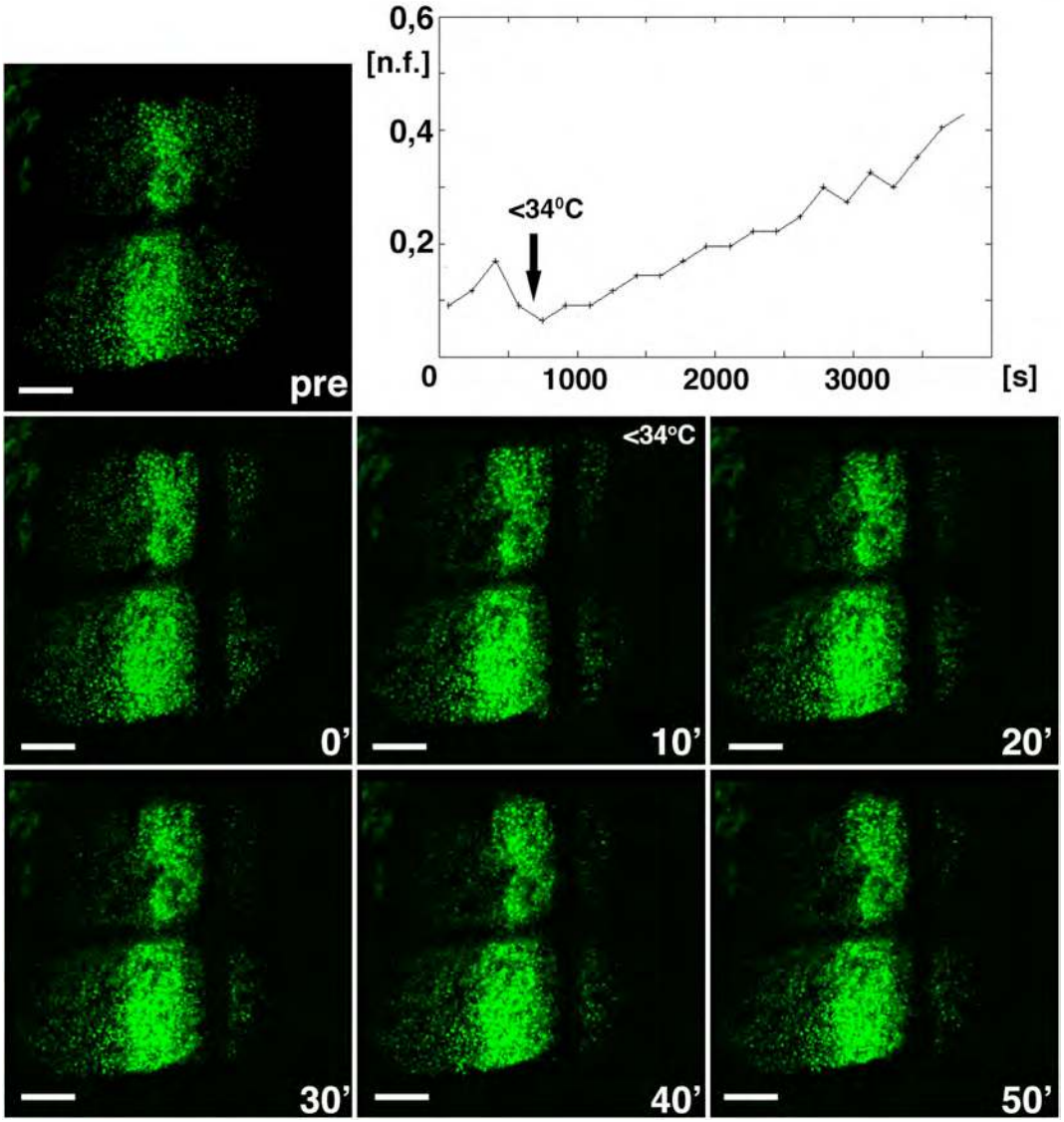

Taken together, the FRAP experiments demonstrate that a blockage of endocytosis by the Dynamin mutant *shibire* occurs very fast, approximately 10 minutes are sufficient to impair endocytosis. In addition, FRAP recovery kinetics reveal that blockage of endocytosis at the receiving territory stops GFP-Dpp movement: neither diffuse fluorescent signal nor bright fluorescent punctate structures are present in the bleached Dynamin mutant *shibire* tissue. This suggests that endocytosis is essential for Dpp propagation throughout the target tissue to form a long-range gradient.

Unlike the “shibire rescue assay”, where endocytosis is blocked for six hours to monitor how blocking endocytosis in the receiving cells influences the formation of the Dpp gradient on the levels of intracellular and extracellular ligand (Entchev et al., 2000), the FRAP experiment allows to analyze the effect of blocking endocytosis on Dpp movement directly. In addition, a long endocytic block makes it difficult to interpret the obtained results, since during this time period the steady-state distribution of the ligand, the receptor, members of the extracellular matrix, and cytoskeleton-mediated movement could be changed. In my case, FRAP analysis of “shibire rescue” discs revealed that block of endocytosis after a short time of only 10 minutes led to the rapid impairment of Dpp movement.
The FRAP recovery kinetics indicate that Dynamin-mediated endocytosis plays a key role in Dpp gradient formation. This changes the working hypothesis that both transport mechanisms, extracellular diffusion and planar transcytosis, contribute equally to the spreading of the morphogen throughout the tissue. However, more experiments need to be done to validate the conclusion that endocytic trafficking through the receiving cells is the major mechanism for Dpp gradient formation.

3.3 Characterizing Dpp trafficking along the endocytic pathway

3.3.1 Establishing antibodies to detect Rab proteins

Based on the presented results, the key role of endocytosis during Dpp movement suggests that Dpp trafficking through the endocytic pathway is essential for long-range gradient formation. Trafficking of Dpp at the receiving cells would involve a number of intermediate compartments controlled by Rab proteins (reviewed in Zerial and McBride, 2001). In this context, previous studies provided evidence that Rab proteins play a critical role in the Dpp signalling range (Entchev et al., 2000). In the “Rab mutant assay”, mutants of Rab5 or Rab7 were expressed in the receiving cells. When endocytosis was impaired by

expressing dominant negative Rab5 or degradation was enhanced by expressing dominant gain of function Rab7, the signalling range was reduced. Conversely, an enhanced endocytosis by overexpressing Rab5 led to an expansion of the signalling range (Entchev et al., 2000). This data led to the conclusion that Dpp transport involves Rab5- and Rab7-positive compartments. However, Dpp transport through Rab-positive endosomes has not yet been directly monitored. To study the transport of Dpp through endosomes in wing imaginal discs, antibodies were generated that detect endogenous Rab5-, Rab7-, and Rab11 protein levels controlling early, late, and recycling endosomal trafficking (Fig. 36). In addition, *in vivo* internalization assays were developed that allow monitoring the kinetics of cargo trafficking along the different endocytic compartments (see Materials and Methods).

First the affinity-purified antibodies were characterized. In a set of experiments the specificity of the different Rab antibodies were tested: (1) the antibodies detect overexpression levels of Rab5GFP, Rab7GFP, and Rab11GFP, induced by the GAL4 system using a *vg-GAL4* driver (Fig. 36A, 36C, and 36E), (2) and are titrated out by incubating them, prior to immunostaining, with the particular peptide used to raise the different antibodies (Fig. 36B, 36D, and 36F) (see Materials and Methods).

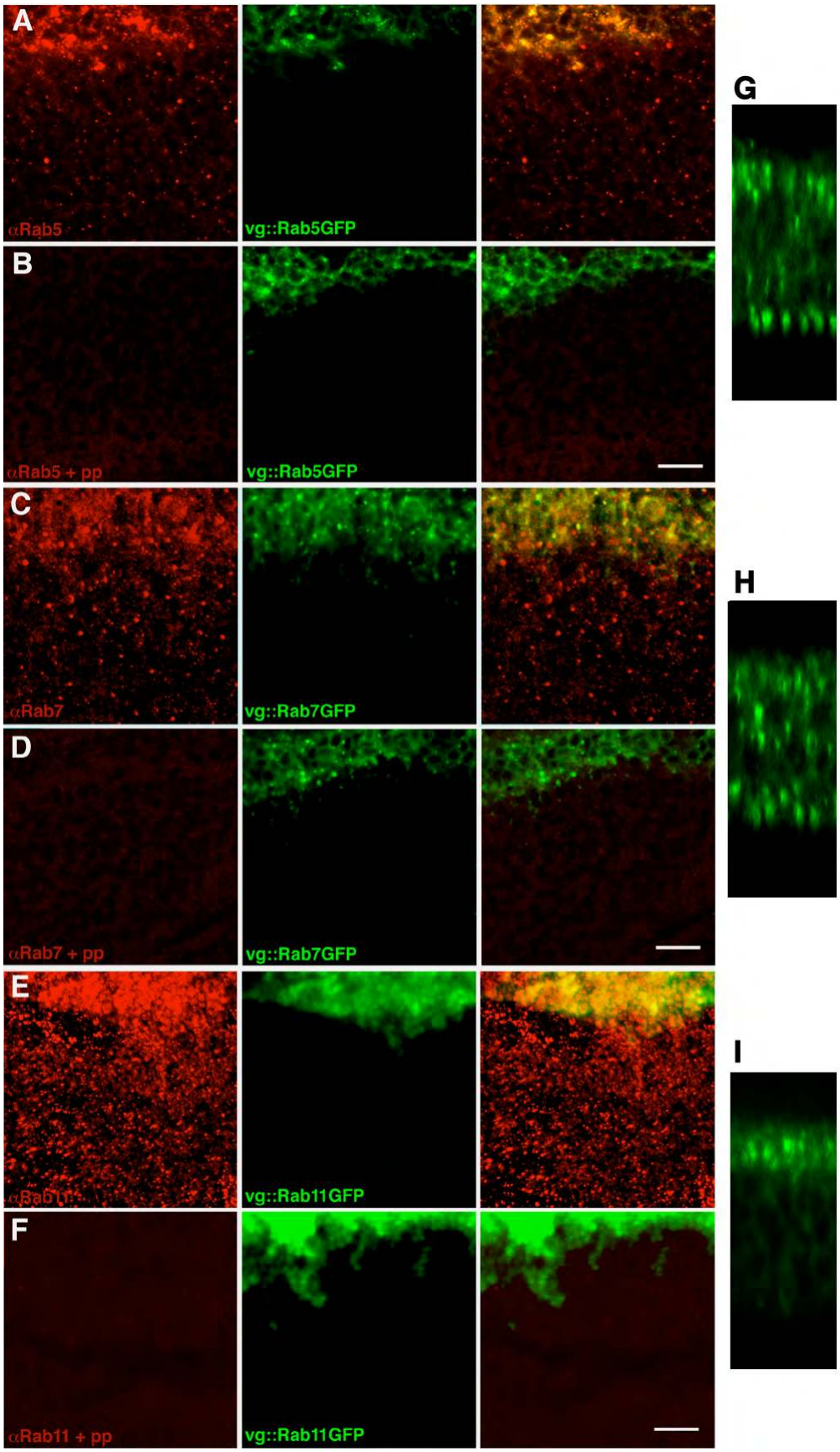
A
αRab5
vg::Rab5GFP
B
αRab5 + pp
vg::Rab5GFP
C
αRab7
vg::Rab7GFP
D
αRab7 + pp
vg::Rab7GFP
E
αRab11
vg::Rab11GFP
F
αRab11 + pp
vg::Rab11GFP
G
H
I

Fig. 36 (previous page): Detecting Rab5/Rab7/Rab11 in *Drosophila* wing disc
A-F) Rab immunostainings of third instar wing discs. A,B) Rab5 staining of wing discs expressing UAS-Rab5GFP under the *vg-GAL4* driver using anti-Rab5 (A) or anti-Rab5 blocked by its corresponding peptide antigen (B). C,D) Rab7 staining of wing discs expressing UAS-Rab7GFP under the *vg-GAL4* driver using anti-Rab7 (C) or anti-Rab7 blocked by its corresponding peptide antigen (D). E,F) Rab11 staining of wing discs expressing UAS-Rab11GFP under the *vg-GAL4* driver using anti-Rab11 (E) or anti-Rab5 blocked by its corresponding peptide antigen (F). G-I) z-sections of wing discs expressing UAS-Rab5GFP (G), UAS-Rab7GFP (H), and UAS-Ra11GFP (I) under the *vg-GAL4*. Note that the different anti-Rab antibodies detect expression levels of RabGFPs induced by the GAL4 system as well as endogenous levels in the wild-type territory, whereas they are abolished when performing a protocol where prior to immunostaining the antibodies were incubated with their corresponding target polypeptide. Other polypeptides did not have any effect (see Materials and Methods). Bars correspond to 10 µm.

All Rab immunostainings in the developing wing cells reveal punctate patterns of endogenous Rab5, Rab7, and Rab11 in the wild-type territory (Fig. 36). These structures correspond to sorting, recycling, and late endosomes to which Rab5, Rab11 and Rab7 mainly associate in steady-state conditions as previously described in mammalian cell culture (Bucci et al., 1992; Stenmark et al., 1994; Chavrier et al., 1990; Feng et al., 1995; Ullrich et al., 1996). Whereas Rab5 and Rab7 positive compartments are localized throughout the apico-basal axis of the wing epithelium (Rab5 compartments are more enriched at the apical and basal part) (Fig. 36G and 36H), Rab11 positive compartments accumulate mainly apically (Fig. 36I). Consistently, in mammalian epithelial cells Rab11 is associated to a subapical compartment (SAC) or apical recycling endosome (ARE) which has been proposed to mediate the recycling and transcytosis of endocytic cargo in epithelial cells (reviewed in Hoekstra et al., 2004). Like in mammalian cells, the recycling endosome labelled by Rab11 is associated to the Golgi apparatus (Urbe et al., 1993; Ullrich et al., 1996). In contrast, the early endosome marked by Rab5 and the late endosome enriched by Rab7 are not in close proximity to the Golgi compartment (Fig. 37).

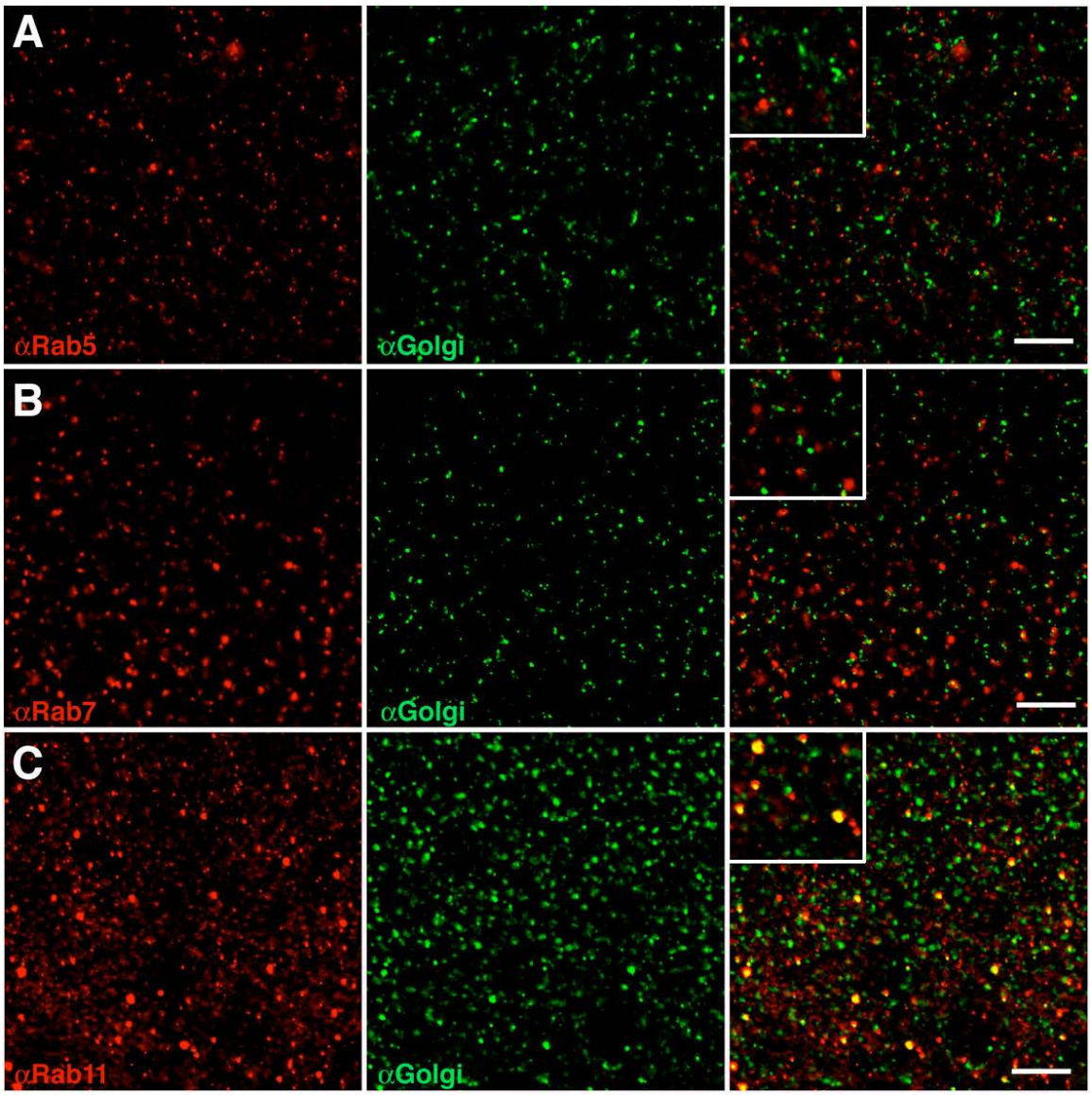

Fig. 37: Rab11 is associated with the Golgi apparatus in *Drosophila* wing disc
A,B, and C) Double labelling of wild-type third instar wing discs showing Golgi immunostaining (green) and Rab immunostaining (red) using anti-Rab5 (A), anti-Rab7 (B) or anti-Rab11 antibody (C). The Golgi membranes were stained with a Golgi-specific antibody that recognizes a 120 kDa integral Golgi membrane protein, colocalizing with rabbit anti *Drosophila* β-COP antibodies by fluorescence microscopy in *Drosophila* S2 cells (Stanley et al., 1997). Note that Rab5 and Rab7 endosomes poorly colocalize with Golgi (less than 5 % (n=3)), whereas Rab11 positive compartments are in close proximity to Golgi membranes (33 % ± 6 (n=3). Bars correspond to 10 µm.

3.3.2 Establishing an in vivo internalization assay

In order to understand the role of endocytic trafficking during signalling mediated by Dpp, the endocytic compartments were further characterized by an *in vivo* internalization assay. Developing fluid phase endocytosis assays using Dextran coupled to various dyes in pulse-chase experiments allowed monitoring the kinetics of fluid phase trafficking through the endocytic compartments during the signalling event (see Materials and Methods) (Berlin and Oliver, 1980; Ohkuma and Poole, 1978). Two distinct endocytic compartments could be distinguished *in vivo* and after fixation in combination with Rab5 and Rab7 immunostaining: an early and a late endocytic compartment (Fig. 38). After 10 minutes of Dextran pulse, the soluble marker is present in punctate structures (Fig. 38A), representing early endosomes containing Rab5 (Fig. 38B). After subsequent chase for 60 minutes at room temperature, Dextran reaches late vesicles that are distinct from early endocytic compartments (Fig. 38A). A subpopulation of those vesicles contains Rab7 (Fig. 38E). Hence, the soluble marker Dextran follows the endocytic pathway to early endosomes and then to late endocytic compartments.

Fig. 38 (next page): Distinguishing between distinct early and late endocytic compartments in *Drosophila* wing disc

A) Double labelling to visualize early endocytic compartments in a wild-type third instar wing disc where Texas Red Dextran accumulates after 10 minutes incubation (red). Double labelling to visualize late endocytic compartments in a wild-type third instar wing disc where Fluorescein Dextran accumulates after 10 minutes incubation and 60 minutes chase (green). Note that there is poor colocalization (less than 5 % (n=3)) of Texas Red Dextran with Fluorescein Dextran (merge in the right panel).

B,C) Double labelling in a wild-type third instar wing disc to visualize early endocytic compartments where Texas Red Dextran accumulates after 10 minutes incubation (green) in combination with Rab immunostaining (red) using anti-Rab5 (B) or anti-Rab7 (C). Note that colocalization of Rab5 with Dextran can be observed in 95 % ± 3 (n=3) of the punctate structures, whereas Rab7 endosomes poorly colocalize with Dextran (less than 5 % (n=3)).

D,E) Double labelling in a wild-type third instar wing disc visualizing late endocytic compartments where Texas Red Dextran accumulates after 10 minutes incubation and 60 minutes chase (green) in combination with Rab immunostaining (red) using anti-Rab5 (D) or anti-Rab7 (E). Note that colocalization of Rab7 with Dextran can be observed in 80 % ± 10 (n=3) of the punctate structures, whereas Rab5 endosomes poorly colocalize with Dextran (less than 5 % (n=3)). Bars correspond to 10 µm.

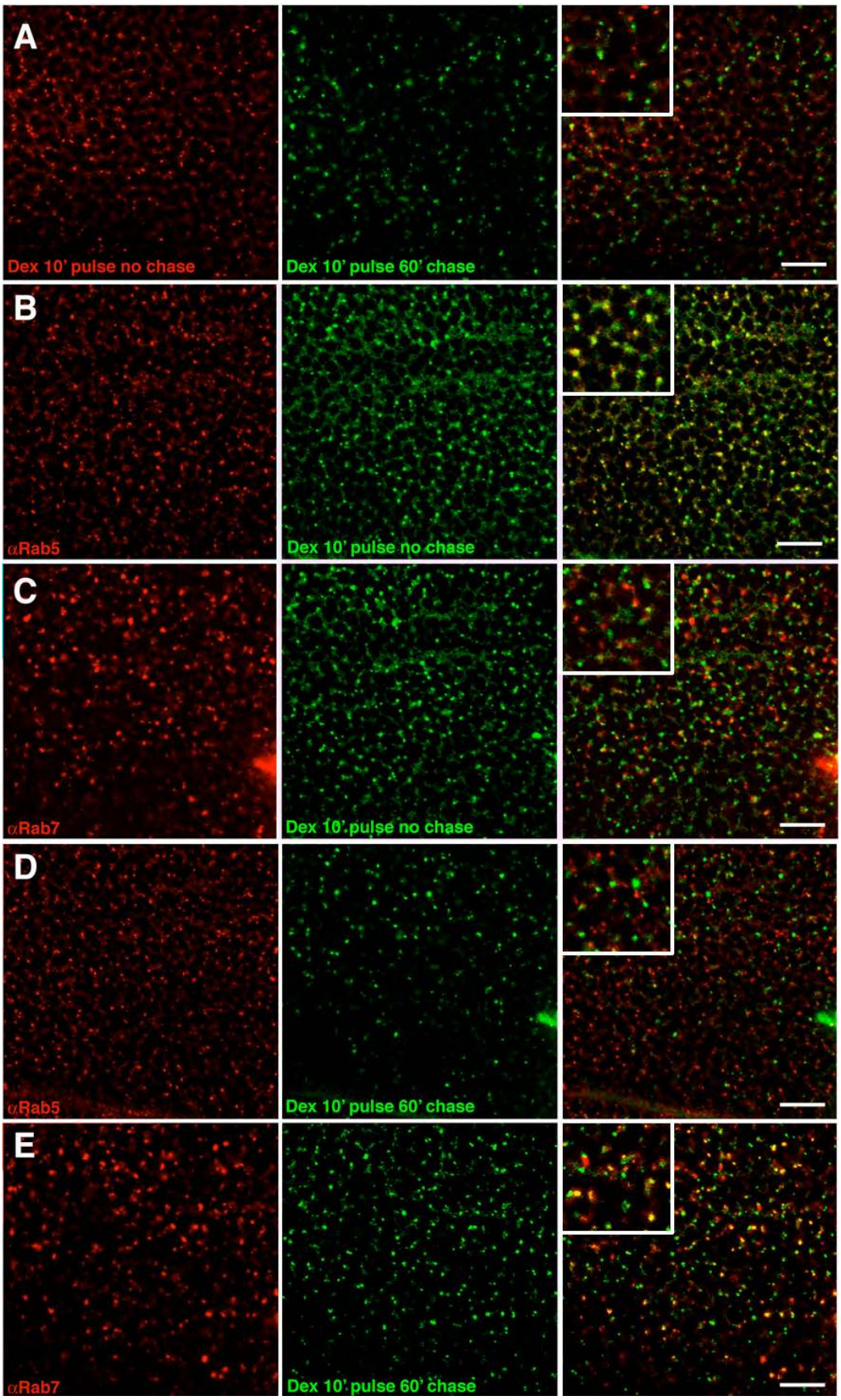
A
Dex 10' pulse no chase
Dex 10' pulse 60' chase
B
αRab5
Dex 10' pulse no chase
C
αRab7
Dex 10' pulse no chase
D
αRab5
Dex 10' pulse 60' chase
E
αRab7
Dex 10' pulse 60' chase

3.3.3 GFP-Dpp is localized in endosomal structures at the receiving cells

Capitalizing on the developed endocytic markers, the distribution of GFP-Dpp at the receiving cells was analyzed. Since more than 90 % of GFP-Dpp appears at the receiving cells primarily in punctuate structures confined to the apical part of the columnar wing imaginal disc epithelium (Entchev et al., 2000), apical GFP-Dpp was monitored in combination with the different subpopulations of endosomes marked by Rab immunostaining. In the most apical part of the epithelial cells, the ligand is present in Rab11 endosomes, representing subapical compartments (SAC) or apical recycling endosomes (ARE). In addition, GFP-Dpp accumulates in early and late endosomes visualized by Rab5 and Rab7 immunostaining, respectively (Fig. 39).

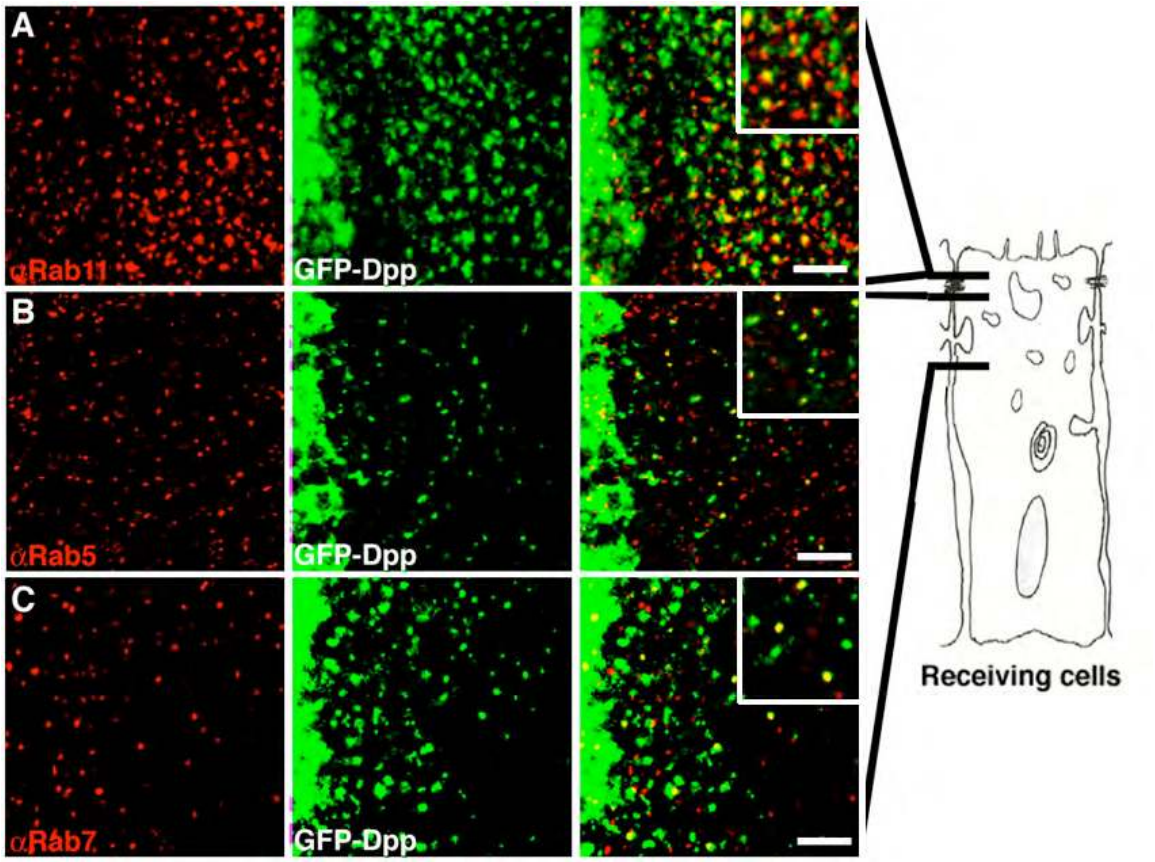

Fig. 39: GFP-Dpp is trafficking through Rab5, Rab7, and Rab11 endosomes in the receiving cells
A,B and C) Double labelling showing GFP-Dpp (green) in combination with Rab immunostaining (red) using anti-Rab11 (A), anti-Rab5 (B) or anti-Rab7 (C) from a *dpp-*

GAL4/UAS-GFP-Dpp **larva. Note that GFP-Dpp is colocalizing with Rab11 positive compartments (22 % ± 4 (n=3)) at the most apical part of the epithelial receiving cells (see right illustration). In addition, GFP-Dpp can be found in Rab5 (38 % ± 6 (n=3)) and Rab7 (24 % ± 3 (n=3)) positive endosomes at the apical part of the receiving cells. Bars correspond to 10 µm.**

GFP-Dpp distribution was also examined by internalized Dextran, performed under experimental conditions where the fluid phase marker labelled either the early (Fig. 40A) or the late endosomal compartments (Fig. 40B) (see Materials and Methods). In agreement with the Rab immunostainings, GFP-Dpp colocalizes with internalized Dextran marking the early as well as late endosomes.

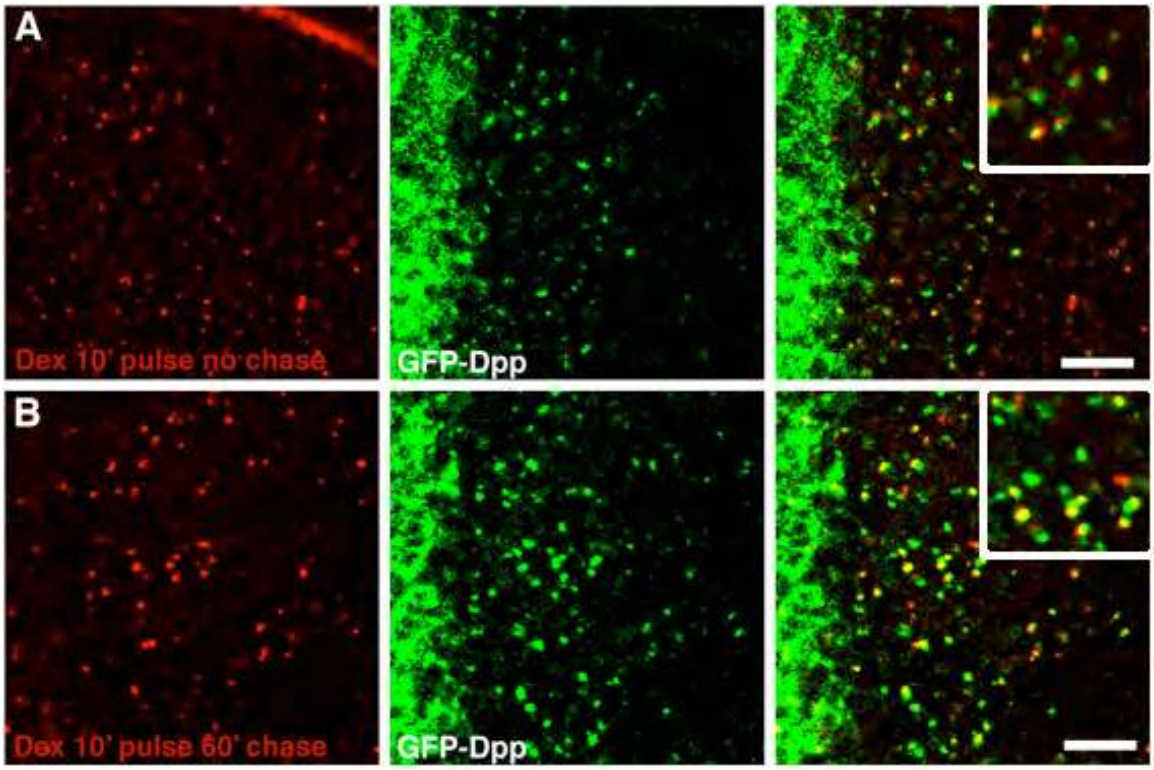

Fig. 40: GFP-Dpp is localized in endocytic compartments marked by Dextran uptake
A,B) Double labelling in a *dpp-GAL4/UAS-GFP-Dpp* third instar wing disc showing GFP-Dpp (green) and early endocytic compartments where Texas Red Dextran (red) accumulates after 10 minutes incubation (A) and late endocytic compartments where Texas Red Dextran (red) accumulates after 10 minutes incubation and 60 minutes chase (B), respectively. Note that GFP-Dpp can be found in early (40 % ± 5 (n=3)) as well as late endocytic compartments (31 % ± 3 (n=3)) at the apical part of the epithelial receiving cells. Bars correspond to 10 µm.

Taken together, most of GFP-Dpp (around 80 %) traffics through endosomes marked by different Rab antibodies and internalized fluorescent Dextran. A significant pool of the ligand accumulates in early (38 % ± 6) and late endosomes (24 % ± 3). Furthermore, GFP-Dpp association with Rab11 (22 % ± 4) in the receiving cells prompts the possibility that the recycling of the ligand occurs via apical recycling endosomes (ARE).

The fact that a minor pool of Dpp is not present in these compartments implies that other endocytic compartments could control the trafficking of the ligand along the endocytic pathway. Recent work in mammalian cells demonstrated that TGF-β receptors are internalized into both caveolin- and EEA1-positive endosomes and reside in both lipid rafts and non-rafts membrane domains (Di Guglielmo et al., 2003). It will be interesting to analyze whether Dpp can also traffic through a clathrin-independent pathway in wing imaginal epithelial cells.

3.4 Establishing a Dpp recycling assay

To address the recycling event of Dpp at the receiving cells, photoactivatable GFP (PAGFP) fused to Dpp was used. The strategy was to follow once photoactivated Dpp upon passage through an endosome at the receiving cell and monitor its movement while trafficking from the endosome to the neighbouring cells. In the following chapter, I demonstrate that PAGFP-Dpp can be photoactivated when expressed in wing imaginal discs. In addition, the signalling activity of the PAGFP-Dpp chimera was validated. Photoactivating PAGFP-Dpp in the whole wing pouch except a small patch of cells allowed us to study the dynamics of PAGFP-Dpp as performed in FRAP experiments for GFP-Dpp. However, activation of a small region (i. e. several cells) in the wing pouch did not result in detectable PAGFP-Dpp movement in the non-photoactivated cells. More analysis needs to be done to visualize PAGFP-Dpp while moving through the receiving cells.

3.4.1 Generating a photoactivatable GFP-Dpp (PAGFP-Dpp) fusion

My results indicate that endocytosis is required for long-range Dpp transport. In addition, GFP-Dpp traffics through Rab positive compartments at the receiving cells. In particular, the ligand is associated to Rab11 enriched apical recycling endosomes (ARE) which prompts the possibility that Dpp undergoes consecutive rounds of internalization and resecretion through the ARE in order to spread through the target tissue. However, the Dpp resecretion event itself has not yet been directly monitored.

To address specifically the recycling at the receiving cells, a strategy was followed to photouncage Dpp upon passage through an endosome at the receiving cell and monitor its movement while trafficking from the endosome. To do this, an approach was taken where photoactivatable GFP (PAGFP) was fused to Dpp. Previous work reported a photoactivatable variant of the jellyfish *Aequorea victoria* green fluorescent protein (PAGFP) that after intense irradiation with 413 nm light, increases fluorescence 100 times when excited by 488 nm light (Patterson and Lippincott-Schwartz, 2002). Photoactivation is thought to involve a shift in the chromophore population from the neutral phenolic form to the anionic phenolate form. These characteristics offer the possibility to explore the protein dynamics of Dpp by tracking photoactivated ligand that is the only visible GFP in the tissue.

First a cytosolic PAGFP was generated to analyze the characteristics of photoactivation in S2 cells (see Materials and Methods). To study the recycling event of Dpp in wing imaginal discs PAGFP was introduced like GFP (Entchev et al., 2000) in the proform behind the second furin cleavage position (Cui et al., 1998; Cui et al., 2001; Entchev et al., 2000). This way, PAGFP remains tagged at the N-terminus of the processed secreted Dpp protein (see Materials and Methods) (Fig. 41).

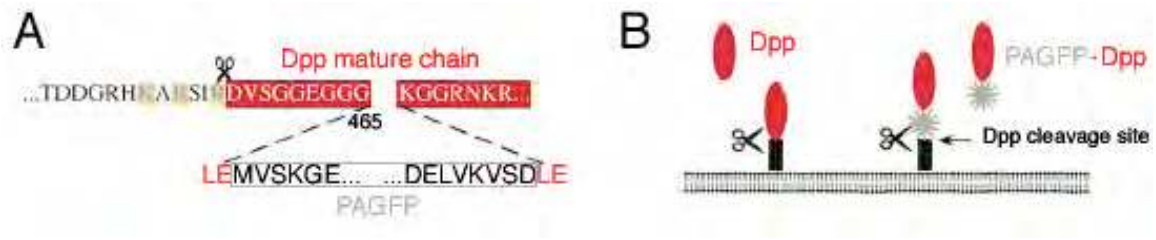

Fig. 41: Generating PAGFP-Dpp
A) Insertion of PAGFP within the Dpp mature protein (red). PAGFP is inserted at the amino acid position 465. The furin cleavage sequence which processes Dpp is depicted in yellow. B) Like Dpp, PAGFP-Dpp is released after furin cleavage at the Trans-Golgi network (Cui et al., 1998) which allows us to follow secreted Dpp after photoactivation.

3.4.2 Photoactivating PAGFP and PAGFP-Dpp in S2 cells

To analyze the characteristics of photoactivation, the rapid conversion of photoactivatable molecules to a green fluorescent state by intense illumination, the cytosolic PAGFP and PAGFP-Dpp were transfected in *Drosophila* S2 cells (see Materials and Methods). The transfected cells were irradiated for several seconds with 400 nm light of a 100 W Hg^{2+} lamp. Before photoactivation, very little fluorescence at 488 nm excitation was seen in the cells expressing cytosolic PAGFP or PAGFP-Dpp (Fig. 42A and 42C). Upon photoactivation with 400 nm light, fluorescence increased at least 50 fold for cytosolic PAGFP and 20 fold for PAGFP-Dpp under 488 nm excitation (Fig. 42B and 42D).

Fig. 42 (next page): Photoactivation and imaging *in vivo* of PAGFP and PAGFP-Dpp in S2 cells
A,B) Cotransfected S2 cells with cytosolic PAGFP under 488 nm excitation (left panel) and DsRed (right panel) prior (A) and after short illumination with 400 nm light (B). C,D) Cotransfected S2 cells with PAGFP-Dpp under 488 nm excitation (left panel) and DsRed (right panel) prior (C) and after short illumination with 400 nm light (D). PAGFP-Dpp is probably present in secretory vesicles in S2 cells.

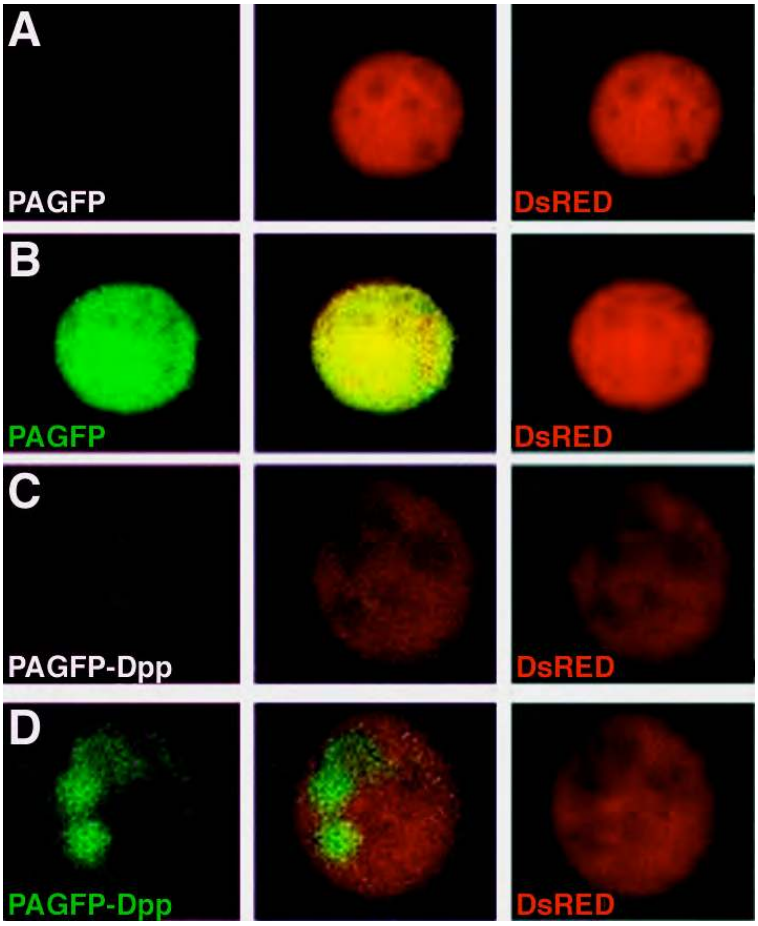

3.4.3 Visualizing PAGFP and PAGFP-Dpp in wing imaginal discs

We then tested whether cytosolic PAGFP and PAGFP-Dpp can be photoactivated when expressed in *Drosophila* wing imaginal discs. First cytosolic PAGFP was considered. Photoactivation was performed in fixed tissue. After 400 nm illumination, the fluorescence increased up to at least 20 fold for cytosolic PAGFP when excited with 488 nm light (Fig. 43). However, basal photoactivation was already visible in the surrounding tissue which was probably caused by exposition to daylight during dissection procedure.

Fig. 43 (next page): Photoactivation and imaging of PAGFP in a fixed wing imaginal disc Photoactivation of cytosolic PAGFP in an *act-GAL4/UAS-PAGFP* third instar wing disc. After short illumination with 400 nm light cytosolic PAGFP is visible in a restricted area (L.P.: Periklis (Laki) Pantazis) under 488 nm excitation. Bar corresponds to 50 µm.

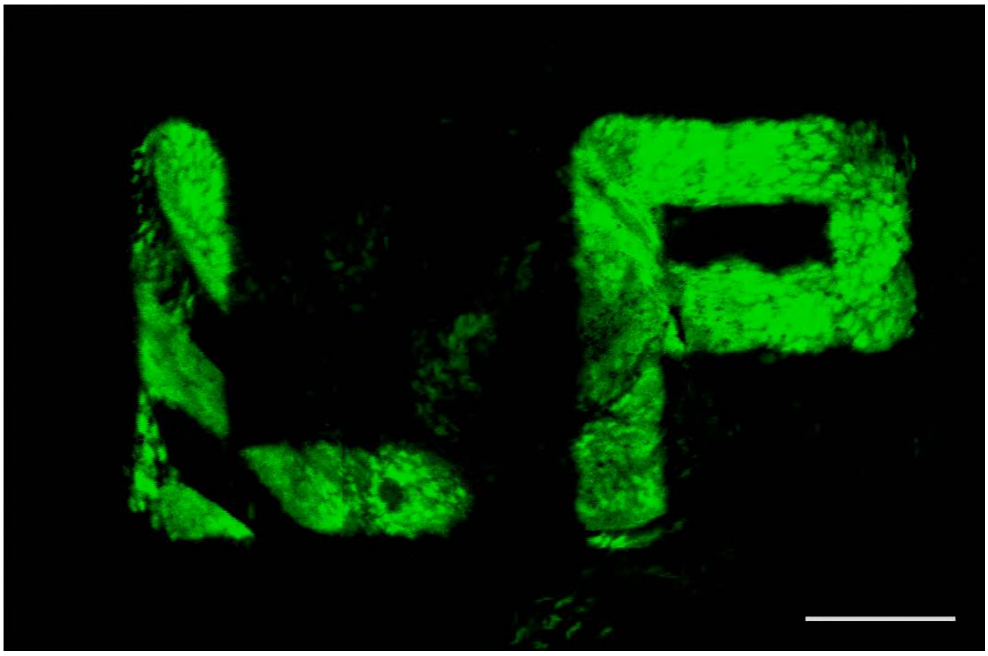

Next PAGFP-Dpp was tested when expressed in wing imaginal discs (Fig. 44). PAGFP-Dpp was driven in the endogenous Dpp expression domain using the *GAL4* gene under the spatial and temporal control of the dpp promoter (*dpp-GAL4*). After photoactivation, fluorescence of PAGFP-Dpp increased in the photoactivated region (Fig. 44B). Like GFP-Dpp, PAGFP-Dpp fluorescence allows subdivision of the wing pouch in two domains: the bright fluorescent signal in the secreting cells and the fluorescent PAGFP-Dpp punctate structures at the receiving territory. Hence PAGFP is secreted from the Dpp expression domain and spreads into the developing target tissue.

Fig. 44 (next page): Photoactivation and imaging of PAGFP-Dpp in a fixed wing imaginal disc

A,B) Photoactivation of PAGFP-Dpp (green) in an *UAS-PAGFP; dpp-GAL4/+* third instar wing disc prior (A) and after short illumination with 400 nm light (B). Cell profiles are labelled with phalloidin (red). Bars correspond to 50 µm.

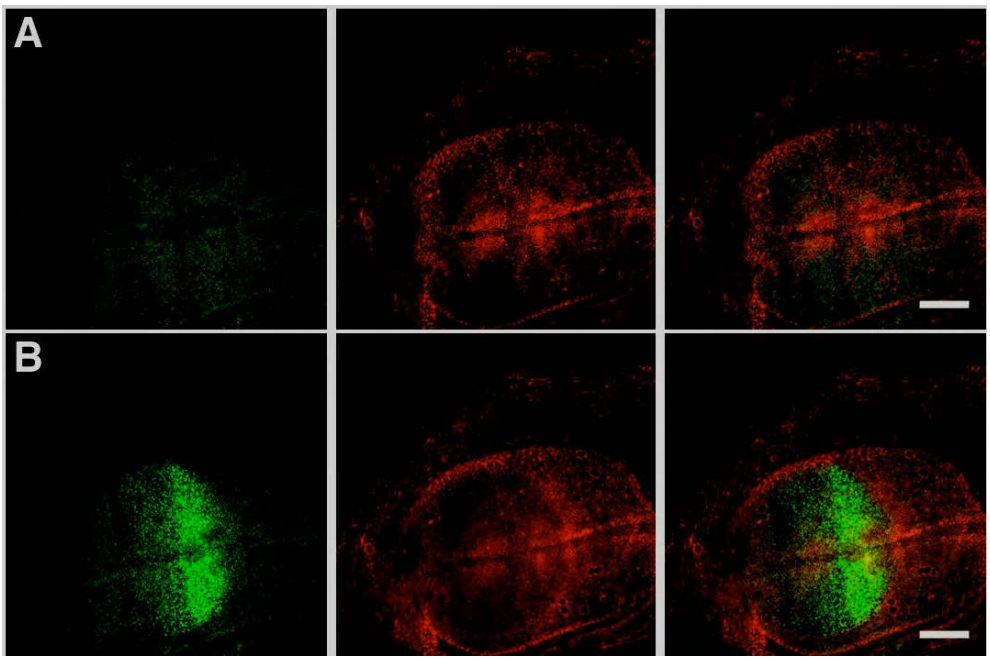

3.4.4 A functional PAGFP-Dpp fusion

Consistent with GFP-Dpp results, PAGFP-Dpp is secreted and can be seen in endocytic punctate structures at the receiving cells. In addition, PAGFP-Dpp overexpression in the endogenous domain with the *dpp-GAL4* driver in a wild-type background also causes imaginal disc overgrowth. To evaluate the signalling activity of PAGFP-Dpp, a rescue experiment was performed in Dpp-defective dpp^{d8}/dpp^{d12} mutant flies (see Materials and Methods). Expression of PAGFP-Dpp in the endogenous Dpp domain restored near normal growth and patterning of the wing imaginal disc in this mutant background (Fig. 45). The PAGFP-GFP activity gradient was visualized in rescued wing discs using an antibody that recognizes phosphorylated Mad (pMad) (Tanimoto et al., 2000). dpp^{d8}/dpp^{d12} wing discs have small wing primordia and express very low levels of pMad (Fig. 45A), consistent with an absence of Dpp activity. Nuclear pMad expression was restored in the rescued wing disc (Fig. 45B). Hence, PAGFP-Dpp is capable of forming a long-range activity gradient in the wing imaginal disc.

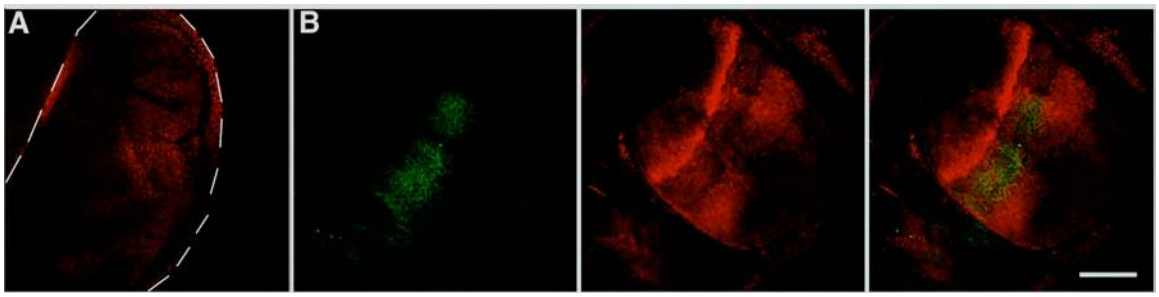

Fig. 45: Rescue of *dpp^{d8}/dpp^{d12}* mutant wing discs by expression of PAGFP-Dpp under *dpp-GAL4* control.
A,B) wing disc without rescue (A) and with rescue by expression of PAGFP-Dpp under *dpp-GAL4* control (B). Double immunolabelling detecting the activity of the PAGFP-Dpp by pMad (red), and photoactivated (400 nm light for several seconds in a restricted region) PAGFP-Dpp visible under 488 nm excitation (green). Note that expression of PAGFP-Dpp in a disc lacking endogenous Dpp (Genotype: *UAS-PAGFP-Dpp/+; dpp^{d8}/dpp^{d12}; dpp-GAL4/+*) restores nuclear pMad expression. Dpp-dependent pMad expression can be seen several cell diameters away from the Dpp production source. However, Dpp-independent pMad expression can be observed outside the wing pouch in the disc lacking endogenous Dpp. Wing imaginal disc orientation: posterior to the right. The shape of the *dpp^{d8}/dpp^{d12}* mutant wing disc is indicated with a white broken line. Bars correspond to 50 µm.

3.4.5 Dynamics of photoactivated PAGFP-Dpp

Activation of PAGFP-Dpp in a small patch of cells in the wing pouch did not result in detectable PAGFP-Dpp movement in the non-photoactivated cells. However, PAGFP signal in the non-photoactivated cells could only be observed *in vivo* when a major part of the PAGFP-Dpp pool was activate, i. e. when almost the whole wing pouch was activated. More analysis will be necessary to visualize a small pool of activated PAGFP-Dpp while moving through the receiving cells.
Therefore, to determine whether PAGFP-Dpp photoactivation can be used as a tool for measuring protein dynamics within living *Drosophila* wing imaginal discs, a major pool of PAGFP-Dpp ligands was photoactivated in the receiving tissue and the recovery in a small non-photoactivated region observed (Fig. 46 and 47). Under low levels of 405 nm excitation, PAGFP-Dpp can be visualized *in vivo* as bright fluorescent signal marking the secreting cells and as dimmer fluorescent punctate structures at the receiving territory (Fig. 46C). Under 488 nm excitation, PAGFP-Dpp shows no or little fluorescence that was probably caused by exposition to daylight during dissection procedure (Fig. 46A).

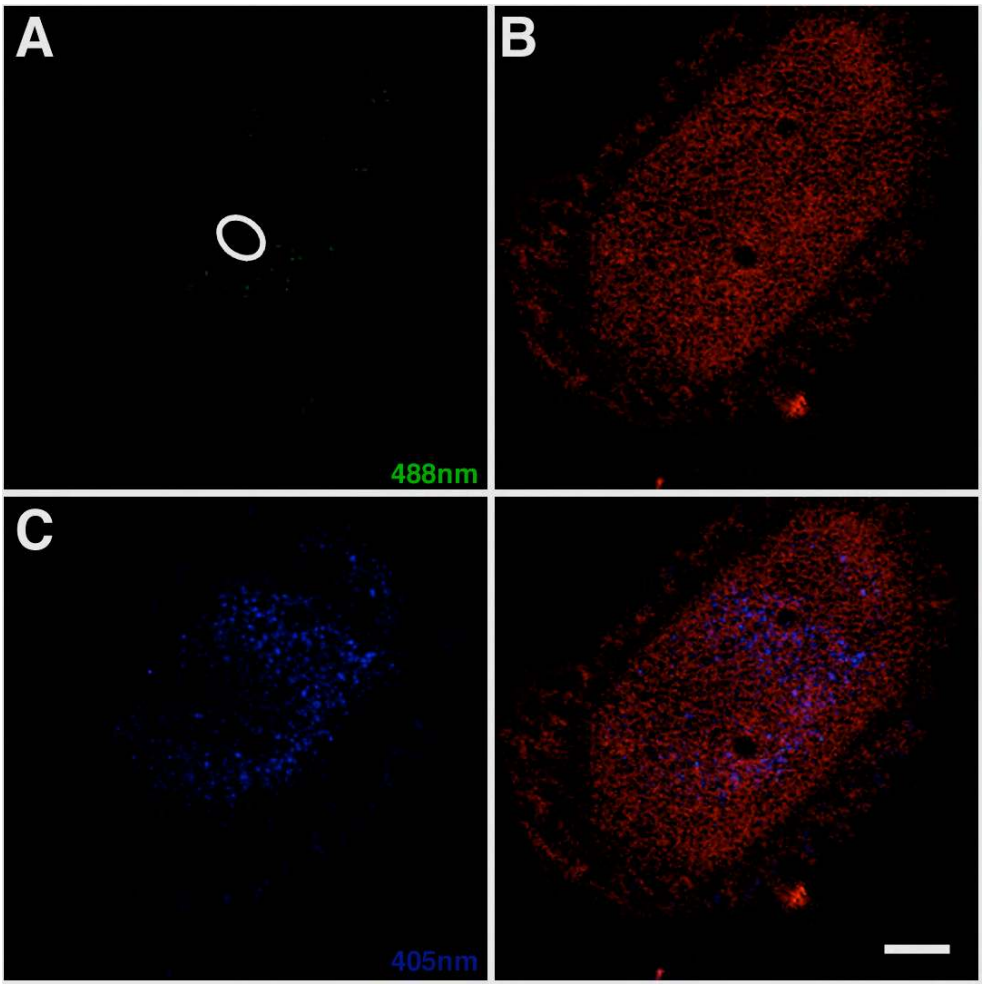

Fig. 46: *In vivo* imaging of PAGFP-Dpp in a living wing imaginal disc
A,C) PAGFP-Dpp in an *UAS-PAGFP-Dpp; dpp-GAL4/+* third instar wing disc was imaged with low levels of 405 nm excitation (C) and 488 nm excitation (A) before photoactivation within the entire wing pouch except the outlined white region. B) Cell profiles are labelled with FM4-64 (red). Note that 405 nm excitation allows visualization and therefore localization of PAGFP-Dpp prior to its photoactivation. Bar corresponds to 30 µm.

After approximately 10 seconds of photoactivation with high levels of 405 nm light within the whole wing pouch except the region outlined in white (Fig. 46A and 47), the pool of PAGFP-Dpp became fluorescent under 488 nm excitation (Fig. 47). The imaging with low levels of 488 nm light showed movement of the photoactivated PAGFP-Dpp ligands into the not activated receiving territory, resulting in an effective diffusion coefficient similar to the previously determined one in FRAP experiments for GFP-Dpp at 25 °C (Fig. 47B).

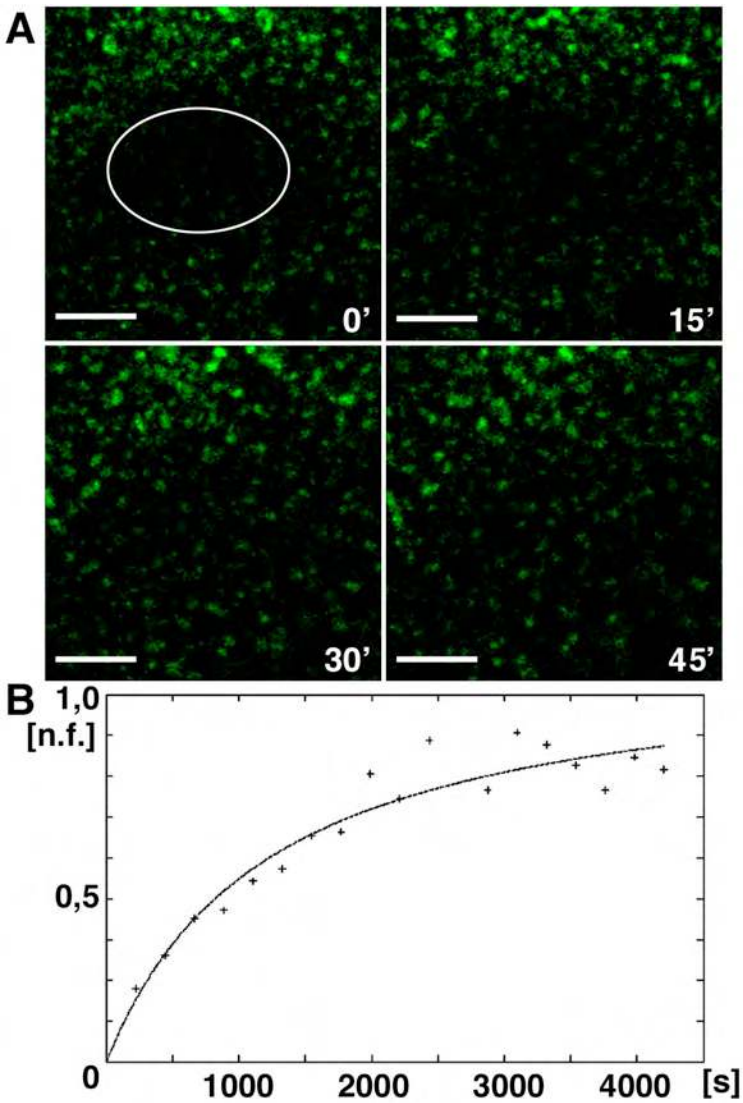

Fig. 47: Photoactivation and *in vivo* imaging of PAGFP-Dpp in a living wing imaginal disc
A) PAGFP-Dpp in an *UAS-PAGFP-Dpp; dpp-GAL4/+* third instar wing disc was imaged with low levels of 488 nm excitation 0, 15, 30, and 45 min after photoactivation. B) Kinetics of recovery of photoactivated PAGFP-Dpp in the outlined receiving tissue. The fluorescence intensity in the non-photoactivated region was measured and plotted as normalized fluorescence (n.f.) over time in seconds (s). The effective diffusion coefficient is approximately D'= 0,0204 $\mu m^2/s$ +/- 0,009 (see Materials and Methods). Bars correspond to 15 µm.

3.4.6 Subcellular photoactivation of PAGFP with a confocal laser-scanning miscroscope (C-LSM)

To address specifically the recycling of Dpp at the target tissue, the photoactivation of PAGFP-Dpp has to occur upon passage through endosomes at a receiving cell. This way, the movement of photouncaged ligand can be tracked while trafficking from the endosome. To do this, subcellular photoactivation of a confocal laser-scanning microscope (C-LSM) was tested. The cytosolic PAGFP was considered. Photoactivation was performed in fixed tissue. After illumination with high levels of 405 nm light for one second the fluorescence increased up to at least 20 fold for cytosolic PAGFP when excited with 488 nm light (Fig. 48).

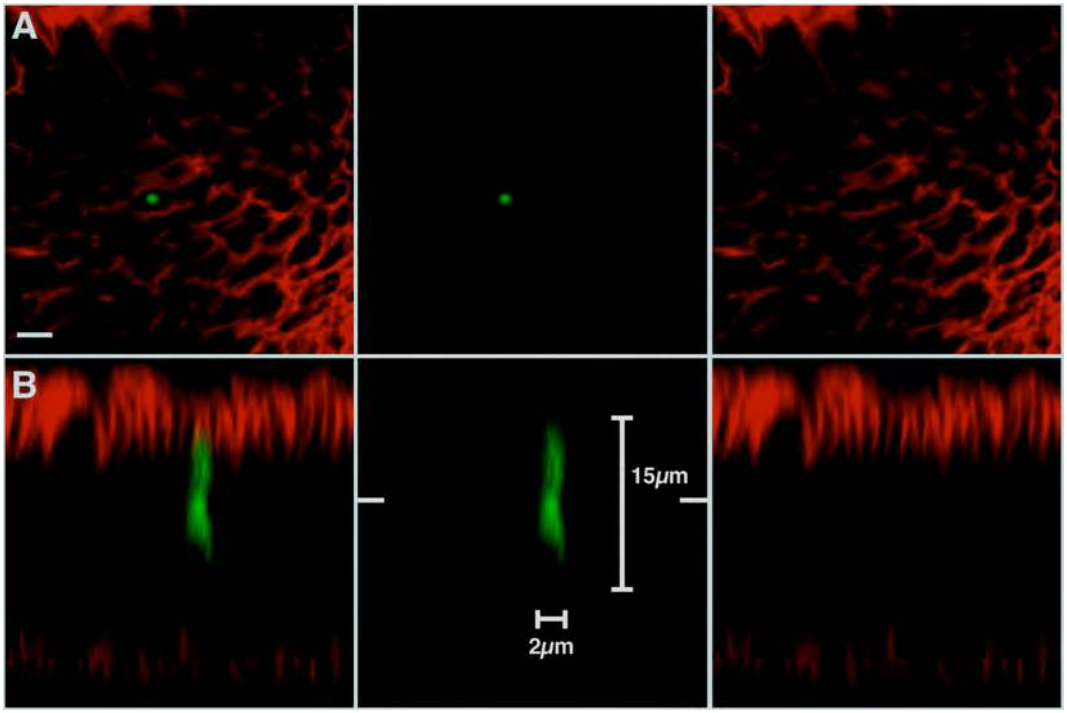

Fig. 48: Subcellular photoactivation of PAGFP in a wing imaginal disc with confocal LSM excitation
A) PAGFP in an *UAS-PAGFP; act-GAL4/+* third instar wing disc was imaged with 488 nm excitation after photoactivation with high levels of 405 nm light with a confocal LSM within a single cell. Cell profiles are labelled with Fasciclin III (red) immunolabelling. B) Axial view of the photoactivated region. Whereas a confocal LSM can activate cytosolic PAGFP within a single cell, the cross-sectional view through the wing epithelium shows that the activation event is not restricted to the focal plane. Bar in A corresponds to 2 µm.

The confocal LSM beam can activate cytosolic PAGFP within a single cell (Fig. 48A). However, this excitation event is not restricted to the focal plane. The z-section through the *Drosophila* wing epithelium shows that the activation beam cannot 'select' an isolated slice within the tissue. A cone shaped activation profile of cytosolic PAGFP is visible which spans over 2 µm in x direction and over approximately 15 µm in z direction (Fig. 48B).
Taken together, the confocal LSM technique cannot activate Dpp within a receiving cell that would allow tracking movement of photouncaged ligand while trafficking from the endosome.

3.4.7 Subcellular photoactivation of PAGFP with a two-photon laser-scanning microspcope (2P-LSM)

In order to achieve a spatial isolated photoactivation event, subcellular photoactivation of a two-photon laser-scanning microscope (2P-LSM) was investigated. Two-photon excitation is based on the probability that two low energy photons arrive 'simultaneously' at a fluorophore and induce an electronic transition comparable to a single high-energy photon at the confocal LSM excitation (Göppert-Mayer, 1931). For example, simultaneous absorption of two red photons can excite a molecular UV-transition. The advantage of two-photon over standard confocal microscopy is the spatial restriction of this excitation event (Denk et al., 1990). Photoactivation of the cytosolic PAGFP in fixed wing imaginal discs with a 2P-LSM was considered. After excitation with low levels of 825 nm laser with a pulse duration of about 100 femtoseconds at a repetition rate of 160 MHz, cytosolic PAGFP absorbed two long-wavelength photons simultaneously, resulting in the increase of the fluorescence up to at least 20 fold (Fig. 49).

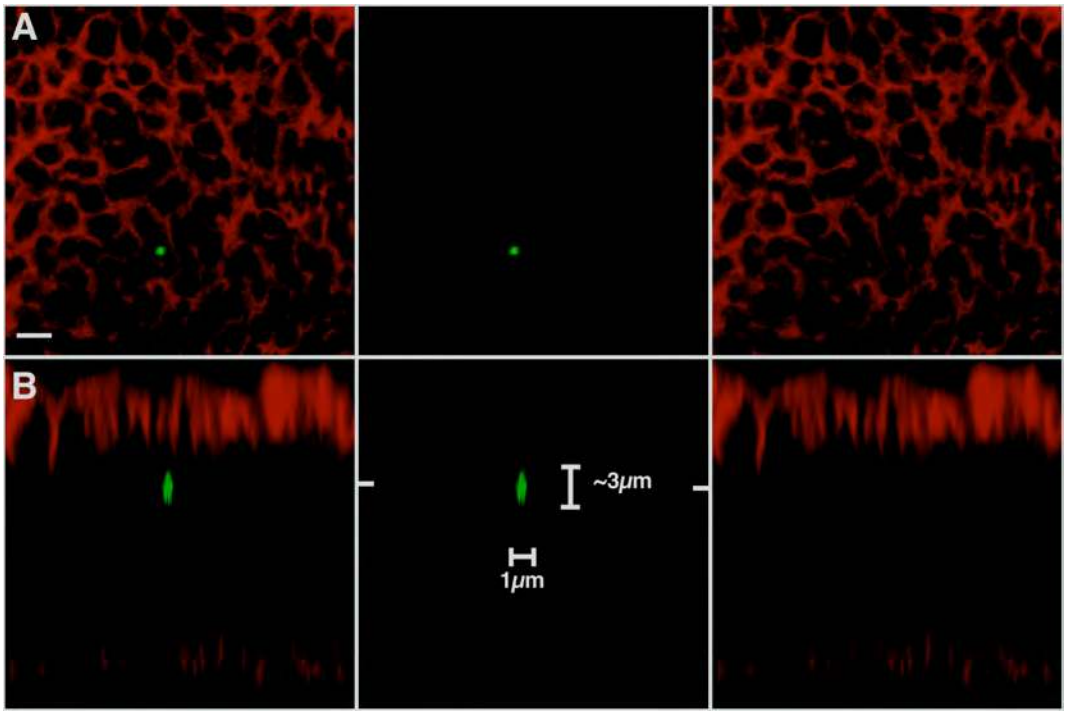

Fig. 49: Subcellular photoactivation of PAGFP in a wing imaginal disc with two-photon LSM excitation
A) PAGFP in an *UAS-PAGFP; act-GAL4/+* third instar wing disc was imaged with 488 nm excitation after photoactivation with pulses of 825 nm light with a two-photon LSM within a single cell. Cell profiles are labelled with Fasciclin III (red) immunolabelling. B) Axial view of the photoactivated region. Note that a two-photon LSM can activate cytosolic PAGFP within a single cell. In addition, the cross-sectional view through the wing epithelium shows that the activation event is approximately restricted to the focal plane. Bar in A corresponds to 2 µm.

The two-photon LSM beam can activate cytosolic PAGFP within a single cell (Fig. 49A). In addition, this excitation event is limited to the focal plane. The cross-sectional view through the *Drosophila* wing epithelium shows that the activation beam can restrict the activation event to an isolated slice within the tissue. Cytosolic PAGFP is visible in a range of 1 µm in x direction and spans only over approximately 3 µm in z direction (Fig. 49B).

Taken together, the two-photon LSM technique can provide spatially resolved photoactivation events within a Dpp receiving cell that would allow tracking movement of photouncaged ligand while trafficking from the endosome.

3.4.8 Photoactivation of PAGFP-Dpp with a two-photon laser-scanning microscope (2P-LSM)

The photoactivation of PAGFP-Dpp was also tested with the two-photon LSM when expressed in wing imaginal discs (Fig. 50). PAGFP-Dpp was driven in the endogenous Dpp expression domain using the *GAL4* gene under the spatial and temporal control of the dpp promoter (*dpp-GAL4*). After photoactivation of fixed tissue with high levels of 825 nm laser with a pulse duration of about 100 femtoseconds at a repetition rate of 100 MHz, fluorescence of PAGFP-Dpp increased in the photoactivated region: bright fluorescent signal in the secreting cells and dimmer fluorescent punctate structures at the receiving territory could be observed (Fig. 50).

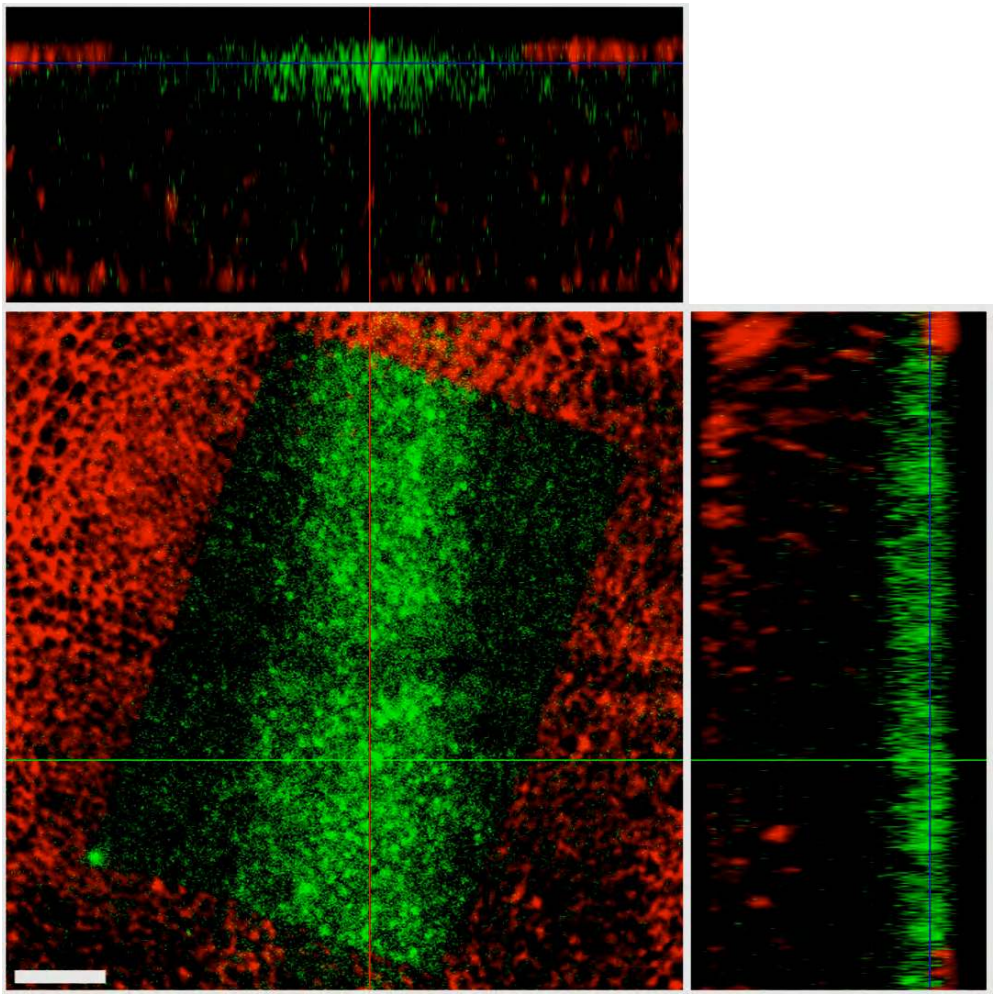

Fig. 50 (previous page): Photoactivation of PAGFP in a wing imaginal disc with a two-photon LSM excitation
Lateral and corresponding axial views of PAGFP-Dpp in an *UAS-PAGFP-Dpp; dpp-GAL4/+* third instar wing disc that was imaged with 488 nm excitation after photoactivation with pulses of 825 nm light with a two-photon LSM. Cell profiles are labelled with phalloidin (red). Note that a two-photon LSM can activate PAGFP-Dpp restricted to a focal plane at the apical part of the wing epithelium. PAGFP-Dpp is visible as bright fluorescent signal marking the secreting cells and dimmer fluorescent punctate structures at the receiving territory. Partial absence of phalloidin signal is due to high laser beam intensity during photoactivation. Bar corresponds to 10 µm.

Using a two-photon excitation system combined with a sensitive confocal LSM comprising a 405 nm laser, it remains to be shown whether activated PAGFP-Dpp upon passage through the endosome within a receiving cell can be tracked from one cell to the neighbouring cell: a key event in the planar transcytosis model of Dpp propagation.

4 Discussion

In the present work, I studied whether the DBTS model, where Dpp transport is based on extracellular diffusion taking into account receptor binding and subsequent internalization, can explain the spreading of Dpp through the target tissue. I compared the implications of this model with direct measurements of the total and cell surface receptor levels as well as the extracellular pool of ligand in wild-type and in endocytosis-defective mosaic tissue. The current DBTS model in which ligand transport is based on extracellular diffusion is inconsistent with the experimental data obtained in the “shibire shadow assay” and the “shibire rescue assay”.

Two results lead to this conclusion. First, the DBTS model can generate transient shadows, but only if the surface receptor levels in the *shi* ^{ts1} clone increase dramatically. As a consequence, this titrates out Dpp while diffusing through the extracellular space, accumulating in the clone. Using receptor antibodies in the “shibire shadow assay”, I could not detect higher levels of surface receptor in the *shi* ^{ts1} clone (see Fig. 25 and 26). Second, in the DBTS model for the “shibire rescue assay”, the levels of both the extracellular Dpp and the surface receptors are dramatically increased in the endocytosis-defective receiving tissue. Such an increase was detected neither for extracellular Dpp (see Fig. 29) nor for the surface receptor levels (see Fig. 27 and 28). Instead, extracellular Dpp entered the receiving tissue over a distance of only 4 – 5 cells. Therefore, the DBTS model cannot explain the experimental data, suggesting that endocytosis plays an active role in the ligand transport beyond the regulation of receptors at the surface.

In addition, by performing FRAP experiments I was able to demonstrate directly that Dynamin-mediated endocytosis is required for Dpp movement through the target tissue. Two results lead to this conclusion. First, after photobleaching a region of interest in the receiving tissue, GFP-Dpp from the neighbouring areas moved into the bleached area in GFP-Dpp expressing wing discs. However,

unbleached GFP-Dpp ligands from the neighbouring areas failed to move into the bleached area when endocytosis was abolished in “shibire rescue” discs at the restrictive temperature (34 °C) (see Fig. 31). Second, fluorescence recovery of GFP signal was only recorded in “shibire rescue” discs after cooling down gradually the tissue from 34 °C to 25 °C (see Fig. 35). This indicates that Dynamin-mediated endocytosis is essential for Dpp movement through the tissue to form a long-range gradient.

Utilizing Rab antibodies and internalized fluorescent Dextran I was also able to demonstrate that GFP-Dpp traffics through early, late and recycling endosomes. In particular, GFP-Dpp association with Rab11 recycling endosomes in the receiving cells prompts the possibility that recycling of ligand occurs via apical recycling endosomes (ARE) (see Fig. 39A).

Finally, I established a recycling assay based on subcellular photoactivation of ligand to address specifically the Dpp recycling event at the receiving cells (see Fig. 49). In the future, this assay will allow us to test whether photouncaged PAGFP-Dpp upon passage through an endosome at the receiving cell will move to neighbouring cells at the target territory.

4.1 Why the DBTS model fails to explain Dpp propagation

In this study, I have shown that the DBTS model cannot explain the observed ligand and receptor profiles during Dpp transport through the target tissue. The discrepancy between the implications of the model and the experimental data cannot be explained by the choice of a particular set of parameters, since the assumption that a high surface receptor concentration is present inside the clone, which is required for shadows to appear in the “shibire shadow assay”, is independent of any choice of parameters (Kruse at al., 2004). In addition, the parameter values were chosen to capture the typical distance over which the ligand extends as well as the characteristic time to reach steady state as previously demonstrated (Entchev et al. 2000).

Yet one wonders why the model is not able to explain Dpp spreading though it integrates many events such as ligand diffusion, receptor binding, internalization and resecretion. This is based on the fact that the ligand transport is only due to diffusion, i. e. ligand-receptor complexes can only be externalized at the same position on the cell surface where they were internalized. The DBTS model ignores the possibility that ligand could also be transported by travelling through cells to reappear at different positions on the cell surface.

The fact that the DBTS model is not sufficient to explain observed Dpp spreading suggests that contributions of receptor trafficking to transport ligand may indeed play an important role. But what are then the relative contributions of both phenomena, extracellular diffusion and intracellular trafficking, to the movement of the ligand through the tissue? Since the parameters of the DBTS model were chosen similar to values measured in a different cellular context, i. e. for the EGF receptor in a cell culture system (Kruse et al., 2004), it will be first necessary to measure directly the different dynamic parameters to address this question, including the diffusion coefficient as well as rates of endocytosis, degradation and recycling of Dpp in the developing wing. To estimate the diffusion coefficient, FRAP experiments in the wing imaginal disc as performed in this study are one approach. This will allow us to estimate the contribution of Dynamin-dependent endocytosis during Dpp gradient formation.

4.2 Dynamin-dependent Dpp transport

In contrast to results presented in this study, recently published experiments by Belenkaya et al. (Belenkaya et al., 2004) implied that Dynamin-mediated endocytosis is not essential for Dpp movement. They indicated that no shadows of extracellular GFP-Dpp could be observed in the “shibire shadow assay”. In addition, extracellular ligand could be detected far away from the source in the “shibire rescue assay”.

In the “shibire shadow assay”, a wave of Dpp emanating from the source is confronted with a *shi* ^{ts1} clone at the restrictive temperature where endocytosis is blocked. A transient shadow of GFP-Dpp was seen behind the clone (Entchev et al., 2000) (see Fig. 5e-g). The shadows are transient because Dpp can move in all directions and after a while the shadows are filled by Dpp coming from the sides. Furthermore, experiments in our lab showed that such shadows could not be observed when *shi* ^{ts1} clones at the restrictive temperature were generated in animals displaying a full, steady-state gradient (Entchev et al., 2000). Therefore three settings are important to keep in mind when performing this experiment:

I) generate a propagation front (i. e. start the experiment at 16 °C, a temperature at which GFP-Dpp expression is low probably due to the thermosensitivity of the GAL4 system),
II) block completely endocytosis in the *shi* ^{ts1} clones (i. e. at 34 °C or above), and
III) monitor GFP-Dpp in the right window to see the transient shadows.

In the experiments by Belenkaya et al., the animals were kept at 18 °C before the initiation of the *shi* ^{ts1} clones (Belenkaya et al., 2004) (see Experimental Procedures), a temperature at which GFP-Dpp forms a gradient that is very similar to conditions at 25 °C. In this situation, no propagation front is generated. This experimental condition is equivalent to look at GFP-Dpp in the presence of *shi* ^{ts1} clones starting from a steady state, a scenario in which no shadows were detected either (Entchev et al., 2000). Furthermore, their “restrictive” temperature is 32 °C (Belenkaya et al., 2004) (see Fig. 3A-D), at which endocytosis is still taking place as demonstrated with FRAP experiments performed in “shibire rescue” wing imaginal discs. Probably because of these two reasons no shadows could be detected in their case.

The same holds true for the “shibire rescue assay” where the temperature treatment was performed again at 32 °C (Belenkaya et al., 2004) (see Fig. 3F). In this experiment, I compared the distribution of extracellular GFP-Dpp when endocytosis was blocked (at 34 °C) at the receiving cells mutant for *shi* ^{ts1} and in heterozygous sibling control animals submitted to the same treatment. In a

situation in which the production of Dpp from the source is the same, I quantified the range of extracellular GFP-Dpp in the *shi* ^{ts1} mutant target tissue *versus* the range in the heterozygous sibling control tissue. The range was dramatically reduced in the *shi* ^{ts1} mutant territory (see Fig. 29). From this result, I concluded that Dynamin-mediated endocytosis is indeed essential for the long-range transport of the extracellular pool of Dpp.

In the report of Belenkaya et al., they looked at GFP-Dpp in a similar experiment. But they compared the range of extracellular Dpp in “shibire rescue” animals at 32 °C (at which GAL4 is highly active thereby causing high levels of expression of GFP-Dpp from the source) *versus* the same genotype at 16 °C (when GAL4 is almost inactive implying low levels of Dpp production from the source) (Belenkaya et al., 2004) (see Fig. 3E and 3F). Since Dpp production is very different at these two temperatures the ranges of extracellular GFP-Dpp in the receiving tissues are not comparable to address the effect of the mutant condition on the spreading of the extracellular pool.

Belenkaya et al. also showed that the total pool of the Dpp receptor, Tkv, accumulated in *shi* ^{ts1} cells upon five hours of endocytic block (see Fig. 4B). This is in contrast to my results. Prompted by the implications of the DBTS model that a block of extracellular Dpp diffusive movement requires an increase of the pool of surface receptors of approximately 20 fold above the normal levels, I analyzed and quantified in my work the pool of surface receptors as well as total receptors. I quantified these parameters in the “shibire shadow assay” and the “shibire rescue assay” compared to wild-type. For this, I generated two new antibodies against the cytosolic and the luminal side of the Thick veins receptor. These reagents allowed determining the levels of the cell surface pool as well as total pool of receptor. I checked the specificity of the antibodies as follows:

I) the detection of a 63 kDa corresponding band in Western Blot experiments (see Fig. 22),
II) the absence of immunostaining in Tkv null mutant clones (*tkv*^{8}) (see Fig. 21),

III) the titration of antibodies by binding to peptides used to generate the antibodies in both stainings and Western Blot (see Fig. 21, 22, and 23), and
IV) the elevated levels of staining in Tkv overexpressing developing tissue (see Fig. 21B and 23B).

In addition, I quantified the levels of overexpression that can be detected by quantitative RT-PCR in overexpressing animals: a factor of less than 5 (probably around 2) can be detected in my immunostainings.

In the “shibire rescue” as well as in the “shibire shadow” animals, no elevated levels of either surface or total receptors could be detected (see Fig. 27 and 28). This implies that if there is an increase of surface receptors, this is lower than 5 fold. Since a 20 fold increase is necessary to account for the formation of shadows, this implies that receptors at the surface are not the reason why *shi* ^{ts1} clones cause the formation of shadows. In addition, no increase, but decrease in the levels of extracellular GFP-Dpp could be observed in the “shibire rescue assay” (see Fig. 29). However, new assays need to be developed to investigate directly the effect on Dpp long-range movement when Dynamin-mediated endocytosis is abolished.

4.3 Addressing the role of Dynamin-mediated endocytosis for Dpp movement: using FRAP as a tool

So far, FRAP analysis have been particular employed in studying trafficking problems related to single cells, e. g. the kinetics of peripheral membrane proteins which are responsible for the formation of COPI vesicles (Presley et al., 2002; Elsner et al., 2003), the mobility of proteins in the mitochondria (Partikian et al., 1998), the lumen of the endoplasmic reticulum (ER) (Dayel et al., 1999), on ER and Golgi membranes (Cole et al., 1996), in the cytoplasm (Seksek et al., 1997) and in the nucleus (Phair and Misteli, 2000), as well as the shuttling of cargo between the different compartments (Girod et al., 1999). To address directly the role of Dynamin-mediated endocytosis for Dpp movement, the

mobility of GFP-Dpp ligands in the wing imaginal disc were measured by analysis of fluorescence photobleaching recovery kinetics (Axelrod et al., 1976).

However, the interpretation of FRAP curves is highly susceptible to misinterpretation. This holds true for the determination of the diffusion coefficient of proteins, which is hampered by the finite time needed for bleaching the region of interest (ROI). In other words, bleaching is assumed to be instantaneous when deriving fitting functions. Yet in my experiments the ROI was bleached in a repetitive manner, i. e. it was scanned several times during the process to achieve a more complete bleaching. In this case, the kinetics of GFP recovery was slow in comparison to the bleaching process and hence it was assumed that the effect was negligible. However, correction terms were indeed considered to account for the fact that there was still some remaining fluorescence after bleaching.

The FRAP experiments demonstrated that Dynamin-mediated endocytosis is essential for Dpp movement through the target tissue. Since movement of GFP-Dpp was absent under conditions were endocytosis was abolished (see Fig. 31), the working hypothesis that both phenomena, extracellular diffusion and intracellular trafficking combined with endocytosis and resecretion, equally contribute to the Dpp current in the developing wing epithelium is rather unlikely.

Why are FRAP experiments able to dissect the contributions of both mechanisms? The advantage of FRAP analysis of “shibire rescue” discs compared to the “shibire rescue assay” is the direct analysis of Dpp movement when endocytosis is blocked after a short time of only 10 minutes. The rapid impairment of Dpp movement under this condition implies that indirect effects like cell surface receptor upregulation that could hinder Dpp while diffusing through the extracellular space is less likely to occur. A caveat of interpreting results obtained in the “shibire rescue assay” is that a block of endocytosis for six hours can cause a change of the steady state of different dynamic parameters, including the diffusion coefficient as well as rates of degradation and recycling of Dpp at the receiving cells.

FRAP experiments open the possibility to further analyze Dpp trafficking within epithelial cells of wing imaginal discs. The use of a temperature-sensitive exocytosis defective syntaxin mutant (Littleton et al., 1998) will be one approach to test whether Dpp movement is also affected. FRAP analysis of the recovery kinetics of GFP tagged Hh or Wg in “shibire rescue” discs would also allow to address directly the role of Dynamin-dependent endocytosis for the gradient formation of both morphogens. Both secreted ligands have been proposed to spread by extracellular diffusion and thereby could serve as negative controls for the scenario of Dynamin-dependent Dpp transport.
The real time analysis enables also to monitor short-term effects on intracellular Dpp movement when drugs affecting endocytic trafficking or the organization of the microtubule and the actin cytoskeleton (e. g. wortmannin, brefeldin A or nocodazole) are applied. FRAP analysis of GFP-Dpp in cell regions expressing different mutants of Rab protein will also address the role of endocytic trafficking during Dpp gradient formation.

4.4 Dpp movement along the endocytic pathway

Trafficking of Dpp at the receiving cells involves a number of intermediate compartments controlled by Rab proteins (reviewed in Zerial and McBride, 2001). In this study I provided evidence that most of GFP-Dpp ligand is present in Rab-enriched endosomes as well as in fluorescent Dextran marked endocytic compartments in *Drosophila* wing imaginal discs (see Fig. 39 and 40). GFP-Dpp ligand accumulates mainly apically in endosomes, and work in our lab indicates that the ligand is restricted to an area between the apical and the septate junctions at the apical part of the epithelial wing cells. In addition, the Dpp receptor Tkv is also concentrated in the same area. Therefore, the trafficking as well as the signalling machinery is probably restricted to the junctional area of wing epithelial cells. This would be consistent with results where the Dpp gradient at the receiving tissue is confined to the apical part of the epithelium

(Entchev et al., 2000). GFP-Dpp degradation then takes place in more basal parts of the cell whereas the recycling of the ligand occurs via apical recycling endosomes (ARE) where Rab11 is present.

However, not all GFP-Dpp is localized in this Rab-positive compartments suggesting that the ligand moves also along other trafficking routes at the receiving cells. In mammalian cell culture, it has been demonstrated that the TGF-β receptor can traffic along both the clathrin-dependent pathway accumulating in EEA1-positive endosomes as well as along a clathrin-independent pathway residing in caveolin-enriched endosomes (Di Guglielmo et al., 2003). This segregation of TGF-β receptors into distinct endocytic compartments is supposed to regulate Smad regulation and receptor turnover. In particular, EEA1-positive endosomes are enriched with SARA promoting TGF-β signalling, whereas Smurfs bound receptors are present in caveosomes required for rapid receptor turnover. So far there is no evidence of caveosome-like structures in *Drosophila*, but it will be interesting to test whether Dpp-Tkv complexes are internalized through a clathrin-independent pathway.

4.5 A Dpp recycling assay

In the process of planar transcytosis, the morphogen spreads throughout the target tissue by consecutive rounds of endocytosis and resecretion (Entchev et al., 2000). Whereas the role of endocytosis has been extensively addressed, Dpp resecretion possibly through the ARE in order to spread through the target tissue has not yet been directly monitored. In the case of Wg in *Drosophila* embryos, it has been shown by *in vivo* imaging of a functional GFP-Wg fusion that morphogen ligands can be secreted from the receiving cells (Pfeiffer et al., 2002). To address the recycling at the receiving cells, a strategy was followed to photoactivate PAGFP-Dpp upon passage through an endosome at the receiving cell using a two-photon LSM (Denk et al., 1990) and monitor its movement while trafficking from the endosome.

Unlike confocal LSM, two-photon excitation occurs only at the beam focus, resulting in spatially resolved photoactivation within a Dpp receiving cell that allows to track the movement of photouncaged ligand while trafficking from the endosome. The penetration depth of confocal microscopy is limited to biological tissue-scattering lengths of approximately 100 µm (Cheong et al., 1990), whereas two photon excitation can offer images 2 – 3 times deeper than confocal LSM (Centonze and White, 1998). Because of the restricted excitation event, deleterious out-of-focus absorptions, photobleaching and phototoxicity are reduced.

Based on the established assay, it will be tested whether activated PAGFP-Dpp can be tracked *in vivo* from one cell to the neighbouring. Possible caveats can be detection problems caused by low intensity of photoactivated ligand moving from cell to cell. To address this, several cells can be activated simultaneously to allow monitoring occurrence of detectable PAGFP-Dpp ligand in a non-photoactivated cell. Furthermore, this experiment offers the possibility to explore the protein dynamics of Dpp by tracking photoactivated ligand that is the only visible GFP in the tissue (Patterson and Lippincott-Schwartz, 2002). Parameters such as endocytosis and recycling of Dpp in the developing wing will be addressed.

5 References

Aberle, H., Haghighi, A. P., Fetter, R. D., McCabe, B. D., Magalhaes, T. R. and Goodman, C. S. (2002). wishful thinking encodes a BMP type II receptor that regulates synaptic growth in Drosophila. Neuron 33, 545-58.

Alberts, B., Bray, D., Lewis, J., Raff, M., Roberts, K. and Watson, J. D. (1994). Molecular Biology of the Cell. NY: Garland Publisher.

Arora, K., Dai, H., Kazuko, S. G., Jamal, J., O'Connor, M. B., Letsou, A. and Warrior, R. (1995). The Drosophila schnurri gene acts in the Dpp/TGF beta signaling pathway and encodes a transcription factor homologous to the human MBP family. Cell 81, 781-90.

Arora, K., Levine, M. S. and O'Connor, M. B. (1994). The screw gene encodes a ubiquitously expressed member of the TGF-beta family required for specification of dorsal cell fates in the Drosophila embryo. Genes Dev 8, 2588-601.

Axelrod, D., Koppel, D. E., Schlessinger, J., Elson, E. and Webb, W. W. (1976). Mobility measurement by analysis of fluorescence photobleaching recovery kinetics. Biophys J 16, 1055-69.

Basler, K. and Struhl, G. (1994). Compartment boundaries and the control of Drosophila limb pattern by hedgehog protein. Nature 368, 208-14.

Belenkaya, T. Y., Han, C., Yan, D., Opoka, R. J., Khodoun, M., Liu, H. and Lin, X. (2004). Drosophila Dpp morphogen movement is independent of dynamin-mediated endocytosis but regulated by the glypican members of heparan sulfate proteoglycans. Cell 119, 231-44.

Bennett, D. and Alphey, L. (2002). PP1 binds Sara and negatively regulates Dpp signaling in Drosophila melanogaster. Nat Genet 31, 419-23.

Berlin, R. D. and Oliver, J. M. (1980). Surface functions during mitosis. II. Quantitation of pinocytosis and kinetic characterization of the mitotic cycle with a new fluorescence technique. J Cell Biol 85, 660-71.

Blair, S. S. (1992). Engrailed expression in the anterior lineage compartment of the developing wing blade of Drosophila. Development 115, 21-33.

Bollenbach, T., Kruse, K., Pantazis, P., González-Gaitán, M. and Jülicher, F. Robust formation of morphogen gradients. Submitted to Phys Rev Lett.

Bradford, M. M. (1976). A rapid and sensitive method for the quantitation of microgram quantities of protein utilizing the principle of protein-dye binding. Anal Biochem 72, 248-54.

Brand, A. H. and Perrimon, N. (1993). Targeted gene expression as a means of altering cell fates and generating dominant phenotypes. Development 118, 401-15.

Briscoe, J., Chen, Y., Jessell, T. M. and Struhl, G. (2001). A hedgehog-insensitive form of patched provides evidence for direct long-range morphogen activity of sonic hedgehog in the neural tube. Mol Cell 7, 1279-91.

Brummel, T. J., Twombly, V., Marqués, G., Wrana, J. L., Newfeld, S. J., Attisano, L., Massagué, J., O´Connor, M. B. and Gelbart, W. M. (1994). Characterization and relationshipof Dpp receptors encoded by the saxophone and thickveins genes in Drosophila. Cell 78, 251-261.

Bryant, P. J. (1975). Pattern formation in the imaginal wing disc of Drosophila melanogaster: fate map, regeneration and duplication. J Exp Zool 193, 49-77.

Bucci, C., Parton, R. G., Mather, I. H., Stunnenberg, H., Simons, K., Hoflack, B. and Zerial, M. (1992). The small GTPase rab5 functions as a regulatory factor in the early endocytic pathway. Cell 70, 715-28.

Campbell, G. and Tomlinson, A. (1999). Transducing the Dpp morphogen gradient in the wing of Drosophila: regulation of Dpp targets by brinker. Cell 96, 553-62.

Centonze, V. E. and White, J. G. (1998). Multiphoton excitation provides optical sections from deeper within scattering specimens than confocal imaging. Biophys J 75, 2015-24.

Chamoun, Z., Mann, R. K., Nellen, D., von Kessler, D. P., Bellotto, M., Beachy, P. A. and Basler, K. (2001). Skinny hedgehog, an acyltransferase required for palmitoylation and activity of the hedgehog signal. Science 293, 2080-4.

Chavrier, P., Parton, R. G., Hauri, H. P., Simons, K. and Zerial, M. (1990). Localization of low molecular weight GTP binding proteins to exocytic and endocytic compartments. Cell 62, 317-29.

Chen, M. S., Obar, R. A., Schroeder, C. C., Austin, T. W., Poodry, C. A., Wadsworth, S. C. and Vallee, R. B. (1991). Multiple forms of dynamin are encoded by shibire, a Drosophila gene involved in endocytosis. Nature 351, 583-6.

Chen, Y. and Schier, A. F. (2001). The zebrafish Nodal signal Squint functions as a morphogen. Nature 411, 607-10.

Cheong, W. F., Prahl, S. A. and Welch, A. J. (1990). A Review of the Optical-Properties of Biological Tissues. Ieee Journal of Quantum Electronics 26, 2166-2185.

Chu, L., Wiley, H. S. and Lauffenburger, D. A. (1996). Endocytic Relay as a Potential Means for Enhancing Ligand Transport through Cellular Tissue Matrices: Analysis and Possible Implications for Drug Delivery. Tissue Engineering 2, 17-38.

Cole, N. B., Smith, C. L., Sciaky, N., Terasaki, M., Edidin, M. and Lippincott-Schwartz, J. (1996). Diffusional mobility of Golgi proteins in membranes of living cells. Science 273, 797-801.

Crick, F. (1970). Diffusion in embryogenesis. Nature 225, 420-2.

Cubas, P., de Celis, J. F., Campuzano, S. and Modolell, J. (1991). Proneural clusters of achaete-scute expression and the generation of sensory organs in the Drosophila imaginal wing disc. Genes Dev 5, 996-1008.

Cui, Y., Hackenmiller, R., Berg, L., Jean, F., Nakayama, T., Thomas, G. and Christian, J. L. (2001). The activity and signaling range of mature BMP-4 is regulated by sequential cleavage at two sites within the prodomain of the precursor. Genes Dev 15, 2797-802.

Cui, Y., Jean, F., Thomas, G. and Christian, J. L. (1998). BMP-4 is proteolytically activated by furin and/or PC6 during vertebrate embryonic development. Embo J 17, 4735-43.

Dayel, M. J., Hom, E. F. and Verkman, A. S. (1999). Diffusion of green fluorescent protein in the aqueous-phase lumen of endoplasmic reticulum. Biophys J 76, 2843-51.

de Renzis, S., Sonnichsen, B. and Zerial, M. (2002). Divalent Rab effectors regulate the sub-compartmental organization and sorting of early endosomes. Nat Cell Biol 4, 124-33.

Denk, W., Strickler, J. H. and Webb, W. W. (1990). Two-photon laser scanning fluorescence microscopy. Science 248, 73-6.

Di Guglielmo, G. M., Le Roy, C., Goodfellow, A. F. and Wrana, J. L. (2003). Distinct endocytic pathways regulate TGF-beta receptor signalling and turnover. Nat Cell Biol 5, 410-21.

Diaz-Benjumea, F. J. and Cohen, S. M. (1993). Interaction between dorsal and ventral cells in the imaginal disc directs wing development in Drosophila. Cell 75, 741-52.

Diaz-Benjumea, F. J. and Cohen, S. M. (1995). Serrate signals through Notch to establish a Wingless-dependent organizer at the dorsal/ventral compartment boundary of the Drosophila wing. Development 121, 4215-25.

Doctor, J. S., Jackson, P. D., Rashka, K. E., Visalli, M. and Hoffmann, F. M. (1992). Sequence, biochemical characterization, and developmental expression of a new member of the TGF-beta superfamily in Drosophila melanogaster. Dev Biol 151, 491-505.

Doherty, D., Feger, G., Younger-Shepherd, S., Jan, L. Y. and Jan, Y. N. (1996). Delta is a ventral to dorsal signal complementary to Serrate, another Notch ligand, in Drosophila wing formation. Genes Dev 10, 421-34.

Dosch, R., Gawantka, V., Delius, H., Blumenstock, C. and Niehrs, C. (1997). Bmp-4 acts as a morphogen in dorsoventral mesoderm patterning in Xenopus. Development 124, 2325-34.

Dudu, V., Pantazis, P. and Gonzalez-Gaitan, M. (2004). Membrane traffic during embryonic development: epithelial formation, cell fate decisions and differentiation. Curr Opin Cell Biol 16, 407-14.

Eldar, A., Rosin, D., Shilo, B. Z. and Barkai, N. (2003). Self-enhanced ligand degradation underlies robustness of morphogen gradients. Dev Cell 5, 635-46.

Elsner, M., Hashimoto, H., Simpson, J. C., Cassel, D., Nilsson, T. and Weiss, M. (2003). Spatiotemporal dynamics of the COPI vesicle machinery. EMBO Rep 4, 1000-4.

Entchev, E. V., Schwabedissen, A. and Gonzalez-Gaitan, M. (2000). Gradient formation of the TGF-beta homolog Dpp. Cell 103, 981-91.

Ericson, J., Rashbass, P., Schedl, A., Brenner-Morton, S., Kawakami, A., van Heyningen, V., Jessell, T. M. and Briscoe, J. (1997). Pax6 controls progenitor

cell identity and neuronal fate in response to graded Shh signaling. Cell 90, 169-80.

Faucheux, M., Netter, S., Bloyer, S., Moussa, M., Boissonneau, E., Lemeunier, F., Wegnez, M. and Theodore, L. (2001). Advantages of a P-element construct containing MtnA sequences for the identification of patterning and cell determination genes in Drosophila melanogaster. Mol Genet Genomics 265, 14-22.

Feng, Y., Press, B. and Wandinger Ness, A. (1995). Rab 7: An important regulator of late endocytic membrane traffic. J. Cell Biol. 131, 1435-1452.

Ferguson, E. L. and Anderson, K. V. (1992a). Decapentaplegic acts as a morphogen to organize dorsal-ventral pattern in the Drosophila embryo. Cell 71, 451-61.

Ferguson, E. L. and Anderson, K. V. (1992b). Localized enhancement and repression of the activity of the TGF-beta family member, decapentaplegic, is necessary for dorsal-ventral pattern formation in the Drosophila embryo. Development 114, 583-97.

Filmus, J. and Selleck, S. B. (2001). Glypicans: proteoglycans with a surprise. J Clin Invest 108, 497-501.

Fischer, J. A., Giniger, E., Maniatis, T. and Ptashne, M. (1988). GAL4 activates transcription in Drosophila. Nature 332, 853-6.

Gelbart, W. M. (1989). The decapentaplegic gene: a TGF-beta homologue controlling pattern formation in Drosophila. Development 107 Suppl, 65-74.

Gierer, A. (1981). Generation of biological patterns and form: some physical, mathematical, and logical aspects. Prog Biophys Mol Biol 37, 1-47.

Gierer, A. and Meinhardt, H. (1972). A theory of biological pattern formation. Kybernetik 12, 30-9.

Girod, A., Storrie, B., Simpson, J. C., Johannes, L., Goud, B., Roberts, L. M., Lord, J. M., Nilsson, T. and Pepperkok, R. (1999). Evidence for a COP-I-independent transport route from the Golgi complex to the endoplasmic reticulum. Nat Cell Biol 1, 423-30.

Göppert-Mayer, M. (1931). Uber Elementarakte mit zwei Quantensprüngen. Ann Phys (Leipzig) 9. 273–294.

González-Gaitán, M. (2003). Signal dispersal and transduction through the endocytic pathway. Nat Rev Mol Cell Biol 4, 213-24.

Greco, V., Hannus, M. and Eaton, S. (2001). Argosomes. A potential vehicle for the spread of morphogens through epithelia. Cell 106, 633-645.

Groppe, J., Rumpel, K., Economides, A. N., Stahl, N., Sebald, W. and Affolter, M. (1998). Biochemical and biophysical characterization of refolded Drosophila DPP, a homolog of bone morphogenetic proteins 2 and 4. J Biol Chem 273, 29052-65.

Guillén, I., Mullor, J. L., Capdevila, J., Sanchez-Herrero, E., Morata, G. and Guerrero, I. (1995). The function of engrailed and the specification of Drosophila wing pattern. Development 121, 3447-56.

Gurdon, J. B., Dyson, S. and St Johnston, D. (1998). Cells' perception of position in a concentration gradient. Cell 95, 159-62.

Gurdon, J. B., Harger, P., Mitchell, A. and Lemaire, P. (1994). Activin signalling and response to a morphogen gradient. Nature 371, 487-92.

Haerry, T. E., Khalsa, O., O'Connor, M. B. and Wharton, K. A. (1998). Synergistic signaling by two BMP ligands through the SAX and TKV receptors controls wing growth and patterning in Drosophila. Development 125, 3977-87.

Held, L. I. (2002). Imaginal discs : the genetic and cellular logic of pattern formation. Cambridge ; New York: Cambridge University Press.

Herbst, J. J., Opresko, L. K., Walsh, B. J., Lauffenburger, D. A. and Wiley, H. S. (1994). Regulation of postendocytic trafficking of the epidermal growth factor receptor through endosomal retention. J Biol Chem 269, 12865-73.

Hoekstra, D., Tyteca, D. and van, I. S. C. (2004). The subapical compartment: a traffic center in membrane polarity development. J Cell Sci 117, 2183-92.

Ingham, P. W. and Fietz, M. J. (1995). Quantitative effects of hedgehog and decapentaplegic activity on the patterning of the Drosophila wing. Curr Biol 5, 432-40.

Inoue, H., Imamura, T., Ishidou, Y., Takase, M., Udagawa, Y., Oka, Y., Tsuneizumi, K., Tabata, T., Miyazono, K. and Kawabata, M. (1998). Interplay of signal mediators of decapentaplegic (Dpp): molecular characterization of mothers against dpp, Medea, and daughters against dpp. Mol Biol Cell 9, 2145-56.

Irvine, K. D. and Wieschaus, E. (1994). fringe, a Boundary-specific signaling molecule, mediates interactions between dorsal and ventral cells during Drosophila wing development. Cell 79, 595-606.

Jackson, S. M., Nakato, H., Sugiura, M., Jannuzi, A., Oakes, R., Kaluza, V., Golden, C. and Selleck, S. B. (1997). dally, a Drosophila glypican, controls cellular responses to the TGF-ß-related morphogen, Dpp. Development 124, 4113-4120.

Jazwinska, A., Kirov, N., Wieschaus, E., Roth, S. and Rushlow, C. (1999a). The Drosophila gene brinker reveals a novel mechanism of Dpp target gene regulation. Cell 96, 563-73.

Jazwinska, A., Rushlow, C. and Roth, S. (1999b). The role of brinker in mediating the graded response to Dpp in early Drosophila embryos. Development 126, 3323-34.

Kerszberg, M. and Wolpert, L. (1998). Mechanisms for positional signalling by morphogen transport: a theoretical study. J. Theor. Biol. 191, 103-114.

Khalsa, O., Yoon, J. W., Torres-Schumann, S. and Wharton, K. A. (1998). TGF-beta/BMP superfamily members, Gbb-60A and Dpp, cooperate to provide pattern information and establish cell identity in the Drosophila wing. Development 125, 2723-34.

Kim, J., Irvine, K. D. and Carroll, S. B. (1995). Cell recognition, signal induction, and symmetrical gene activation at the dorsal-ventral boundary of the developing Drosophila wing. Cell 82, 795-802.

Kim, J., Sebring, A., Esch, J. J., Kraus, M. E., Vorwerk, K., Magee, J. and Carroll, S. B. (1996). Integration of positional signals and regulation of wing formation and identity by Drosophila vestigial gene. Nature 382, 133-8.

Kirkpatrick, H., Johnson, K. and Laughon, A. (2001). Repression of dpp targets by binding of brinker to mad sites. J Biol Chem 276, 18216-22.

Koch, A. J. and Meinhardt, H. (1994). Biological pattern-formation - from basic mechanisms to complex structures. Rev Mod Phys 66, 1481-1507.

Koppel, D. E., Axelrod, D., Schlessinger, J., Elson, E. L. and Webb, W. W. (1976). Dynamics of fluorescence marker concentration as a probe of mobility. Biophys J 16, 1315-29.

Kruse, K., Pantazis, P., Bollenbach, T., Julicher, F. and Gonzalez-Gaitan, M. (2004). Dpp gradient formation by dynamin-dependent endocytosis: receptor trafficking and the diffusion model. Development 131, 4843-56.

Kutty, G., Kutty, R. K., Samuel, W., Duncan, T., Jaworski, C. and Wiggert, B. (1998). Identification of a new member of transforming growth factor-beta superfamily in Drosophila: the first invertebrate activin gene. Biochem Biophys Res Commun 246, 644-9.

Laemmli, U. K. (1970). Cleavage of structural proteins during the assembly of the head of bacteriophage T4. Nature 227, 680-5.

Lander, A. D., Nie, Q. and Wan, F. Y. (2002). Do morphogen gradients arise by diffusion? Dev Cell 2, 785-96.

Lauffenburger, D. A. and Linderman, J. J. (1993). Receptors: models for binding, trafficking, and signalling. NY: Oxford University Press.

Lecuit, T., Brook, W. J., Ng, M., Calleja, M., Sun, H. and Cohen, S. M. (1996). Two distinct mechanisms for long-range patterning by Decapentaplegic in the Drosophila wing. Nature 381, 387-93.

Lecuit, T. and Cohen, S. M. (1998). Dpp receptor levels contribute to shaping the Dpp morphogen gradient in the Drosophila wing imaginal disc. Development 125, 4901-4907.

Letsou, A., Arora, K., Wrana, J. L., Simin, K., Twombly, V., Jamal, J., Staehling-Hampton, K., Hoffmann, F. M., Gelbart, W. M., Massagué, J. et al. (1995). Drosophila Dpp Signaling Is Mediated by the punt Gene Product: A Dual Ligand-Binding Type II Receptor of the TGF-beta Receptor Family. Cell 80, 899-908.

Lewis, P. M., Dunn, M. P., McMahon, J. A., Logan, M., Martin, J. F., St-Jacques, B. and McMahon, A. P. (2001). Cholesterol modification of sonic hedgehog is required for long-range signaling activity and effective modulation of signaling by Ptc1. Cell 105, 599-612.

Lippincott-Schwartz, J., Snapp, E. and Kenworthy, A. (2001). Studying protein dynamics in living cells. Nat Rev Mol Cell Biol 2, 444-56.

Littleton, J. T., Chapman, E. R., Kreber, R., Garment, M. B., Carlson, S. D. and Ganetzky, B. (1998). Temperature-sensitive paralytic mutations demonstrate that

synaptic exocytosis requires SNARE complex assembly and disassembly. Neuron 21, 401-13.

Lo, P. C. and Frasch, M. (1999). Sequence and expression of myoglianin, a novel Drosophila gene of the TGF-beta superfamily. Mech Dev 86, 171-5.

Marques, G., Bao, H., Haerry, T. E., Shimell, M. J., Duchek, P., Zhang, B. and O'Connor, M. B. (2002). The Drosophila BMP type II receptor Wishful Thinking regulates neuromuscular synapse morphology and function. Neuron 33, 529-43.

Martinez Arias, A. (2003). Wnts as morphogens? The view from the wing of Drosophila. Nat Rev Mol Cell Biol 4, 321-5.

Maschat, F., Serrano, N., Randsholt, N. B. and Geraud, G. (1998). engrailed and polyhomeotic interactions are required to maintain the A/P boundary of the Drosophila developing wing. Development 125, 2771-80.

Massagué, J. (1998). TGF-beta signal transduction. Annual Review of Biochemistry 67, 753-791.

McDowell, N., Gurdon, J. B. and Grainger, D. J. (2001). Formation of a functional morphogen gradient by a passive process in tissue from athe early Xenopus embryo. Int. J. Dev. Biol. 45, 199-207.

Minami, M., Kinoshita, N., Kamoshida, Y., Tanimoto, H. and Tabata, T. (1999). brinker is a target of Dpp in Drosophila that negatively regulates Dpp-dependent genes. Nature 398, 242-6.

Nakato, H., Futch, T. A. and Selleck, S. B. (1995). The division abnormally delayed (dally) gene: a putative integral membrane proteoglycan required for cell division patterning during postembryonic development of the nervous system in Drosophila. Development 121, 3687-702.

Nellen, D., Affolter, M. and Basler, K. (1994). Receptor serine/threonine kinases implicated in the control of Drosophila body pattern by decapentaplegic. Cell 78, 225-37.

Nellen, D., Burke, R., Struhl, G. and Basler, K. (1996). Direct and long-range action of a DPP morphogen gradient. Cell 85, 357-68.

Neumann, C. J. and Cohen, S. M. (1996). Distinct mitogenic and cell fate specification functions of wingless in different regions of the wing. Development 122, 1781-9.

Neumann, C. J. and Cohen, S. M. (1997). Long-range action of Wingless organizes the dorsal-ventral axis of the Drosophila wing. Development 124, 871-80.

Newfeld, S. J., Padgett, R. W., Findley, S. D., Richter, B. G., Sanicola, M., de Cuevas, M. and Gelbart, W. M. (1997). Molecular evolution at the decapentaplegic locus in Drosophila. Genetics 145, 297-309.

Nguyen, M., Parker, L. and Arora, K. (2000). Identification of maverick, a novel member of the TGF-beta superfamily in Drosophila. Mech Dev 95, 201-6.

Novick, P. and Zerial, M. (1997). The diversity of Rab proteins in vesicle transport. Current Opinion in Cell Biology 9, 496-504.

Nybakken, K. and Perrimon, N. (2002). Heparan sulfate proteoglycan modulation of developmental signaling in Drosophila. Biochim Biophys Acta 1573, 280-91.

Ohkuma, S. and Poole, B. (1978). Fluorescence probe measurement of the intralysosomal pH in living cells and the perturbation of pH by various agents. Proc Natl Acad Sci U S A 75, 3327-31.

Panganiban, G. E., Reuter, R., Scott, M. P. and Hoffmann, F. M. (1990). A Drosophila growth factor homolog, decapentaplegic, regulates homeotic gene expression within and across germ layers during midgut morphogenesis. Development 110, 1041-50.

Parker, L., Stathakis, D. G. and Arora, K. (2004). Regulation of BMP and activin signaling in Drosophila. Prog Mol Subcell Biol 34, 73-101.

Partikian, A., Olveczky, B., Swaminathan, R., Li, Y. and Verkman, A. S. (1998). Rapid diffusion of green fluorescent protein in the mitochondrial matrix. J Cell Biol 140, 821-9.

Patterson, G. H. and Lippincott-Schwartz, J. (2002). A photoactivatable GFP for selective photolabeling of proteins and cells. Science 297, 1873-7.

Penton, A., Chen, Y., Staehling-Hampton, K., Wrana, J. L., Attisano, L., Szidonya, J., Cassill, J. A., Massague, J. and Hoffmann, F. M. (1994). Identification of two bone morphogenetic protein type I receptors in Drosophila and evidence that Brk25D is a decapentaplegic receptor. Cell 78, 239-50.

Pfeiffer, S., Alexandre, C., Calleja, M. and Vincent, J. P. (2000). The progeny of wingless-expressing cells deliver the signal at a distance in Drosophila embryos. Curr. Biol. 10, 321-324.

Pfeiffer, S., Ricardo, S., Manneville, J. B., Alexandre, C. and Vincent, J. P. (2002). Producing cells retain and recycle Wingless in Drosophila embryos. Curr Biol 12, 957-62.

Phair, R. D. and Misteli, T. (2000). High mobility of proteins in the mammalian cell nucleus. Nature 404, 604-9.

Phelps, C. B. and Brand, A. H. (1998). Ectopic gene expression in Drosophila using GAL4 system. Methods 14, 367-79.

Pignoni, F. and Zipursky, S. L. (1997). Induction of Drosophila eye development by decapentaplegic. Development 124, 271-8.

Pirrotta, V. (1988). Vectors for P-mediated transformation in Drosophila. Biotechnology 10, 437-56.

Podos, S. D., Hanson, K. K., Wang, Y. C. and Ferguson, E. L. (2001). The DSmurf ubiquitin-protein ligase restricts BMP signaling spatially and temporally during Drosophila embryogenesis. Dev Cell 1, 567-78.

Porter, J. A., Young, K. E. and Beachy, P. A. (1996). Cholesterol modification of Hedgehog signaling proteins in animal development. Science 274, 255–259.

Posakony, L. G., Raftery, L. A. and Gelbart, W. M. (1990). Wing formation in Drosophila melanogaster requires decapentaplegic gene function along the anterior-posterior compartment boundary. Mech. Dev. 33, 69-82.

Presley, J. F., Ward, T. H., Pfeifer, A. C., Siggia, E. D., Phair, R. D. and Lippincott-Schwartz, J. (2002). Dissection of COPI and Arf1 dynamics in vivo and role in Golgi membrane transport. Nature 417, 187-93.

Pyrowolakis, G., Hartmann, B., Muller, B., Basler, K. and Affolter, M. (2004). A simple molecular complex mediates widespread BMP-induced repression during Drosophila development. Dev Cell 7, 229-40.

Raftery, L. A. and Sutherland, D. J. (1999). TGF-beta family signal transduction in Drosophila development: from Mad to Smads. Dev Biol 210, 251-68.

Raftery, L. A., Twombly, V., Wharton, K. and Gelbart, W. M. (1995). Genetic screens to identify elements of the decapentaplegic signaling pathway in Drosophila. Genetics 139, 241-54.

Ramírez-Weber, F. A. and Kornberg, T. B. (1999). Cytonemes: cellular processes that project to the principal signaling center in Drosophila imaginal Discs. Cell 97, 599-607.

Ray, R. P. and Wharton, K. A. (2001). Context-dependent relationships between the BMPs gbb and dpp during development of the Drosophila wing imaginal disk. Development 128, 3913-25.

Reits, E. A. and Neefjes, J. J. (2001). From fixed to FRAP: measuring protein mobility and activity in living cells. Nat Cell Biol 3, E145-7.

Riddle, R. D., Johnson, R. L., Laufer, E. and Tabin, C. (1993). Sonic hedgehog mediates the polarizing activity of the ZPA. Cell 75, 1401-16.

Ruberte, E., Marty, T., Nellen, D., Affolter, M. and Basler, K. (1995). An absolute requirement for both the type II and type I receptors, punt and thickveins, for dpp signaling in vivo. Cell 80, 889-897.

Sampath, T. K., Rashka, K. E., Doctor, J. S., Tucker, R. F. and Hoffmann, F. M. (1993). Drosophila transforming growth factor beta superfamily proteins induce endochondral bone formation in mammals. Proc Natl Acad Sci U S A 90, 6004-8.

Sanicola, M., Sekelsky, J., Elson, S. and Gelbart, W. M. (1995). Drawing a stripe in Drosophila imaginal disks: negative regulation of decapentaplegic and patched expression by engrailed. Genetics 139, 745-56.

Schneider, I. (1972). Cell lines derived from late embryonic stages of Drosophila melanogaster. J Embryol Exp Morphol 27, 353-65.

Sekelsky, J. J., Newfeld, S. J., Raftery, L. A., Chartoff, E. H. and Gelbart, W. M. (1995). Genetic characterization and cloning of mothers against dpp, a gene required for decapentaplegic function in Drosophila melanogaster. Genetics 139, 1347-58.

Seksek, O., Biwersi, J. and Verkman, A. S. (1997). Translational diffusion of macromolecule-sized solutes in cytoplasm and nucleus. J Cell Biol 138, 131-42.

Selleck, S. B. (2000). Proteoglycans and pattern formation: sugar biochemistry meets developmental genetics. Trends Genet 16, 206-12.

Simmonds, A. J., Brook, W. J., Cohen, S. M. and Bell, J. B. (1995). Distinguishable functions for engrailed and invected in anterior-posterior patterning in the Drosophila wing. Nature 376, 424-7.

Skeath, J. B. and Carroll, S. B. (1992). Regulation of proneural gene expression and cell fate during neuroblast segregation in the Drosophila embryo. Development 114, 939-46.

Sonnichsen, B., De Renzis, S., Nielsen, E., Rietdorf, J. and Zerial, M. (2000). Distinct membrane domains on endosomes in the recycling pathway visualized by multicolor imaging of Rab4, Rab5, and Rab11. J Cell Biol 149, 901-14.

Soumpasis, D. M. (1983). Theoretical analysis of fluorescence photobleaching recovery experiments. Biophys J 41, 95-7.

Spencer, F. A., Hoffmann, F. M. and Gelbart, W. M. (1982). Decapentaplegic: a gene complex affecting morphogenesis in Drosophila melanogaster. Cell 28, 451-61.

St Johnston, D. (2002). The art and design of genetic screens: Drosophila melanogaster. Nat Rev Genet 3, 176-88.

St Johnston, R. D., Hoffmann, F. M., Blackman, R. K., Segal, D., Grimaila, R., Padgett, R. W., Irick, H. A. and Gelbart, W. M. (1990). Molecular organization of the decapentaplegic gene in Drosophila melanogaster. Genes Dev 4, 1114-27.

Stanley, H., Botas, J. and Malhotra, V. (1997). The mechanism of Golgi segregation during mitosis is cell type-specific. Proc Natl Acad Sci U S A 94, 14467-70.

Staples, R. R. and Ramaswami, M. (1999). Functional analysis of dynamin isoforms in Drosophila melanogaster. J Neurogenet 13, 119-43.

Starbuck, C. and Lauffenburger, D. A. (1992). Mathematical model for the effects of epidermal growth factor receptor trafficking dynamics on fibroblast proliferation responses. Biotechnol Prog 8, 132-43.

Stenmark, H., Valencia, A., Martinez, O., Ullrich, O., Goud, B. and Zerial, M. (1994). Distinct structural elements of rab5 define its functional specificity. Embo J 13, 575-83.

Strigini, M. and Cohen, S. M. (1997). A Hedgehog activity gradient contributes to AP axial patterning of the Drosophila wing. Development 124, 4697-705.

Strigini, M. and Cohen, S. M. (2000). Wingless gradient formation in the Drosophila wing. Curr Biol 10, 293-300.

Tabata, T. and Kornberg, T. B. (1994). Hedgehog is a signaling protein with a key role in patterning Drosophila imaginal discs. Cell 76, 89-102.

Tabata, T., Schwartz, C., Gustavson, E., Ali, Z. and Kornberg, T. B. (1995). Creating a Drosophila wing de novo, the role of engrailed, and the compartment border hypothesis. Development 121, 3359-69.

Tanimoto, H., Itoh, S., ten Dijke, P. and Tabata, T. (2000). Hedgehog creates a gradient of DPP activity in Drosophila wing imaginal discs. Mol Cell 5, 59-71.

Teleman, A. A. and Cohen, S. M. (2000). Dpp gradient formation in the Drosophila wing imaginal disc. Cell 103, 971-80.

Torroja, C., Gorfinkiel, N. and Guerrero, I. (2004). Patched controls the Hedgehog gradient by endocytosis in a dynamin-dependent manner, but this internalization does not play a major role in signal transduction. Development 131, 2395-408.

Tsukazaki, T., Chiang, T. A., Davidson, A. F., Attisano, L. and Wrana, J. L. (1998). SARA, a FYVE domain protein that recruits Smad2 to the TGFbeta receptor. Cell 95, 779-791.

Tsuneizumi, K., Nakayama, T., Kamoshida, Y., Kornberg, T. B., Christian, J. L. and Tabata, T. (1997). Daughters against dpp modulates dpp organizing activity in Drosophila wing development. Nature 389, 627-31.

Turing, A. M. (1952). The Chemical Basis of Morphogenesis. Philosophical Transactions of the Royal Society of London Series B-Biological Sciences 237, 37-72.

Ullrich, O., Reinsch, S., Urbe, S., Zerial, M. and Parton, R. G. (1996). Rab11 regulates recycling through the pericentriolar recycling endosome. J Cell Biol 135, 913-24.

Urbe, S., Huber, L. A., Zerial, M., Tooze, S. A. and Parton, R. G. (1993). Rab11, a small GTPase associated with both constitutive and regulated secretory pathways in PC12 cells. FEBS Lett 334, 175-82.

Vervoort, M., Crozatier, M., Valle, D. and Vincent, A. (1999). The COE transcription factor Collier is a mediator of short-range Hedgehog-induced patterning of the Drosophila wing. Curr Biol 9, 632-9.

Vincent, J. P. and Dubois, L. (2002). Morphogen transport along epithelia, an integrated trafficking problem. Dev Cell 3, 615-23.

Waltzer, L. and Bienz, M. (1999). A function of CBP as a transcriptional co-activator during Dpp signalling. Embo J 18, 1630-41.

Wang, Q. T. and Holmgren, R. A. (1999). The subcellular localization and activity of Drosophila cubitus interruptus are regulated at multiple levels. Development 126, 5097-106.

Wharton, K. A., Ray, R. P. and Gelbart, W. M. (1993). An activity gradient of decapentaplegic is necessary for the specification of dorsal pattern elements in the Drosophila embryo. Development 117, 807-22.

Wharton, K. A., Thomsen, G. H. and Gelbart, W. M. (1991). Drosophila 60A gene, another transforming growth factor beta family member, is closely related to human bone morphogenetic proteins. Proc Natl Acad Sci U S A 88, 9214-8.

Willert, K., Brown, J. D., Danenberg, E., Duncan, A. W., Weissman, I. L., Reya, T., Yates, J. R. and Nusse, R. (2003). Wnt proteins are lipid-modified and can act as stem cell growth factors. Nature 423, 448-52.

Wolpert, L. (1969). Positional information and the spatial pattern of cellular differentiation. J Theor Biol 25, 1-47.

Wrana, J. L., Attisano, L., Wieser, R., Ventura, F. and Massague, J. (1994). Mechanism of activation of the TGF-beta receptor. Nature 370, 341-347.

Xie, T., Finelli, A. L. and Padgett, R. W. (1994). The Drosophila saxophone gene: a serine-threonine kinase receptor of the TGF-beta superfamily. Science 263, 1756-9.

Xu, T. and Harrison, S. D. (1994). Mosaic analysis using FLP recombinase. Methods Cell Biol 44, 655-81.

Yamashita, H., ten Dijke, P., Franzen, P., Miyazono, K. and Heldin, C. H. (1994). Formation of hetero-oligomeric complexes of type I and type II receptors for transforming growth factor-beta. J Biol Chem 269, 20172-8.

Yang, Y., Drossopoulou, G., Chuang, P. T., Duprez, D., Marti, E., Bumcrot, D., Vargesson, N., Clarke, J., Niswander, L., McMahon, A. et al. (1997). Relationship between dose, distance and time in Sonic Hedgehog-mediated regulation of anteroposterior polarity in the chick limb. Development 124, 4393-404.

Zecca, M., Basler, K. and Struhl, G. (1995). Sequential organizing activities of engrailed, hedgehog and decapentaplegic in the Drosophila wing. Development 121, 2265-78.

Zecca, M., Basler, K. and Struhl, G. (1996). Direct and long-range action of a wingless morphogen gradient. Cell 87, 833-44.

Zerial, M. and McBride, H. (2001). Rab proteins as membrane organizers. Nature Reviews Molecular Cell Biology 2, 107-216.

Zhu, H., Kavsak, P., Abdollah, S., Wrana, J. L. and Thomsen, G. H. (1999). A SMAD ubiquitin ligase targets the BMP pathway and affects embryonic pattern formation. Nature 400, 687-93.

Appendix

Abbreviations

BSA	bovine serum albumin
$CaCl_2$	calcium chloride
CH_3OH	methanol
CH_3COOH	acetic acid
CO_2	carbon dioxid
DNA	deoxyribonucleic acid
ECL	enhanced chemiluminescence
E.coli	*Escherichia coli*
EDTA	ethylene diamine tetraacetate
EEA1	early endosomal autoantigen 1
EtOH	ethanol
FLP-FRT	site-specific FLP recombinase-FLP recombination target
FRT	FLPase recombination target
GDP	guanosine diphosphate
GFP	green fluorescent protein
GST	glutathione-*S*-transferase
GTP	guanosine triphosphate
Hg^{2+}	mercury
HRP	horseradish peroxidase
KCl	potassium chloride
KDa	kilo Dalton
KH_2PO_4	potassium hydrogen phosphate
LB medium	Luria-Bertani medium
mA	milliAmpère
$MgCl_2$	magnesium chloride

MW	molecular weight
NaCl	sodium chloride
Na_2HPO_4	sodium hydrogen phosphate
PAGFP	photoactivatable green fluorescent protein
PBS	phosphate-buffered saline
PCR	polymerase chain reaction
PIPES	piperazine-*N,N'*-bis(2-ethanesulfonic acid)
SDS	sodium dodecyl sulfate
TEMED	N,N,N',N',-tetramethylethylenediamine
TGF	transforming growth factor
UV	ultraviolet
V	volt
W	watt

Additional abbreviations are introduced and explained in the text.
Symbols of multiples (e. g. µ, n, etc.) and SI units are not listed.

Movie description

All movies are provided in high and low resolution.

wt25/34 as well as shibirerescue25/32 (low/high)

Each movie shows a third instar wing imaginal disc pouch projection (out of six individual sections) expressing GFP-Dpp (green) from a *dpp-GAL4/UAS-GFP-Dpp* larva (wt25/34) or from a *shi* ^{ts1}*; UAS-Dynamin*$^{+}$/+*; dpp-GAL4/UAS-GFP-Dpp* larva (shi25/32). GFP-Dpp gradients were imaged at 25°C/34°C (for discs with a wild-type receiving territory) or 25°C/32°C (for the “shibire rescue” discs) before, and approximately one hour after photobleaching of GFP-Dpp in a narrow stripe of 10 µm width (see Materials and Methods). The recovery of the fluorescent signal was measured by confocal time-lapse microscopy (composed of two minutes intervals). In all conditions, GFP-Dpp ligands from the neighbouring areas move subsequently into the bleached area. Recovered GFP-Dpp appears first as a diffuse fluorescent signal and later as bright fluorescent punctate structures.

shibirerescue34 (low/high)

The movie shows a third instar wing imaginal disc pouch projection (out of six individual sections) expressing GFP-Dpp (green) from a *shi* ^{ts1}*; UAS-Dynamin*$^{+}$/+*; dpp-GAL4/UAS-GFP-Dpp* larva. The GFP-Dpp gradient was imaged before, and approximately one hour after photobleaching of GFP-Dpp in a narrow stripe of 10 µm width at the restrictive temperature (34°C) where was blocked at the receiving territory (see Materials and Methods). Under this condition, no recovery of the fluorescent signal was measured by confocal time-lapse microscopy. Five independent FRAP movies showed similar absence of recovery.

shibirerescue34->25 (low/high)

The movie shows a third instar wing imaginal disc pouch projection (out of six individual sections) expressing GFP-Dpp (green) from a *shi* ^{ts1}*; UAS-Dynamin*$^{+}$/+*; dpp-GAL4/UAS-GFP-Dpp* larva. The GFP-Dpp gradient was imaged at 34°C before, and for 10 minutes after photobleaching of GFP-Dpp in a narrow stripe of 10 µm width (see Materials and Methods). Following the dynamics of GFP-Dpp for approximately 10 minutes at the restrictive temperature, the wing imaginal disc was then cooled down gradually to 25°C. Recovery of the fluorescent signal was measured only after the release of the temperature block.

Publications during PhD

Dudu V*, **Pantazis P***, González-Gaitán M
Membrane traffic during embryonic development: epithelial formation, cell fate decisions and differentiation. Curr Opin Cell Biol. 2004 Aug; 16(4):407-14.

Kruse K*, **Pantazis P***, Bollenbach T, Jülicher F, González-Gaitán M
Dpp gradient formation by dynamin-dependent endocytosis: receptor trafficking and the diffusion model. Development 2004 Oct; 131(19):4843-56.

Bollenbach T, Kruse K, **Pantazis P**, González-Gaitán M, Jülicher F
Robust formation of morphogen gradients. Submitted to Phys Rev Lett.

*contributed equally

Statement / Versicherung

I herewith declare that I have produced this paper without the prohibited assistance of third parties and without making use of aids other than those specified; notions taken over directly or indirectly from other sources have been identified as such. This paper has not previously been presented in identical or similar form to any other German or foreign examination board.

The thesis work was conducted from 01.03.2001 to 01.11.2004 under the supervision of Dr. Marcos González-Gaitán at the Max Planck Institute of Molecular Cell Biology and Genetics in Dresden.

Hiermit versichere ich, dass ich die vorliegende Arbeit ohne unzulässige Hilfe Dritter und ohne Benutzung anderer als der angegebenen Hilfsmittel angefertigt habe; die aus fremden Quellen direkt oder indirekt übernommenen Gedanken sind als solche kenntlich gemacht. Die Arbeit wurde bisher weder im Inland noch im Ausland in gleicher oder ähnlicher Form einer anderen Prüfungsbehörde vorgelegt.

Die vorgelegte Arbeit wurde vom 01.03.2001 bis 01.11.2004 unter der Aufsicht von Dr. Marcos González-Gaitán am Max Planck Institut für Molekulare Zellbiologie und Genetik in Dresden durchgeführt.

Dresden, 01.11.2004,

Periklis Pantazis

HSSS AdminTools (c) 2001, last visited: Wed Feb 02 15:52:21 CET 2005